THE HOLOCENE HISTORY OF LAKE KIVU (EAST AFRICA): NEW PERSPECTIVES FROM NEW CORES.

A THESIS

SUBMITTED TO THE FACULTY OF THE UNIVERSITY OF MINNESOTA BY

JILLIAN EMILIA VOTAVA

IN PARTIAL FULFILLMENT OF THE REQUIREMENTS FOR THE DEGREE OF

MASTER OF SCIENCE

THOMAS C. JOHNSON AND ROBERT E. HECKY

JULY 2014

ACKNOWLEDGEMENTS

First and foremost I wish to acknowledge my thesis advisors, Dr. Bob Hecky and Dr. Tom Johnson, for the opportunity to work on such a project. The Lake Kivu system is far from simple and this project has provided many thought-provoking discussions with some of the most experienced researchers in tropical African limnology and paleoclimatology. I am grateful for their patience, encouragement, and thorough critiques over the past two years. I thank Tom especially, for the once in a lifetime adventure to Lake Malawi in January 2013. I thank Dr. Steve Colman for his thoughtful and meticulous review of this thesis as well as the extra opportunities to be aboard the R/V Blue Heron. All of the faculty, staff, and fellow graduate students of the Large Lakes Observatory helped in the success of my graduate career; whether it was offering advice on methodologies and specific instruments or just offering camaraderie. Specifically, I thank Sarah Grosshuesch for LLO lab support, Bryan Bandli for training and help on the X-Ray Diffractometer, Molly O'Beirne and Julia Halbur for organic geochemistry training, tea-times, and overall good mental health; The crew of the Blue Heron, Capt. Mike King, Rual Lee, Johnny Simenson, and Peter Norick, for their hospitality and inclusiveness; Lisa Sundberg for the opportunity to give back and be a part of Great Lakes science outreach; Fellow graduate students Rozhan Zakaria, Jiying Li, Dan Titze, Lucas Gloege, Messias Macuiane, and (practically a grad student) Nick Spano for their perspectives on Large Lakes, modern science, and life.

Finally I wish to thank my family, Mom, Dad, Jenny, Jessy, and Spencer, for their unquestioning support of my scientific pursuits, even when that meant moving 400 miles away and "up-nort" to unspeakable winter temperatures. I also thank the Kerkoves of Ironwood, MI for all the produce and hospitality over the years. Last, but not least, I especially thank my life partner and best friend, Marcel Kerkove, for his mutual support of graduate school and the nightly literary adventures with Thurber-hounds and hitch-hiking across the galaxy (apparently the answer is 42).

This research project was funded in large part through a MacArthur Foundation Grant titled, "Dynamics of the Lake Kivu System: Geological, Biological and Hydrographic Impacts on Biodiversity and Human Wellbeing". Additional financial support came from a 2013 GSA Student Research grant and RA support through UMD's Geological Sciences department.

ABSTRACT

Lake Kivu lies at the heart of East Africa's rift lakes in a volcanically active region. Hydrothermal seeps impose a complex stratification regime with heated, high-salinity waters entering below 280 m water depth. Previous detailed studies of fossil diatoms and mineralogy of the sediment record suggest this hydrothermal activity began 5,000 years BP. Unfortunately, dating bulk organic matter of these original cores was problematic due to dissolved volcanogenic CO_2.

This study offers a new chronology and a detailed perspective on the limnologic history of Lake Kivu through investigation of carbonates and bulk organic matter from sediment cores recovered in 2012 and 2013. A Holocene history was compiled by ^{14}C dating of recovered terrestrial macro fossils from a deep, central basin core, and by ^{210}Pb geochronology of recent sediments from a near-shore core. Water levels in Lake Kivu rose during the African Humid Period (AHP) pluvial from 12 ka to 5 ka. Authigenic $CaCO_3$ deposition began around 4.2 ka in the deep, main basin with all subsequent carbonate intervals composed of endogenic aragonite. A solute budget reveals that most of the Ca^{2+} ion is supplied at depth via the hydrothermal seeps and suggests that this sub-lacustrine input was initiated just prior to onset of carbonate deposition. Stable isotopic analyses of $\delta^{13}C_{aragonite}$ and $\delta^{13}C_{OM}$ both indicate slight enrichment beyond the expected kinetic fractionation and above other East African lakes suggesting volcanogenic influence on water column DIC began around 4.2 ka. Some of the alternating intervals of carbonate deposition and cessation in the late-Holocene, and associated $\delta^{18}O_{aragonite}$ enrichment, coincide with records of drought from nearby Lake Edward, such as at the AHP termination, at 2 ka, and during the Little Ice Age. This suggests a climate overprint on the predominantly volcanogenic record of carbonate sedimentation in Lake Kivu.

Table of Contents

List of Tables

List of Figures

1 INTRODUCTION

1.1 LAKE KIVU

Eastern Africa plays host to some of the world's oldest and deepest great lakes. Active volcanism and tectonic rifting that starts at the triple junction in the Gulf of Aden (~12°N), between the African, Arabian and Indian plates, and extends through East Africa as far south as the Zambezi River delta (~18°S) has created this unique chain of lakes (Figure 1.1). Nowhere else on Earth's surface is there such a geological system that serves as a modern analog for the formation of early ocean basins (Degens, 1973).

Sediments from these East African lakes contain an exceptional record of the tropical climate history of the African continent. High sedimentation rates on the order of 100 cm/ 1,000 years (ky) and minimal bioturbation, yields sediment records that can be resolved to decades, if not individual years (Johnson and Odada, 1996). Sediment records from many of these lakes have provided valuable information regarding past regional climate variability, for which few other climate records exist. Some of the East African rift lakes are better studied (especially Victoria, Malawi, and Tanganyika) than others.

One of the lesser studied lakes is Lake Kivu, located at 2°S latitude between the Republic of Rwanda and the Democratic Republic of the Congo and, although not the deepest of the rift lakes, presents many interesting geological and limnological quandaries. Sediment cores from Kivu were last recovered in the early 1970's as part of a Kivu-Tanganyika expedition by the Woods Hole Oceanographic Institute and yielded a great deal of published work on the limnological history of Kivu referenced throughout this study. Here we report on the environmental history of Lake Kivu over the past 12,000 years, based on the analyses of carbonates and bulk organic matter from new sediment cores recovered in 2012 and 2013.

Situated at one of the highest points in the East African rift valley, the surface of Lake Kivu is just over 1400 meters above sea level, with Lake Edward 180 km to the north and Lake Tanganyika 150 km to the south (Fig. 1.2). Although Lake Kivu sits above both Edward and Tanganyika, its outflow is south via the Ruzizi River to Lake Tanganyika. The relatively recent (i.e. late-Pleistocene) volcanic eruptions of the Virunga volcanoes just north of Lake Kivu have blocked the earlier northern connection to Lake Edward and the Lake Victoria basins (Degens *et al.*, 1972).

The extremely close proximity of volcanic activity to Lake Kivu makes it unique among the rift lakes. Indeed two of these volcanoes are still active; Nyirongongo and Nyamlagira (Fig. 1.2),

the latter having most recent lava flows erupted in 2002 with devastating effects to the people living in communities along Kivu's north shore. Volcanic activity significantly affects the lake chemistry with saline water entering the lake at depth via hydrothermal seeps. Hydrothermal activity and increased salinity in the sub-lacustrine environment forces the lake into a highly complex stratification regime with warmer, more saline waters at the bottom than at the surface, so-called *crenogenic meromixis*, as first described in detail by Degens *et al.* (1972). Deep waters of Kivu contain high amounts of dissolved carbon dioxide (CO_2) and methane (CH_4) associated with volcanism and benthic methanogens, respectively (Schmid *et al.*, 2005). The significant methane inventory in Lake Kivu's water column (60 km^3 at STP) has recently gained the attention of the surrounding nations as a potential economic resource. Similar to the Cameroonian crater-lake, Nyos, which de-gassed in the mid 1980's causing many fatalities however, Lake Kivu poses a potentially catastrophic geo-hazard to the highly populated cities and villages surrounding the basin. Previous sedimentological and paleolimnological studies of Kivu suggest that volcanism, and the associated hydrothermal water, has played a major role in the stability of the stratification and chemistry of the overlying water column (Stoffers and Hecky, 1978; Haberyan and Hecky, 1987). The extent to which the sediment record of Lake Kivu is influenced by this sub-lacustrine input has not been investigated in detail. Climate is generally thought to be the major driver of physical, chemical, and geologic changes of any large lake, yet given the interesting situation of Lake Kivu, the relative influence of climate and volcanism on the lake's environmental history remains an open question. The goal of this study is to investigate the hydrothermal and climate influences through signals recorded in the carbonate minerals and bulk organic matter from sediment cores recovered in 2012/ 13.

Figure 1.1 East African Rift Lakes

The African continent with inset of the Great African Rift Lakes in eastern Africa. Lake Kivu is indicated by the red arrow, along the Western Rift Valley and located ~150 km north of Lake Tanganyika. Kivu and Tanganyika are hydrologically connected via the Ruzzizi River flowing south. Lake Edward is located just south-west of Lake George. Lake Challa for reference in section 4.1.3. Images:www.tulane.edu and www.globalgreatlakes.org

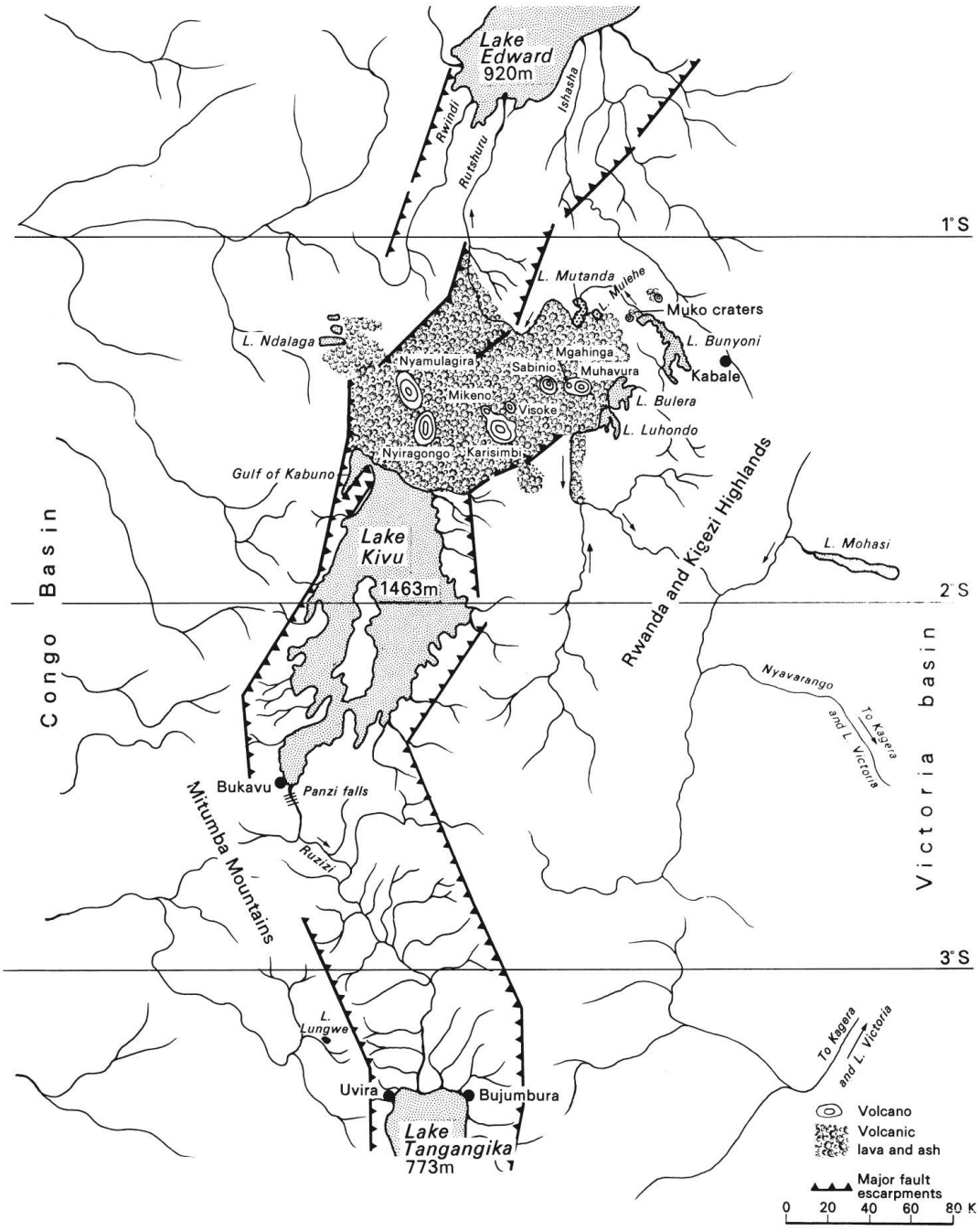

Figure 1.2 Lake Kivu Tectonic Setting

The Western Rift valley between Lake Edward in the north and Lake Tanganyika in the south. The Virunga Volcanic province blocks Kivu from Edward. Note the elevation differences between the lake surfaces. Kivu's lake surface sits 1,463 meters above sea level. Figure from Beadle (1974).

1.2 BACKGROUND

Lake Kivu has a surface area of 2370 km^2 and a mean depth of 245 m; with the maximum depth reaching 485 m in the northern basin (e.g. see morphometry data compiled by Muvundja *et al.*, 2009). The lake is composed of two main basins, eastern and northern, and a few smaller basins (Figure 1.3) divided by a north-south trending plutonic sill of Precambrian origin (Degens *et al.*, 1972). As mentioned above, Kivu's water column is unusual, with warmer temperatures at the bottom (~26°C) than at the surface (24.3°C). This is maintained by the higher salinity of the deep water (~6 g/L) and results in a density differential of about 0.002 g/cc between the surface mixed layer (0 to 60 m) and the hypolimnion (Figure 1.4; Schmid *et al.*, 2005). As a result, Kivu is meromictic and permanently stratified, with high concentrations of CO_2 and CH_4 in the hypolimnion. The major geo-hazard potential of Kivu lies in the fact that if these supersaturated, gas-charged bottom waters were disturbed and moved upward a sufficient distance, the pressure release would cause spontaneous, and catastrophic, de-gassing. This is the Lake Kivu of modern times, but was it always this way? Stoffers and Hecky (1978) discussed evidence for lake level fluctuations by as much as -300 m and +100 m relative to the present, and suggested that the lake has not always had outflow to Tanganyika. Haberyan and Hecky (1987) found drastic changes in the late-Holocene sedimentological record that included peculiar brown layers of gel-like consistency a few centimeters thick and were associated with: (1) increased organic matter, (2) cessation in carbonate precipitation, (3) input of volcanic ashes, and (4) major shifts in diatom assemblages. Using these bulk organic proxies, the authors proposed these changes as evidence for large limnic eruption events (i.e. mixing of surface and bottom waters resulting in rapid changes in water chemistry) caused by the onset of volcanic activity and hydrothermal inputs around 5,000 years ago. The stratigraphic record of Lake Kivu, spanning the past 12,000 years or so, is quite dynamic and serves as motivation for this study.

The precipitation of authigenic carbonates in freshwater lakes is mainly affected by water chemistry and therefore, changes in carbonate mineralogy and occurrence down-core can be used as a direct proxy for changes in lake water chemistry through time (Kelts and Hsü, 1978). This study entailed analyses for carbonate mineralogy and isotopic composition of carbonates and bulk organic matter. In most lakes, carbonates precipitate from the epilimnion and any changes in their isotopic composition ($\delta^{13}C$ and $\delta^{18}O$) record the evolution of the water body as a whole (Talbot, 1990). Generally, $\delta^{13}C$ from organic carbon in large lakes is isotopically light due to fractionation derived from aquatic photosynthesis or methanogenesis (-6 to -40‰ and -40‰ to -90‰, respectively). Alternatively, $\delta^{13}C$ derived from volcanic gas is relatively heavy (-10 to

+10‰) (Sharp, 2007). The investigation of $\delta^{13}C$ can highlight the sources of carbon within the carbonate sediments of Lake Kivu if sufficient difference exists between the biogenic carbon (via fractionation of atmospheric CO_2) and hydrothermal/volcanogenic carbon.

In most lakes of simple hydrology, precipitation and evaporation control the water's isotopic signature of oxygen (and hydrogen). In Lake Kivu this phenomenon is complicated by hydrothermal inputs of H_2O and CO_2 at depth. Degens *et al.* (1972) found the surface waters of Kivu to be enriched in $\delta^{18}O$ (+3.5‰) relative to the saline deep waters (-0.5‰). The surface water likely has evaporative enrichment while the bottom waters are more similar to the local meteoric waters (-3‰; Rozanski *et al.*, 1993). The groundwater is heated due to active volcanism, and in the presence of plutonic rocks which are isotopically heavy (+6 to +10‰ $\delta^{18}O$; Hoefs, 1997) with respect to the water (-3‰), the interaction results in altered rocks that are slightly depleted in $\delta^{18}O$ and hydrothermal waters that are slightly enriched (more positive ‰) in $\delta^{18}O$ compared to the original meteoric water.

This study also entailed cursory microscopic examination of the sediment for diatom assemblages and other sedimentary components. These observations were combined with the mineralogical and isotopic results to further our understanding of the environmental history of Lake Kivu throughout the Holocene.

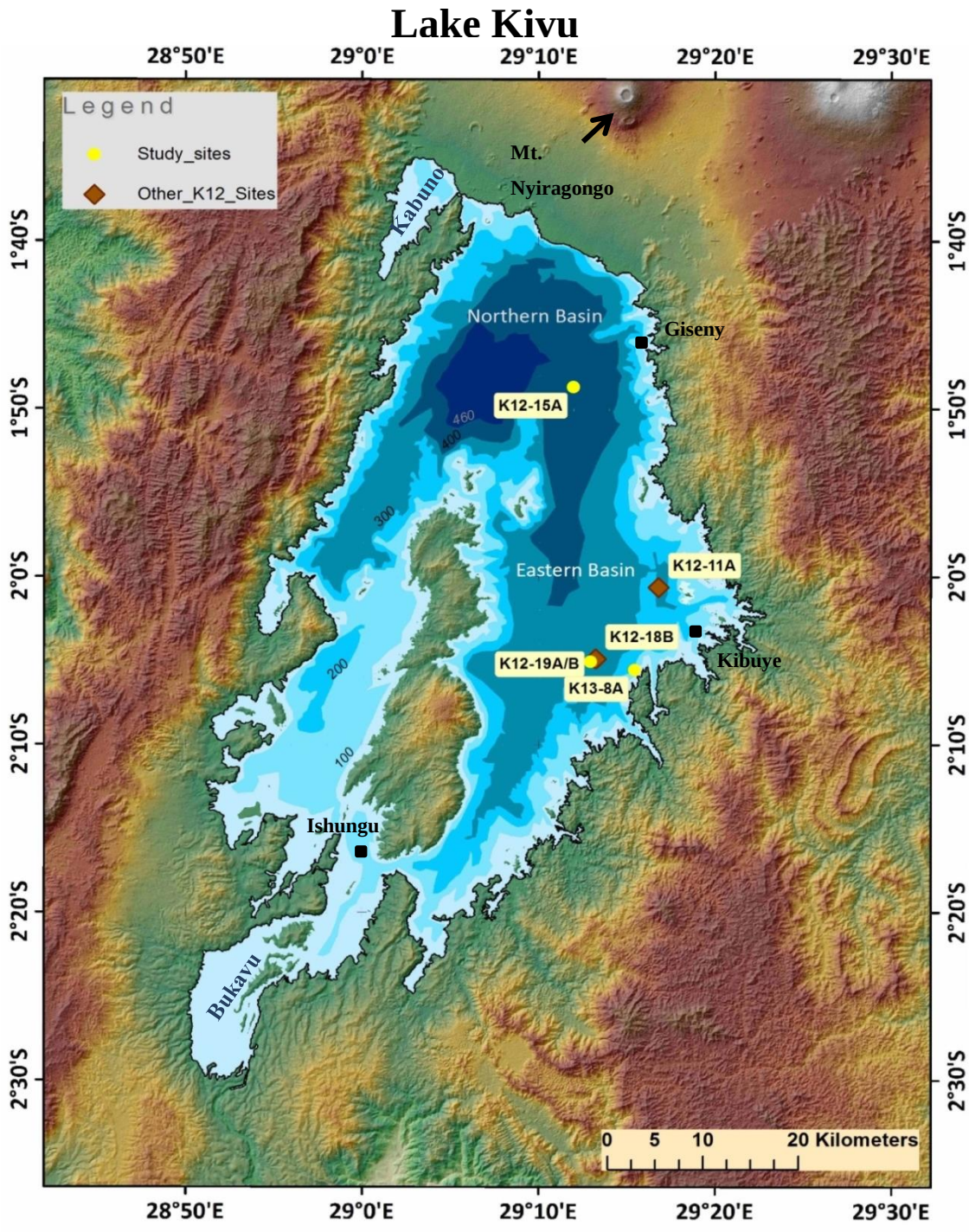

Figure 1.3 Lake Kivu Study Sites

Topographic/ bathymetric detail of Lake Kivu with coring sites mentioned in this study highlighted in tan labels. Black squares: study sites of Pasche *et al.* (2010). Regional SRTM Digital Elevation Model (DEM) joined to bathymetry by (Hubert Zal). Colored lake contours are in meters. Note the steep terrain and the two volcanoes near the top of the image. Kabuno and Bukavu basins labeled for reference.

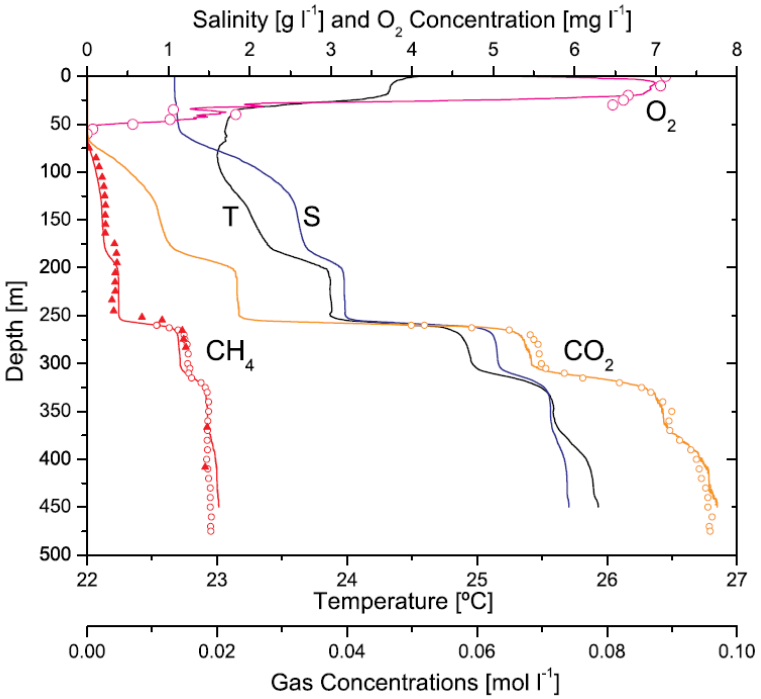

Figure 1.4 Lake Kivu's Water Column

Figure reported by Schmid *et al.* (2005) with temperature (T), salinity (S), and gas concentrations (O_2, CO_2, and CH_4) measured in February 2004. Kivu's mixed layer varies seasonally between 50 and 70 m water depth.

2. MATERIALS AND METHODS

All materials used in this study were recovered on two separate field campaigns to Lake Kivu aboard the R/V Kilindi, a University of Syracuse transportable research vessel. The first occurred 10^{th} – 18^{th} January, 2012 (designated MANGO-KIVU12- in the LacCORE archive) and the other occurred 14^{th} – 16^{th} March, 2013 (MANGO2-KIVU13-). The cores from these expeditions are hereafter referred to with the prefix K12 and K13, respectively.

2.1 SEDIMENT CORES

Seismic profiles from previous surveys conducted by Chris Scholz and workers (2010 – 2012) contributed to coring site selection. Sediments were retrieved either with a gravity corer or a Kullenberg piston corer lined with standard polycarbonate plastic tubes ~7cm in diameter. At individual sites, length of continuous sediment recovered varied from 10 centimeters to over 8 meters. Successful recovery of sediment cores from this lake is very difficult due to the gas-charged bottom- and pore-waters. Degassing effects often led to sediment mixing in the upper, most fluid portions of the cores, especially at recovery depths greater than 200m. Upon recovery, the cores were cut into roughly 1.5 meter sections for ease of shipment and processing in the laboratory. Cores were then sealed and shipped to the National Lacustrine Core Facility, LacCORE, at the University of Minnesota (Minneapolis, MN). After arrival at LacCORE, cores were split open lengthwise with one half deemed the "working" and the other deemed the "archive" half. Working halves were processed first by taking high-resolution, color photographic images and then scanned for magnetic susceptibility (SI, 10^{-5}) with a Geotek MSCL-XYZ split core logger. After logging for magnetic properties, each core section was described by filling out an Initial Core Description (ICD) sheet, generally following the classification scheme of Schnurrenberger *et al.* (2003). During initial description cores were examined for macrofossils which were then extracted and placed in labeled glass vials for later use (See Chronology below). Working halves were wrapped in saran-wrap, placed in labeled D-tubes, and brought to the core storage facility at the Large Lakes Observatory (LLO) on the Duluth campus for further analysis.

For the purposes of this project (to investigate the inorganic carbonate record) four cores were chosen to study in detail. The piston-core K12-15A was originally deemed the best for acquiring a long, Holocene, stratigraphic record for Lake Kivu with over 7 meters of sediment recovered from its deep (455m), distal location in the Northern Basin (Figure 1.3). With only the

top 40-50cm of the record being disturbed, it was hoped that additional gravity cores could be correlated to develop a complete stratigraphy up to present-day conditions. Despite its distal location however, subsequent sedimentological analyses and seismic interpretation work by C. Scholz and X. Zhang (manuscript in press) confirmed the presence of many turbidite sequences throughout the core amounting to a total of 3 meters of the record. Thereafter attention switched to the Eastern Basin and piston core K12-19A (352m water depth). In addition to having far fewer turbidite sequences than K12-15A, this core also had an accompanying gravity core (K12-19B) with minimal disturbance, datable recovered macrofossils, and over 8 meters of sediment stratigraphy to investigate. As mentioned above, maintaining undisturbed sediment stratigraphy during the coring process is very difficult under the modern Lake Kivu conditions and some disturbance/ displacement, especially in the upper 1 meter, is expected. K12-19A's top-most section (0 to 140cm) is greatly disturbed and hence the need for the gravity cores. K12-19B (68cm long) was analyzed in place of K12-19A's top-most section but also showed clear evidence of coring disturbance (e.g. some displaced, rotated beds and units). During the second field campaign emphasis was placed in this Eastern Basin locale and, using modifications learned from the first field expedition, a number of gravity cores were successfully recovered with seemingly intact stratigraphy. Core K13-8A was chosen for its remarkable continuity, shallower location, and proximity to other studies of modern Lake Kivu sedimentation (e.g. "Kibuye" core used in Pasche *et al*., 2010; Pasche *et al*., 2011).

2.2 LITHOLOGIC COMPONENT OBSERVATIONS

The high-resolution images and ICDs form the basis of the lithostratigraphic observations of the cores. In addition, the mineralogy and diatom assemblages were investigated in certain depth intervals to put together a more comprehensive stratigraphy. Here I focus on methods for the three cores most heavily analyzed for this study: K12-19A, K12-19B, and K13- 8A.

2.2.1 – MINERALOGY

Dominant mineralogy for select intervals (greater than 2.5% TIC) was determined by dry powder X-Ray Diffractometry (XRD) on a Phillips X'pert MPD diffractometer with a theta-theta goniometer and a copper anode x-Ray tube in the University of Minnesota Duluth's (UMD) Research Instrumentation Laboratory. Samples were prepared by creating a slurry of sediment and de-ionized water (DI) in a watch-glass which was then transferred onto a 5 cm by 5 cm glass slide and allowed to dry (via air or hotplate). Glass slides were labeled directly with a permanent

marker. Each sample was run on a 1 second time step with a 1° filter from 10° to 45° 2θ at 40kV and 40mA with CuK_{α} radiation (λ= 1.5418Å). Peaks were identified using the software suite X'Pert High Score by matching peaks to a searchable database of minerals. Using the literature of previous Lake Kivu sediment investigations many of the carbonate-forming minerals were considered, including: aragonite, Mg-calcite, dolomite, siderite, and mono-hydrocalcite as well as some other minerals like pyrite, quartz, kaolinite (clay), and feldspars (Stoffers and Hecky, 1978; Botz *et al.*, 1988).

2.2.2 - DIATOMS

Smear slides created from raw sediment (usually individual laminations) were used for the qualitative microscopic analysis of sediment composition. The piston core (K12-19A) was sampled at least to 20 cm intervals, while the gravity cores (K12-19B and K13-8A) were sampled at 10 cm intervals. An Olympus polarizing-light microscope with 100X and 200X magnification was used to identify the major sediment components. To aid in this process, general smear slide description forms, available through LacCORE and LRC, were used to guide the observations. Diatoms were not counted and instead overall dominance of two distinct morphologies was noted. Common (>5%) morphologies and size, pennate vs. centric dominance, and presence/ absence of key taxa and minerals were all documented on the forms. The major diatom taxa could be identified in smear slides aided by reference to Haberyan and Hecky (1987), Gasse *et al.* (1983), and Gasse (1986). These include: *Chaetoceros sp.*, *Nitschia* sp., *Stephanodiscus* sp., *Rhopalodia* sp., and *Melrosia* sp.

2.3 BULK CARBON ANALYSES

Sediment cores were sampled at 1 cm to 5 cm intervals depending on the overall length and resolution desired. Table 2.1 details the four cores discussed in this study and to what extent each was sampled. Between 1 cm^3 and 2 cm^3 of wet material was extracted, placed in pre-weighed 20 mL plastic vials, weighed, freeze-dried in a Labconco Freeze Dry system (-40°C; <130mBar), reweighed, and then homogenized by agate mortar/ pestle.

Table 2.1: Sediment Core Sampling Details

Core	Location (lat., long.)	Water Depth (m)	Core Length (cm)	Sampling interval
K12-15A	-1.813, 29.200	455	691	0.5cm every 5cm, from 0cm to 686cm depth
K12-19A	-2.058, 29.216	352	856.5	0.5cm every 5cm, from 90cm to 838cm depth
K12-19B	" "	352	68	0.5 cm every 2cm, from 0 to 64cm depth
K13-8A	-2.094, 29.257	96	73	1cm continuous 0 to 20cm, then every 5cm, 25 to 70cm depth

2.3.1 – TOTAL CARBON

Total carbon (TC) for K12-15A, and K13-8A was determined using a UIC Carbon Furnace CM5300 and Coulometer CM5014 system where approximately 20 mg of sample was combusted at 950° C in an O_2 atmosphere and the resulting CO_2 was titrated, quantitatively measured, and values reported as % C. Precision of the coulometer was determined by running lab-grade pure $CaCO_3$ before and between every 5 or 10 samples and operation deemed acceptable when ±0.25% C (of the needed 12% C in 100% $CaCO_3$) was achieved.

2.3.2 – TOTAL INORGANIC CARBON

Total inorganic carbon (TIC) for all cores was determined directly using the UIC Coulometer and Acidification Module CM5130 where approximately 20 mg of sample was acidified in 2N HCl and the evolved CO_2 was titrated, quantitatively measured, and values reported as % C. As with the TC analysis, instrument set-up was kept in the acceptable ±0.25% C range.

2.3.3 – TOTAL ORGANIC CARBON

Organic carbon content can be measured multiple ways, both directly and indirectly. For sediments analyzed by coulometry (K13-8A), organic carbon (OC) was determined by difference: %TC - %TIC. For core K12-15A, % OC and % N were determined on acidified samples using the Elemental Analyzer (EA) during pre-combustion for isotopic analysis of organic ^{13}C and ^{15}N

(See Stable Isotope Analyses section 2.5.2 - Bulk Organic Matter). In addition, organic carbon was determined for the cores (K12-19A, K12-19B, and K13-8A) by Loss on Ignition (LOI) modified from Heiri *et al.* (2001) and Santisteban *et al.* (2004). Dried, weighed samples (WS) of about 100 mg were placed in weighed crucibles and set overnight (at least 12 hours) in a drying-oven at 105° C then allowed to cool in a desiccator before reweighing (DW_{105}). The crucibles were then placed in the muffle furnace (Thermolyne FA1730) and combusted at 550° C for 4 hours and allowed to cool in the oven before reweighing (DW_{550}). Organic carbon (% OC) was calculated with the following relationships:

$$LOI_{550} = \frac{100 * (DW_{105} - DW_{550})}{WS}$$

$$\%OC = \frac{LOI_{550}}{2}$$

Both methods of OC determination yielded similar results for K13-8A with reproducibility for most samples better than ± 1.5% C.

2.4 Chronology and Age Models

2.4.1 – AMS ^{14}C Dating

Piston cores K12-19A and K12-11A yielded the most macrofossils (vascular plant remains) for analysis; however, fossils were also recovered from other cores as well. A total of 14 recovered macrofossils (8 from K12-19A, 4 from K12-11A, 1 from K12-18A, and 1 from K12-18B) were sent off for radio carbon analysis to Beta Analytics (Miami, FL) for accelerator mass-spectrometry of ^{14}C following their online general guidelines for preparing geological samples. Results were reported as conventional radiocarbon ages (i.e. years before AD 1950) with a precision of ± 50 years or better. Later these were converted to calibrated years before present (cal. yr BP) using CalPal – online (www.calpal-online.de), and an age model was created by linear regression of these calibrated ages against sediment depth.

2.4.2 – ^{210}Pb Dating of Bulk Sediments

Gravity core K13-8A was sampled in 1cm increments (~1cc) continuously to 10cm depth, then every 2cm to 20cm depth (plus additional "background" samples at 25 and 30 cm depth). Samples were freeze-dried, homogenized by agate mortar/ pestle and sent for analysis of ^{210}Pb at

the Department of Soil Science at the University of Manitoba (Winnipeg, Canada). ^{210}Pb activity was determined by alpha spectroscopy and values were reported in Becquerels per gram (Bq/g) with the standard deviation around ± 0.03 Bq/g. Sediment depth-age relations were modeled a few different ways: linear, constant rate of supply (CRS), and rapid steady state mixing (RSSM). The linear model is the simplest but also the least useful to interpreting natural systems since it assumes there has been no change in sedimentation rate (Appleby, 2001; Gale, 2009). The most commonly used model is the CRS model which assumes a constant atmospheric ^{210}Pb flux but allows the sediment supply to vary. It is an integrative model that takes into account cumulative dry bulk density and the total ^{210}Pb inventory down-core (Robbins, 1978; MacKenzie *et al.*, 2011). The RSSM model adds an additional metric to account for sediment reworking by benthic organisms (Robbins and Edington, 1975). Given that Lake Kivu is anoxic below ~60 m water depth and core K13-8A was recovered in 96 m water depth, bioturbation was not an issue and we applied the CRS model to this gravity core.

Estimates of dry bulk density at each interval down-core were mainly derived from porosity measurements. Porosity was estimated from the water weight measurements (pre- and post-freeze drying) by the following relationships:

$$\emptyset\ (porosity) = \frac{V_{water}}{(V_{water} + V_{dry\ sed})} = \frac{{}^{M_{water}}/_{\rho_{water}}}{\left({}^{M_{water}}/_{\rho_{water}} + {}^{M_{sed}}/_{\rho_{sed}}\right)}$$

Where V is volume in cm^2, M is mass in grams, and ρ is density in g/cm^3. Sediment density was estimated based on the abundance of (A) organic matter, (B) biogenic silica, and (C) mineral content.

$$\rho_{sed} = A + B + C = \left(\frac{\%TOC}{100} * 2\right) + \left(\frac{\%BSi}{100} * 2\right) + \left(\frac{100 - \%BSi - 2 * \%TOC}{100}\right) * 2.65$$

Where *% BSi* is biogenic silica empirically derived from X-Ray Fluorescence (XRF) Si:Ti ratios using the following relationship:

$$\%BSi = 142.86(Si{:}Ti) - 7.14$$

From the relationship established for Lake Malawi sediment; Johnson *et al.*, 2011.
Dry mass per area (g/cm^2) was estimated at each depth interval sampled in gravity core K13-8A following:

$$dry\ mass\ per\ area\ \left(\frac{g}{cm^2}\right) = (1 - \emptyset) * \rho_{sed} * depth\ interval\ (cm)$$

And the accumulated dry mass per area, taken as the cumulative sum of these at each interval down-core.

2.5 STABLE ISOTOPE ANALYSES

Stable isotopes were analyzed from two sources within the cores: inorganic carbonate minerals (K12-19A, K12-19B, K13-8A) and bulk organic matter (K12-15A, K12-19B, K13-8A). In dealing with any stable isotope, samples are compared to a known standard and reported using the following "delta" nomenclature:

$$\delta\ (‰) = \frac{R_x}{R_s - 1} * 1000$$

$$e.g. \quad \delta^{18}O(‰) = \frac{\left(\frac{^{18}O\ _{sample}}{^{16}O\ _{sample}}\right)}{\left(\frac{^{18}O\ _{VPDB}}{^{16}O_{VPDB}} - 1\right)} * 1000$$

Where R_x is the heavy/light isotope ratio of the sample and R_s is the ratio of a standard.

2.4.1- CARBONATE MINERAL FRACTION ($\delta^{13}C$ and $\delta^{18}O$ of $CaCO_3$)

In order to analyze the stable isotopic composition of the carbonate minerals in our cores, raw sediment samples had to be treated in order to remove organic matter. This involved a 4-step process that is modified from Steinman *et al.* (2012) and the Limnological Research Center (LRC) standard operating procedures (SOP) series. About 1cc of wet sediment was first sieved with 50 ml DI (with a small addition of $NaHCO_3$ to the water to keep the pH slightly elevated) through a #230 steel or Nitex screen sieve and the finer (<63μm) fraction was collected, concentrated via centrifuge and set overnight with a 50-50 bleach-water (~2.625% NaOCl) solution. These "washed" sediments were then rinsed three times, freeze-dried, and homogenized in agate mortar/pestle. Approximately 50 mg of each homogenized sample was sent to the University of Arizona's Environmental Isotope Laboratory for stable carbon and oxygen analysis. Values were reported in per mil (‰) deviation from Vienna PeeDee Belemnite (VPDB) standard and the precision found to be better than 0.1‰.

2.5.2 – BULK ORGANIC MATTER ($\delta^{13}C$ and $\delta^{15}N$ of bulk sediments)

Dried sediment samples were analyzed for carbon and nitrogen stable isotopes using continuous flow isotope ratio mass spectrometry (EA-IRMS) at LLO for K12-15A and at the Stable Isotope Laboratory on the University of Minnesota – Twin Cites campus for K13-8A and K12-19B.

For K12-15A, about 5 mg of dry sediment was used per sample. For the gravity cores, sample masses were optimized from % OC data to yield 0.9 mg C and ranged from 3.3 mg to 21 mg. The dry samples were first treated to remove inorganic carbon by acid fumigation for 6 to 8 hours with 12N HCl in silver (Ag) capsules. After fumes dissipated overnight and the samples oven dried 4 hours at 60°C, the Ag capsules were enclosed in tin (Sn) capsules for analysis on the EA-IRMS. At both labs, analyses were performed on a Costech 4010 ECS coupled to a Thermo-Finnigan Delta+XP IRMS and values reported in conventional delta (δ, ‰) notation relative to the Vienna PeeDee Belemnite (VPDB) standard for carbon and to ambient air (N_2) for nitrogen.

3 RESULTS

3.1 LITHOLOGY

3.1.1 CORE K12-19B

Gravity core 19B (352 m water depth) has a total sediment depth of 65 cm and involves three distinct lithologies (Figure 3.1). The older section of this core, from 65 cm to 36 cm, reveals alternating intervals of homogenized, dark greenish brown diatomaceous silty clay with indistinct laminations (≤ 1 mm) and two intervals of laminated, light brownish orange to brown sapropels that have a unique gel-like texture (here after referred to as "brown layers"). These cohesive beds (typically 1 to 5 cm thick) are very distinct and occur almost ubiquitously throughout the upper 2.5 meters of Kivu sediment cores. In gravity core 19B, two such brown layers occur at 58 cm and 39 cm depth, and both contain up to 30% TOC. The shallowest brown-layer is overlain by laminated, dark greenish brown diatomaceous silty clay from 36 cm to 22.5 cm. This unit is very similar to the underlying diatomaceous silty clay except that it has clear and distinct laminations (~1 mm thick). Both of these diatomaceous layers have low inorganic carbon (1%) and about 15% TOC. Between 22 and 20 cm there is a gradual transition to a laminated, greyish brown and white calcareous silty clay unit, the third major unit of this core. The calcareous unit is the upper unit of this core and has 3% to 4% TIC and 10% TOC, except in the top 0 to 4 cm where TIC drops and TOC rises slightly. Pennate diatom morphologies dominate the entire length of this core with an increased occurrence of centric diatoms below 38 cm. No ash layers were observed.

3.1.2 CORE K13-8A

Gravity core 8A (96 m water depth) was one of the best gravity cores recovered with seemingly intact stratigraphy and a total sediment depth of 74 cm (Figure 3.2). The oldest sediments, from 74 to 53 cm, consist of homogenized, dark greenish brown diatomaceous silty clays with 1% TIC and 20% TOC. There is a gradual transition around 53 cm into a laminated, light brown and greenish grey, calcareous silty clay unit with a distinct contact at 48 cm. This is overlain by a distinct brown-layer from 48 cm to 43 cm. There is a sharp transition at 43 cm to the laminated, calcareous silty clay unit again which continues up to 20 cm depth. This calcareous unit contains 6 – 7% TIC and 8%TOC, which is similar to the other carbonate-rich intervals, but also has interesting carbonate crusts (9.3% TIC) that make up the individual laminations from 27 cm depth right up to the distinct contact at 20 cm with the overlying organic-rich sediments. The

crusts appear broken, or shattered perhaps due to the coring process, but whole pieces up to 1.5 cm in diameter (~1 mm thick) can be extracted with forceps. These are further described in section 3.3, entitled "Carbonate Mineralogy". There is a brief interval of organic-rich, homogenous dark brown sediments with up to 26% TOC from 20 to 18 cm depth before returning to laminated, carbonate-rich sediments. This calcareous interval extends up to 11.5 cm depth but is interrupted between 14 – 13 cm depth by another brown-layer. This brief interval has distinct contacts with the carbonate intervals. Above this, there is a transition to homogenous, dark greenish brown diatomaceous silty clays from 11.5 cm to 5 cm. This organic-rich interval has almost no inorganic carbon (< 0.5% TIC) and ~17% TOC. The top 5 cm, the most recent and modern- day sediments, consist of the calcareous silty clays with 5 – 6%TOC and TIC. Pennate diatoms dominate from 0.5 cm to at least 51 cm depth. Centric diatoms occur below 14 cm depth, except in the region of the carbonate crusts at 21 cm. Below 60 cm centric diatoms become more common than the pennate forms. An ash layer was encountered near the base of this core at 65.5 cm depth, with a peak in magnetic susceptibility and no diatoms observed in smear slide.

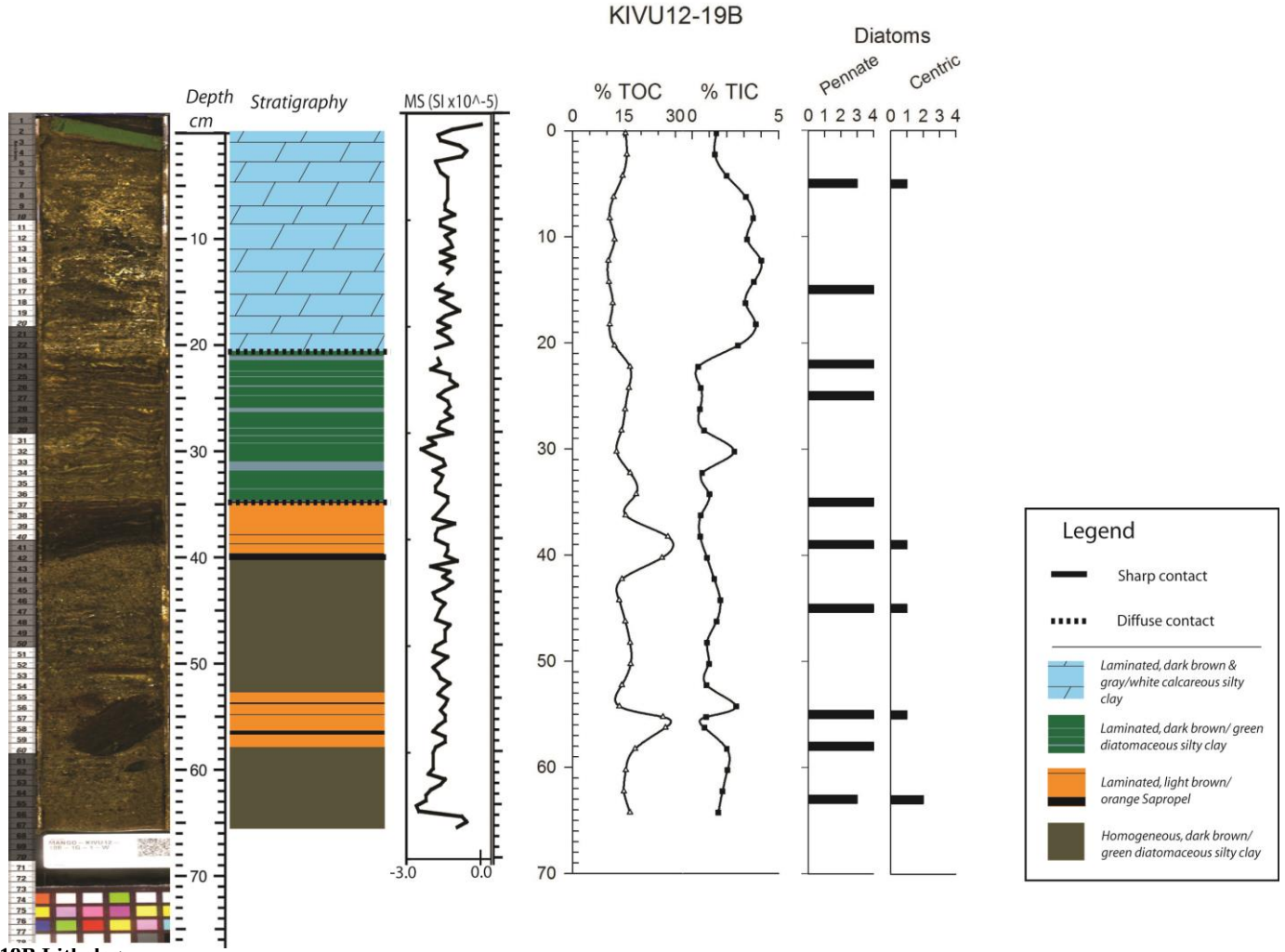

Figure 3.1 - K12-19B Lithology

Core image, stratigraphy, magnetic susceptibility (SI, $x10^{-5}$), total organic carbon (%), total inorganic carbon (%), and diatom abundances (qualitative) versus depth from sediment top. Diatoms: 0 – none/ trace, 1 – rare (5%), 2 – common (5-25%), 3 – abundant (25-50%), 4 – dominant (>50%).

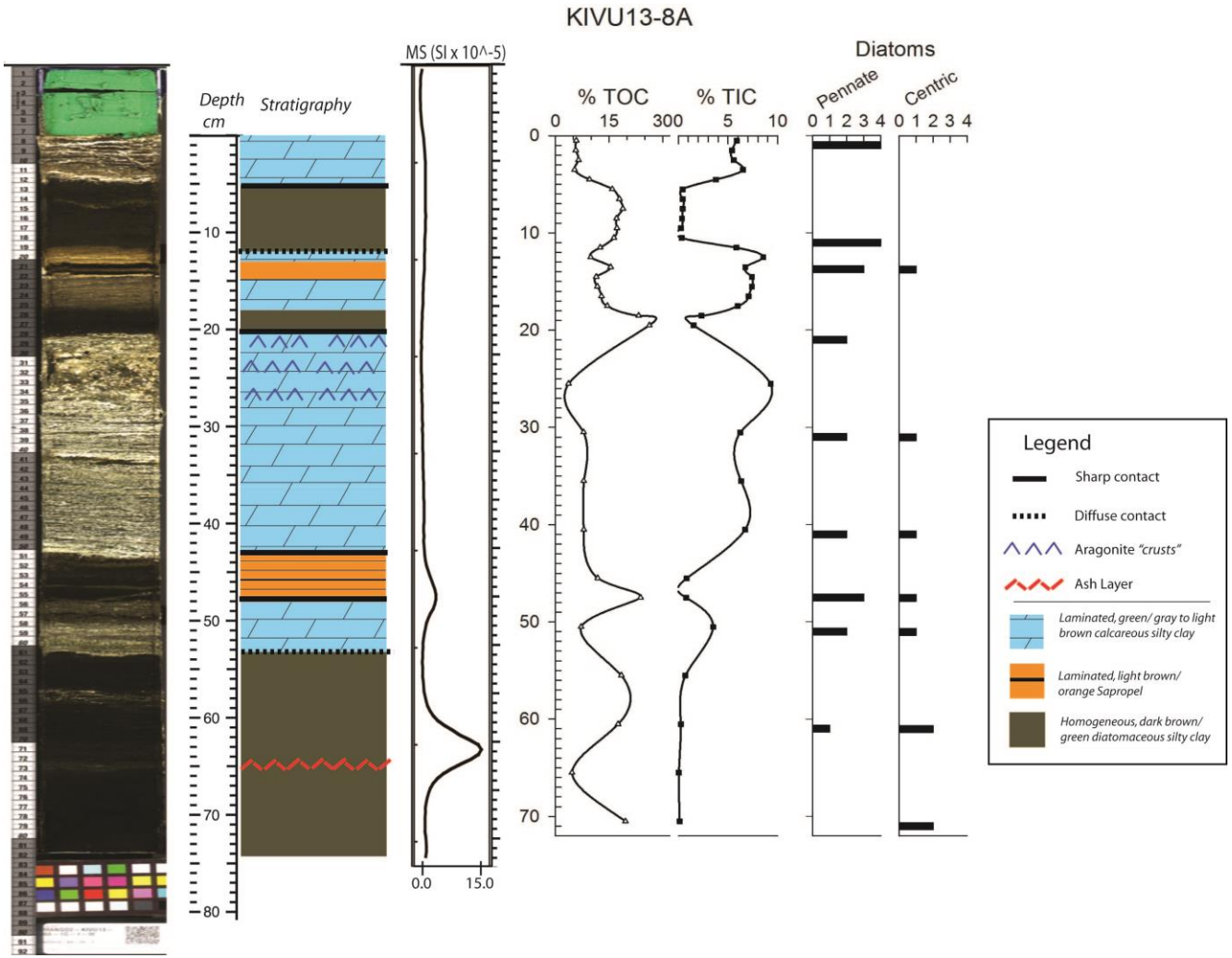

Figure 3.2 - K13-8A Lithology

Core image, stratigraphy, magnetic susceptibility (SI, x10^{-5}), total organic carbon (%), total inorganic carbon (%), and diatom abundances (qualitative) versus depth from sediment top. Diatoms: 0 – none/ trace, 1 – rare (5%), 2 – common (5-25%), 3 – abundant (25-50%), 4 – dominant (>50%).

3.1.3 CORE K12-19A

Piston core 19A (352 m water depth) contains over 8 meters of sediment (839.5 cm) that spans most of the Holocene (see following Chronology section). Besides a few intervals of turbidites and the upper-most section (0 to 122 cm) being disturbed, likely due to gas expansion and escape during recovery (see Methods chapter), this core contains remarkable stratigraphy (Figure 3.3). The very base of this core (from 839.5 to ~832 cm depth) consists of coarse sands and a whole quartz cobble just small enough to fit inside the core tube liner (~4 cm in diameter). This coarse unit is overlain by a compact, fine-grained clay interval from 832 to 825 cm depth. Above this clay there is a distinct contact and change in lithology to finely laminated (≤ 5 mm) dark brownish green to light olive, diatomaceous silty clay containing about 9% TOC and virtually no TIC (< 0.1%). These conditions persist for nearly 5 meters up the core to a sediment depth of ~340 cm. This long interval of laminated, organic-rich sediment is interrupted by at least three major (≥10 cm) turbidity flows centered at 680, 575, and 545 cm depth. In this lower interval, macrofossils are relatively common and numerous ash layers appear throughout (Figure 3.1.3). The TOC record averages around 10.2% but reaches as high as 19.4% (720 cm) and as low as 2.5% (581 cm) while the TIC record remains insignificant. The rise to 1.2%TIC around 580 cm occurs in a turbidite interval and should not be considered to reflect local conditions. Significant changes in lithology do occur however, immediately above at 340 cm depth. There is a sharp rise in TIC to > 3% by 3 meters depth, peaking at 4.9% at 280 cm. This new interval consists of laminated, gray to light olive calcareous silty clays with diffuse lower and upper contacts. A small (5 cm) turbidite at 305 cm is capped by a massive diatomite (>1 cm thick) and this sequence occurs again at the upper contact of this carbonate-rich interval, 240 cm depth. Immediately above this diatomite, at 235 cm depth, TIC drops to near zero and TOC rises above 15% into a laminated, light brown to orange sapropel layer. A distinct brown-layer occurs at 220 cm, above which there is a gradual transition to darker brown laminated, organic-rich sediments with a sharp upper contact at 200 cm depth. From 200 cm to 158 cm TIC rises to near 4% with a peak of 5.5% at 188 cm in this upper interval of laminated gray to green calcareous silty clay. This carbonate period is interrupted by an ash layer at 193 cm and has a sharp upper contact into another brown-layer. At 154 cm TIC drops to < 0.5% and TOC rises to 31.9%, but by 150 cm TOC returns to near 15% and there is another gradual transition in the sediments to dark greenish brown laminated diatomaceous silty clay.

The lower, organic-rich portion of 19A (340cm to bottom) has a centric diatom dominance, largely consisting of the taxa *Stephanodiscus*, especially throughout the interval from 715 cm to

615 cm where these are the only diatom morphology encountered. Throughout the lower carbonate interval, and through the turbidite, centric and pennate forms seem to occur equally. Above ~235 cm, through the alternating brown layers/ organic-rich and carbonate-rich intervals, pennate diatoms occur in higher abundance than centric forms. *Chaetoceros* were observed mostly in the organic layer between the two carbonate intervals (223 cm to 200 cm depth), but also into the upper carbonate interval (198 to 178 cm depth), as illustrated in Figure 3.3. Even though *Chaetoceros* was identified for a brief interval in this record, in smear slide not more than a dozen or so individuals were encountered, occurring in much less abundance than either the pennate *Nitschia* or the centric *Stephanodiscus*.

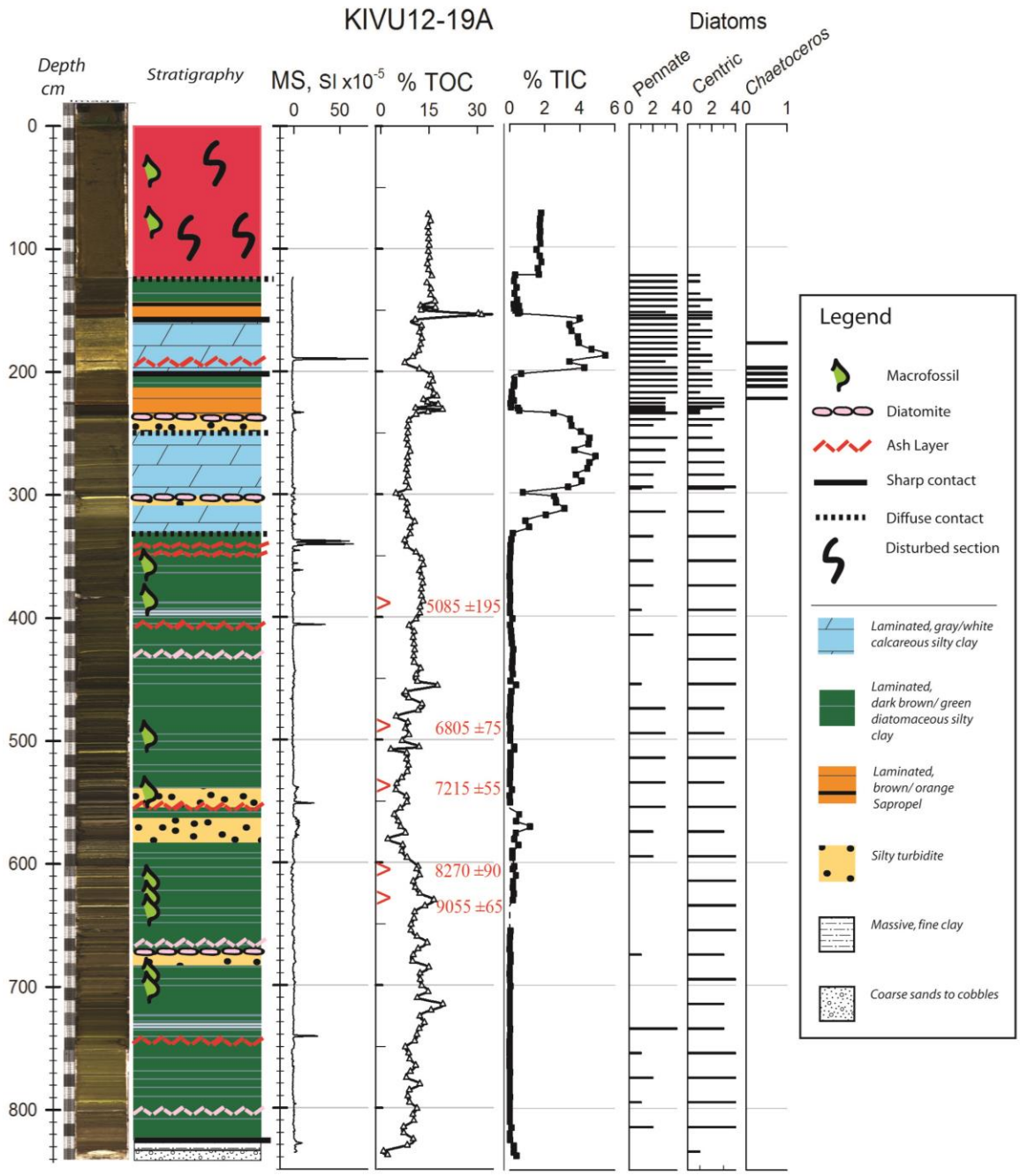

Figure 3.3 - K12-19A Lithology

Core image, stratigraphy, magnetic susceptibility (SI, x10^{-5}), total organic carbon (%), total inorganic carbon (%), and diatom abundances (qualitative) versus depth from sediment top. Diatoms: 0 – none/ trace, 1 – rare (5%), 2 – common (5-25%), 3 – abundant (25-50%), 4 – dominant (>50%); *Chaetoceros*: present (1)/ absent (0). Red ">" symbols in %TOC plot are AMS dated macrofossils in cal yr BP with 1SD.

3.1.4 CORE K12-15A

The top section of piston core 15A (455 m water depth) shows signs of better recovery than 19A, with only the top 30 - 40 cm disturbed and homogenized by gas escape, however this long core (691 cm) contains numerous turbidites thicker than 15 cm throughout the record (Figure 3.4). This core did not hit a coarse layer such as we observe at the base of 19A. The lower-most unit of 15A consists of laminated, dark greenish brown diatomaceous silty clays from 691 cm to ~500 cm depth with TOC averaging 7.9% and TIC <0.15%. A silty turbidite interrupts the record from 685 cm to ~670 cm. There are numerous ash layers in this unit and three diatomite layers (~1 cm thick) occur around 658, 610, and 525 cm depth. Around 500 cm depth there is a gradual transition into lighter, greenish grey laminated calcareous silty clays. These calcareous conditions (~3.4% TIC) exist up to 246 cm depth but the interval is heavily diluted by massive turbidites >20 cm thick. Each of these major turbidites is capped by a diatomite 1 – 2 cm thick. In every instance throughout this interval, the base of the turbidite is a gradual transition from the laminated, calcareous clays, while the upper contact is distinct, with a diatomite layer. An ash layer occurs near the base of this interval at 495 cm depth and two more occur right above the first turbidite/ diatomite sequence at 430 and 428 cm depth. A macrofossil was recovered at the base of a turbidite, 410 cm depth, but was not dated. This calcareous interval ends with a gradual transition into the turbidite, around 280 cm, which is capped at 246 cm by a diatomite. A fine ash layer occurs above this at 245 cm depth in the overlying organic-rich sediments. The upper section of this core, from 245 cm to 40 cm, is an alternating sequence between laminated organic-rich and calcareous silty clays. The first brown-layer occurs right above the fine ash layer at 245 cm depth up to 241 cm and is overlain by laminated dark brownish green diatomaceous silty clays from 241 cm to 205 cm when there is a gradual transition back to calcareous clays. This organic interval is marked by an average increase in TOC from 11% to 15.7% and a decrease in TIC from 3.6% to 0.5%. A turbidite/ diatomite cap sequence interrupts this unit from 230 cm to 215 cm depth. TOC % becomes variable from 10% to 38% in the sediments <250 cm depth whereas it was very constant (~11%) throughout the underlying calcareous unit. At 205 cm there is a gradual transition back to laminated greenish gray calcareous silty clays. This carbonate-rich (3% TIC) interval terminates abruptly at 160 cm depth into a light brown and orange sapropel. Two ash layers were observed at 198 cm and 187 cm depth. Organic-rich (0.35% TIC, 18% TOC) sediments prevail from 160 cm to 50 cm depth with a turbidite/ diatomite cap interruption from ~120 cm to 195 cm depth. Sapropelic brown layers occur at 155, 130, 95, and 70 cm depth and are marked by sharp rises in TOC to near 30%. The first brown-layer, at 155 cm, is only ~3cm

thick and was missed in the systematic sampling regime of every 5 cm, which explains the lack of a sharp increase to near 30% TOC. At 50 cm depth there is a gradual transition from laminated dark greenish brown organic sediments back to laminated, olive- grey calcareous silty clays. This laminated carbonate interval extends for only 10 cm before turning into disturbed, broken stratigraphy, in the top section.

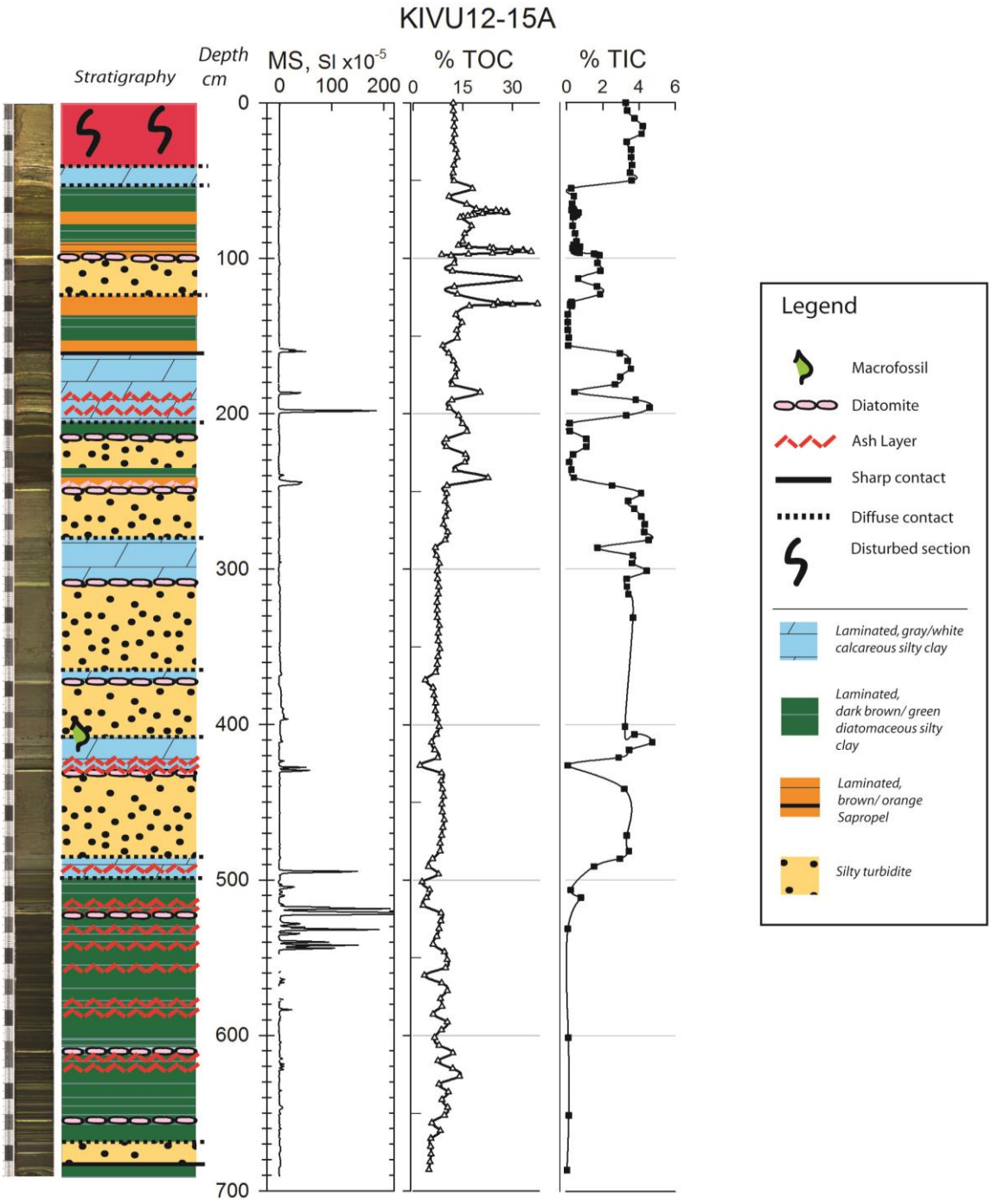

Figure 3.4 - K12-15A Lithology

Core image, stratigraphy, magnetic susceptibility (SI, x10^{-5}), total organic carbon (%), and total inorganic carbon (%) versus depth from sediment top.

3.2 CHRONOLOGY

3.2.1 RADIOCARBON CHRONOLOGY

Good chrono-stratigraphic control was achieved over the lower half of piston core K12-19A, from 5,000 to 9,000 cal yr BP (Figure 3.5, Table 3.1). Of the 12 macrofossils analyzed for radiocarbon, I used 6 (5 from K12-19A, 1 from K12-18B; Table 3.1) which yield a significant linear regression after calibration (R^2= 0.99). Other dated macrofossils yielded poor results or anomalously young ages (gray triangles in Figure 3.5; Table 3.1).

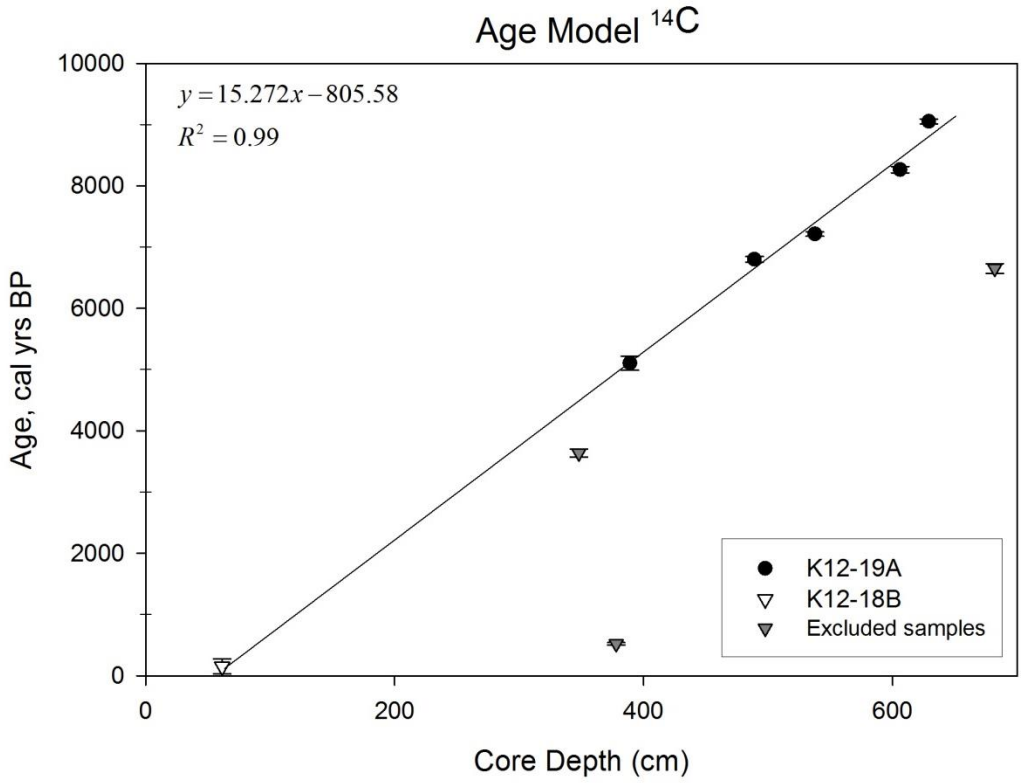

Figure 3.5 – Radiocarbon Age Model
AMS radiocarbon dating of terrestrial macrofossils; shown here as calibrated years before present (cal yr BP) versus depth in core. This yields an average linear sedimentation rate of 65.5 cm kyr^{-1}. Less compaction and degassing disturbance in the top-most sections of the cores most likely causes the regression to not cross the origin. Macrofossils from 19A: black circles; from 18B: open triangle. Gray-filled triangles are the dates excluded from this regression.

For the shallowest age a macrofossil from the nearby coring location site K12-18A/B was used. Core K12-18B is believed not to have over-penetrated and this macrofossil (twig) came from the base of a cohesive brown layer unit with stratigraphic integrity maintained. Based on this age model the base of lacustrine sediments in 19A was deposited about 11,700 cal yr BP.

Table 3.1: Material analyzed for Accelerator Mass Spectrometry ^{14}C ages.
See map (Figure 1.3) for core locations.

***-** excluded from regression in Figure 3.2.1; **§-** data not shown; **NA**- not available; **n.d**.- not determined

BETA	Core-Sect.	Depth (sect.) cmblf	Material	δ^{13}C ‰	AMS Age (^{14}C yr BP)	Age (cal yr BP)
347837	Kivu-00	modern	terrestrial	-30.4	103.7 ± 0.3 %MC	n.d. **§**
347843	18B-1G-1	(61.5) 61.5	macroplant	-24.9	180 ± 122	190 ± 110
347839	11A-1K-4	(40) 378	macroplant	-25.6	490 ± 30	520 ± 20 *****
347840	11A-1K-6	(5) 499	wood	NA	1290 ± 30	n.d. **§**
347841	11A-1K-7	(49) 664.5	macroplant	NA	1110 ± 30	n.d. **§**
347844	19A-1K-4	(55) 348	macroplant	-27.1	3390 ± 30	3635 ± 65*****
347845	19A-1K-5	(12.5) 389	macroplant	-26.1	4440 ± 30	5104 ± 117
347846	19A-1K-6	(45.5) 489	macroplant	-27.8	5960 ± 30	6800 ± 44
347847	19A-1K-6	(94) 537.5	macroplant	-31.6	6270 ± 40	7212 ± 36
347848	19A-1K-7	(18) 606	macroplant	-27.1	7430 ± 40	8265 ± 52
347849	19A-1K-7	(35) 629	macroplant	-25.7	8100 ± 40	9051 ± 40
347850	19A-1K-7	(89.5) 681	macroplant	NA	5840 ± 30	6650 ± 80 *****

Based on the ash layers, stratigraphic markers, and seismic profiles, cores 19A and 15A were correlated following Zhang *et al.* (submitted) as illustrated below in Figure 3.6. After correlation, the extent to which the turbidites have diluted the 15A record becomes apparent. Using the deposition rate between horizons B and B1, the base of 15A is estimated to have been deposited around 7,160 cal yr BP.

Table 3.2 : Dating of Stratigraphic Horizons in K12-15A
See Figure 3.6 for reference to horizons and correlation between 19A and 15A.

Horizon	Depth in 19A, cm	Age, cal yr BP	Depth in 15A, cm
A	190	2097	199
A1	232	2739	245
A2	296	3716	429
B	340	4389	520
B1	407	5412	583

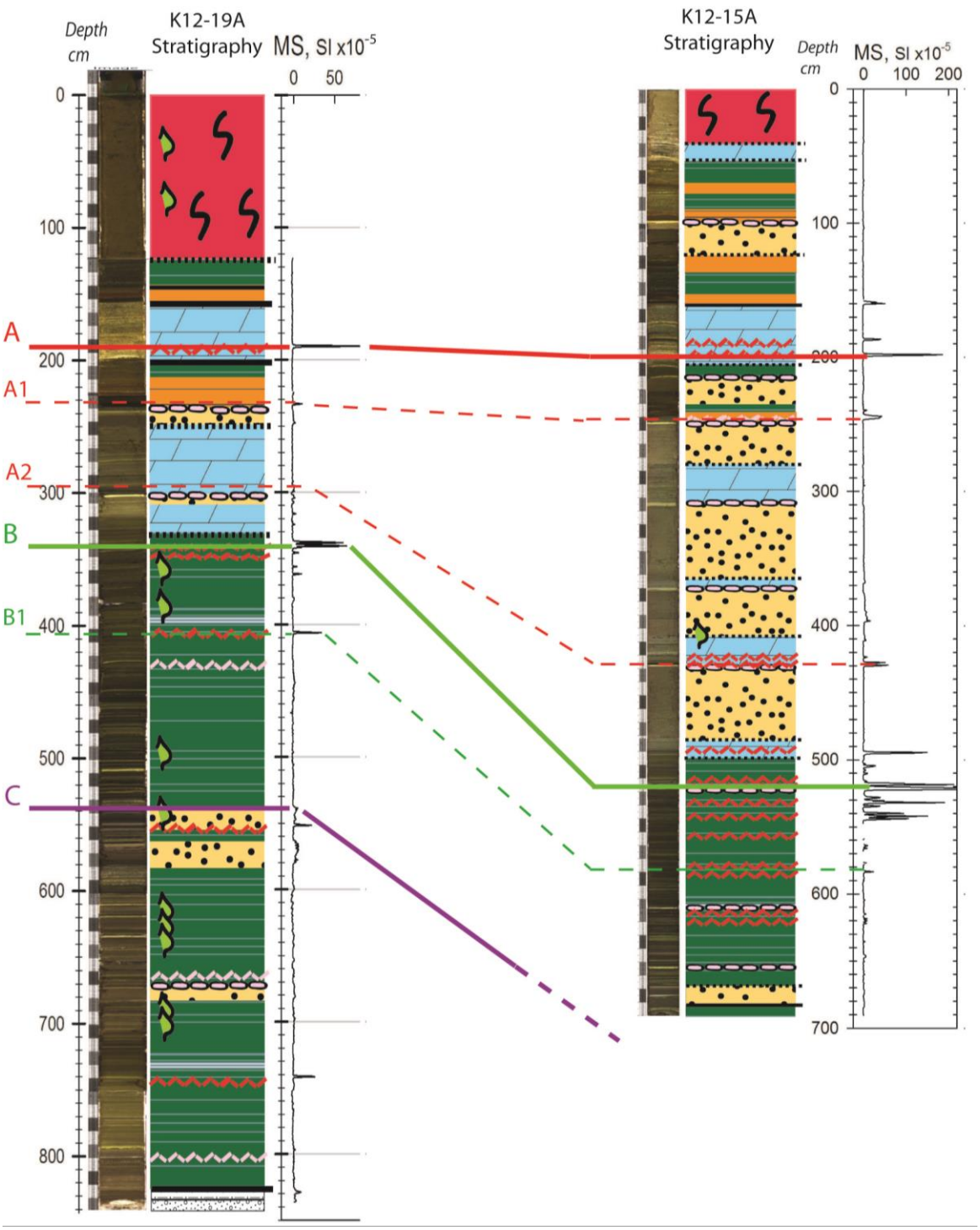

Figure 3.6 – Age model stratigraphic correlation between 19A and 15A

Correlations between K12-19A and K12-15A based on seismic horizons (solid lines: A, B, and C) by C. Scholz and workers on Lake Kivu 2010 – 2012, ash layers, and other distinct stratigraphic markers (dashed lines). The base of 15A is younger than 7,200 cal yr BP.

3.2.2 ^{210}PB CHRONOLOGY

Lead-210 analysis of our gravity core K13-8A reveals variable sedimentation rates over the past 125 years. Here we applied the constant rate of supply (CRS) model instead of the rapid steady state mixing (RSSM) model as this core was recovered from below the uppermost chemocline, in anoxic waters with little bioturbation. The top-most sediments (< 5 cm) have clear, intact laminations of carbonate mud and a distinct contact with the underlying homogeneous, organic-rich layer. This stark contrast in lithology likely accounts for the change in slope (change in sedimentation rate) around 5cm depth rather than zoo-benthos reworking, which is what the RSSM model takes into account.

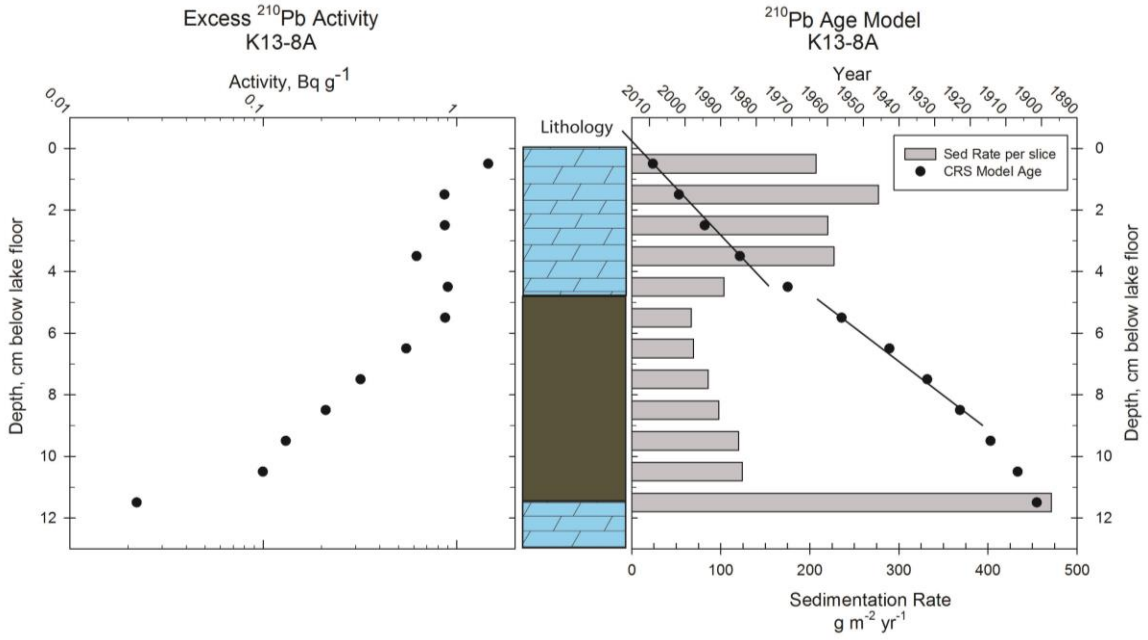

Figure 3.7 – ^{210}Pb Age Model
Lead-210 dating of bulk sediment from the top 0 -12 cm portion of core K13-8A; Left: excess ^{210}Pb activity; Center: lithology from Figure 3.2; Right: constant rate of supply (CRS) modeled year (dots) and estimated sedimentation rate (horizontal bars) versus depth in core. These samples yield an average linear sedimentation rate of 93 cm /ky and an average (0- 12cm) CRS sediment flux of 173 g/m^2 /y. Lines represent the two separate regressions used for applying the age model as discussed in text.

The top 0-5 cm depth CRS average sedimentation rate is 207 g/m^2/y. The next 5-11 cm depth CRS average sedimentation rate is 94 g/m^2/y. This increase in sedimentation rate and change to carbonate-rich material in very recent sediments is consistent with Pasche *et al.* (2010), who saw distinct changes at ~8.5 cm depth in their Kibuye core (190 m water depth) with a switch from underlying organic-rich into carbonate-rich sediments (Figure 1.2 for core location). Pasche *et al.* (2010) report a core average sedimentation rate of 287 g/m^2/y, a carbonate layer sedimentation rate of 263 g/m^2/y, and organic layer sedimentation rate of 89 g/m^2/y.

As the ^{210}Pb isotope has a short half-life of just 22.3 years, using it to date sediments beyond 110 -120 years is not feasible (Gale, 2009) and as such, ^{210}Pb ages of sediments deposited before 1900 in core 8A are not reliable. Nevertheless, using the distinct sedimentation rates for the two major lithology units derived from the upper 10 cm, we applied linear sedimentation rates (i.e. years per cm depth) in a piecewise manner down the entire length of the core based on lithology. The slope of the first four ^{210}Pb samples (0.5 – 3.5 cm) were used to define the carbonate-rich linear sedimentation rate of ~8 years/ cm (R^2= 0.9939), while the slope of the samples from 5.5 to 8.5 cm depth were used to define the organic-rich linear sedimentation rate of ~11 years/ cm (R^2=0.9924). Application of this model for core 8A from 1 to 74 cm depth suggests the base of this core was deposited circa 1315 AD (Table 3.3).

Table 3.3 – ^{210}Pb Age Model for K13-8A
Two linear sed rates applied based on lithology; carbonate: 8.0627 yrs/cm; organic: 11.023 yrs/cm.

Depth, cm	Year
1	2005
10	1918
20	1819
30	1739
40	1658
50	1571
60	1469
70	1359
74	1315

We are confident that both gravity cores 8A and 19B capture the present-day sediment top due to their high porosity ($\varphi = 0.93$ and 0.96, respectively) with the differences in lithology due to their locations. Carbonate precipitation and sedimentation likely exceeds any dissolution in the shallow-water, near-shore location of 8A than in the deeper, off-shore location of 19B. The lack of an ash layer in 19B that is present in 8A however, forces the assumption that 19B encompasses a record above this event. See Appendix 1: Sediment Core Data Tables for porosity and water content estimates of all four cores.

3.3 CARBONATE MINERALOGY

X-ray diffraction (XRD) analyses of several intervals of cores K12-19A/B and K13-8A showed aragonite to be the only significant carbonate mineral present (Figure 3.8). Although not sampled for XRD analysis, some of the cohesive "brown layers" displayed distinct siderite ($FeCO_3$) crystals identified under polarizing-light microscopy (Figure 3.9). See Appendix 3: X-Ray Diffraction Mineralogy for more information.

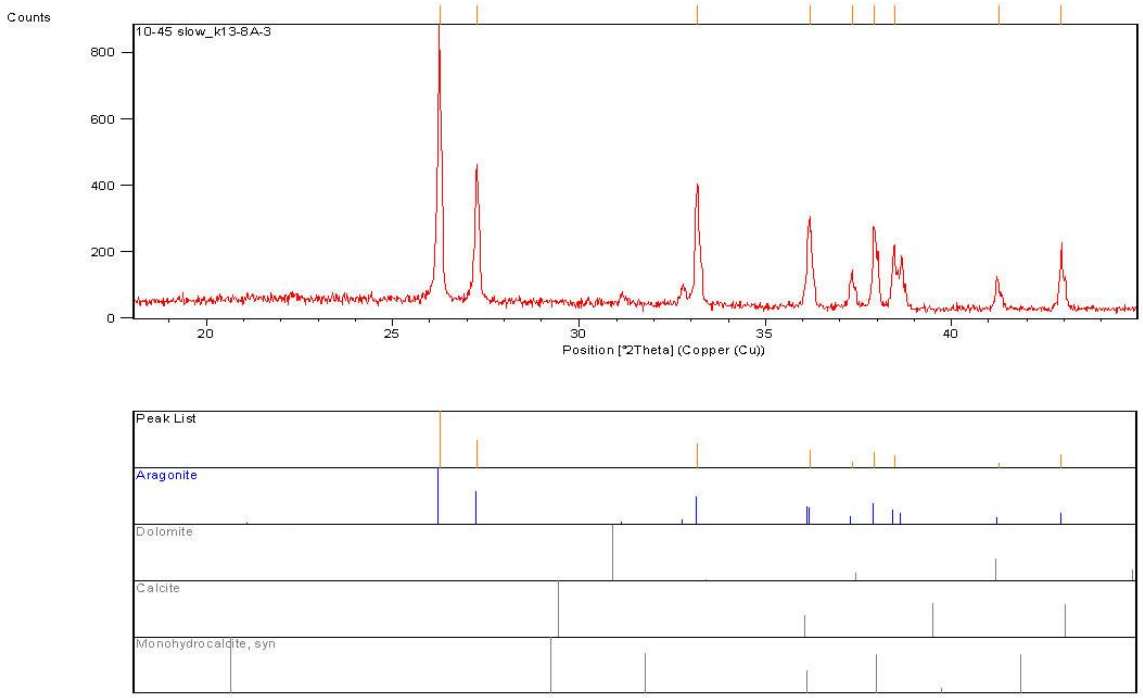

Figure 3.8 – Aragonite XRD scan from K13-8A
Top panel: sample XRD scan result from 23 cm depth identifying the "crusts" as aragonite. Note 2θ position for dominant peaks of calcite, dolomite, and mono-hydrocalcite (lower panel), all clearly absent from this carbonate sample.

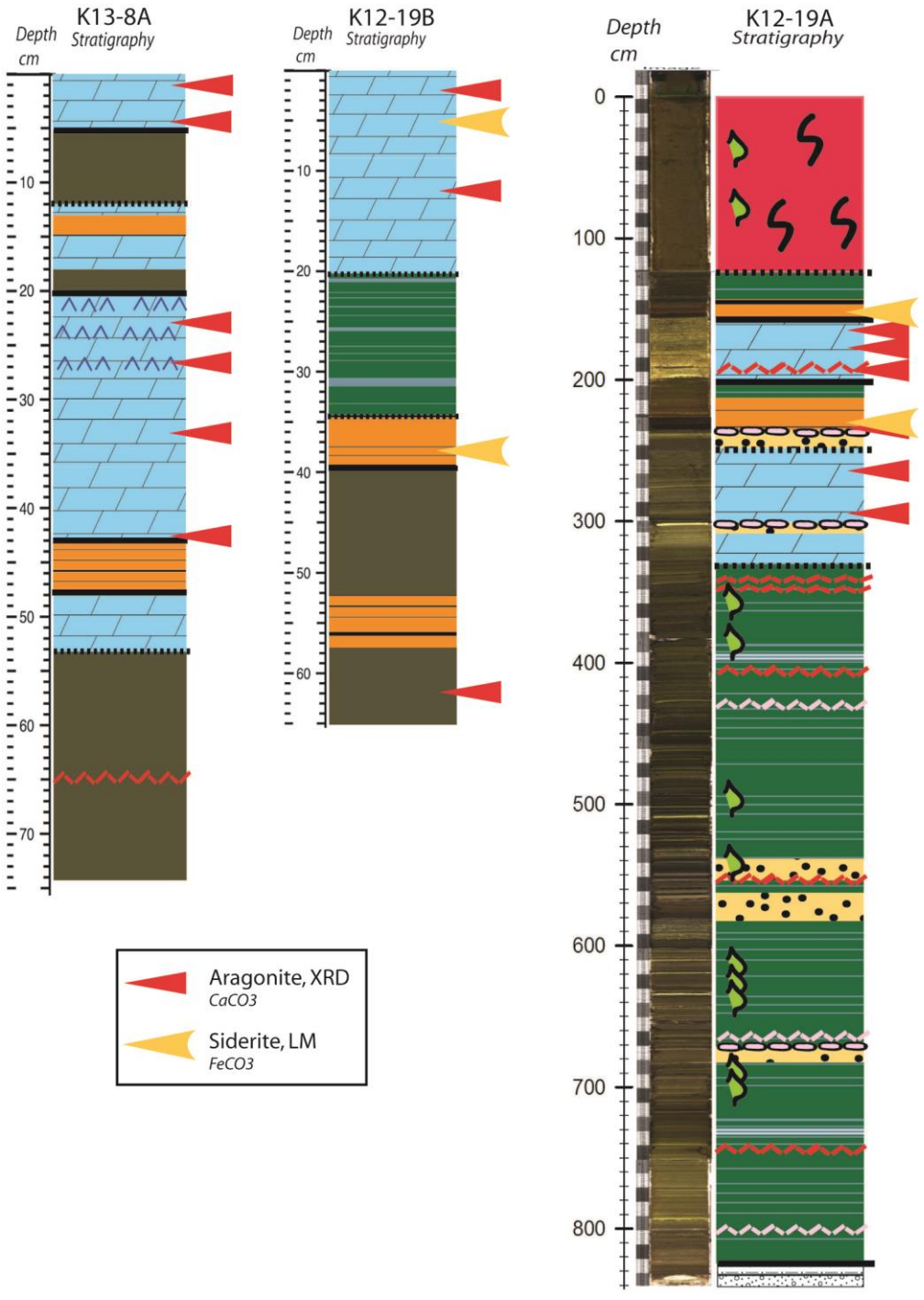

Figure 3.9 – Carbonate Mineralogy
Represntation of which units XRD samples were taken from for each core. Red arrow: dominant peak aragonite; yellow arrow: siderite crystals identified in smear slide under polarizing light microscope(LM).

3.4 CARBONATE ISOTOPES

3.4.1 CARBONATE ISOTOPES OF K12-19B

Most striking about the carbon and oxygen carbonate isotopes from K12-19B is their apparent covariance down-core (Figure 3.10). These values, which range from 3.56‰ to 6.52‰ ^{13}C and 0.48‰ to 2.86‰ ^{18}O, are in the range expected based on previous work in the eastern and northern basins by Botz *et al.* (1988) who report 4.3‰ – 5.8‰ ^{13}C and 0.7‰ – 4.3‰ ^{18}O. No major trends down-core can be discerned; however, there is one major excursion to lower values (3.56‰ ^{13}C, 0.48‰ ^{18}O) at 30.5 cm depth which is the only sample analyzed from within the laminated, diatomaceous silty clay unit. A rise in %TIC at this horizon suggests that a subtle, carbonate-rich lamination was indeed sampled however.

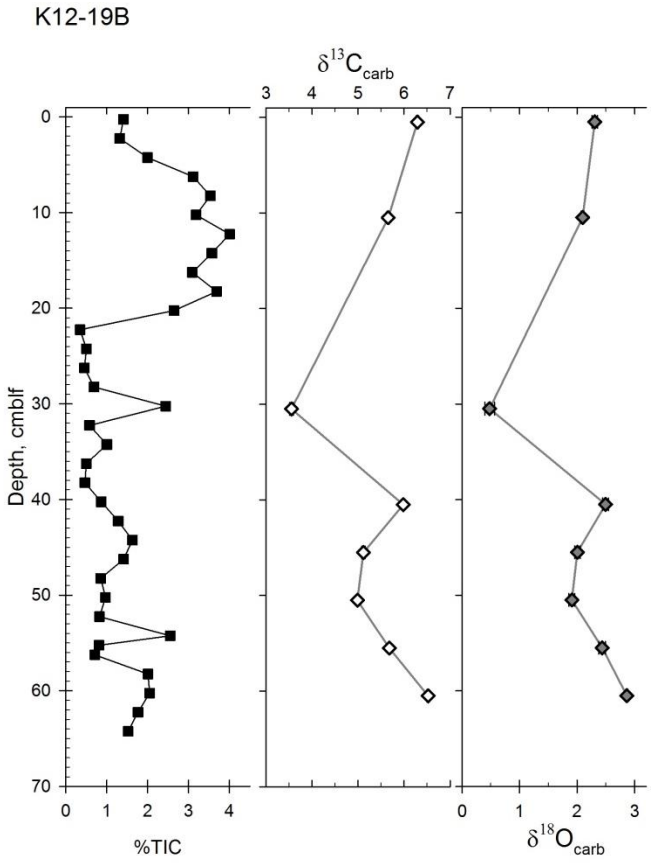

Figure 3.10 – Carbonate Isotopes core K12-19B

Percent TIC and δ-values for ^{13}C and ^{18}O of the carbonate fraction versus depth. Isotope values reported in per mil deviation from VPDB with error bars of 1SD.

3.4.2 CARBONATE ISOTOPES OF K13-8A

As with 19B, the carbon and oxygen isotopes tend to co-vary down-core (Figure 3.11). In K13-8A, ^{13}C ranges from 5.13‰ to 8.62‰ and ^{18}O from 1.56‰ to 3.79‰ (Figure 3.11). These values are also in the range expected from previous work, with more enriched $\delta^{13}C$ values closer to the shoreline and from shallower water (Botz *et al.*, 1988). The oldest sediments sampled, deposited ca. 1500 AD, have values of 5.1‰ ^{13}C and 1.6‰ ^{18}O and became more enriched in both C and O after that until ~1650 AD where the values stabilize around 7.6‰ and 3.5‰, respectively. The highest $\delta^{13}C$ value (8.62‰) occurs at 1785 AD from the interval of aragonite "crusts". Carbon, and to a lesser extent oxygen, become slightly more depleted from around 1860 AD to the modern-day calcareous sediments of ~6.5‰ $\delta^{13}C$ and ~2.75‰ $\delta^{18}O$.

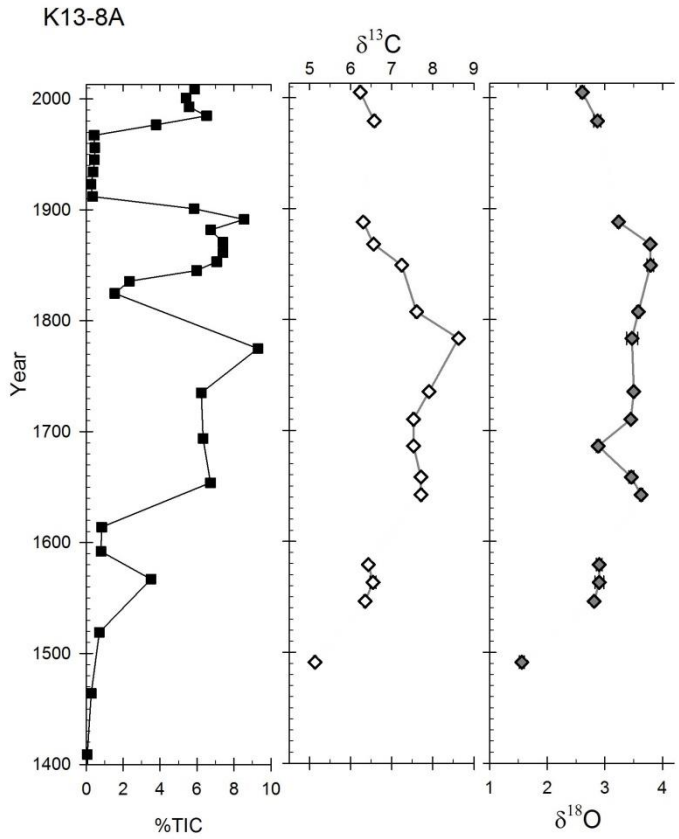

Figure 3.11 – Carbonate Isotopes core K13-8A
Percent TIC and δ-values for ^{13}C and ^{18}O of the carbonate fraction versus year of deposition (estimated from ^{210}Pb). Isotope values reported in per mil deviation from VPDB with error bars of 1SD.

3.4.3 Carbonate Isotopes of K12-19A

Though variable, the isotopes measured from the two carbonate intervals in piston core 19A show an enrichment trend from the onset of carbonate at 4,200 cal yr BP to cessation at 1,600 cal yr BP, rising from 5.3‰ to 7‰ $\delta^{13}C$ and from 1.5‰ to 3.45‰ $\delta^{18}O$ (Figure 3.12). Values are more variable for both carbon and oxygen in the older carbonate interval from 4,200 BP to 2,700 BP, while they appear more stable during the following carbonate interval from 2,200 BP to 1,600 BP. Again, as within the gravity cores, carbon and oxygen generally co-vary down-core.

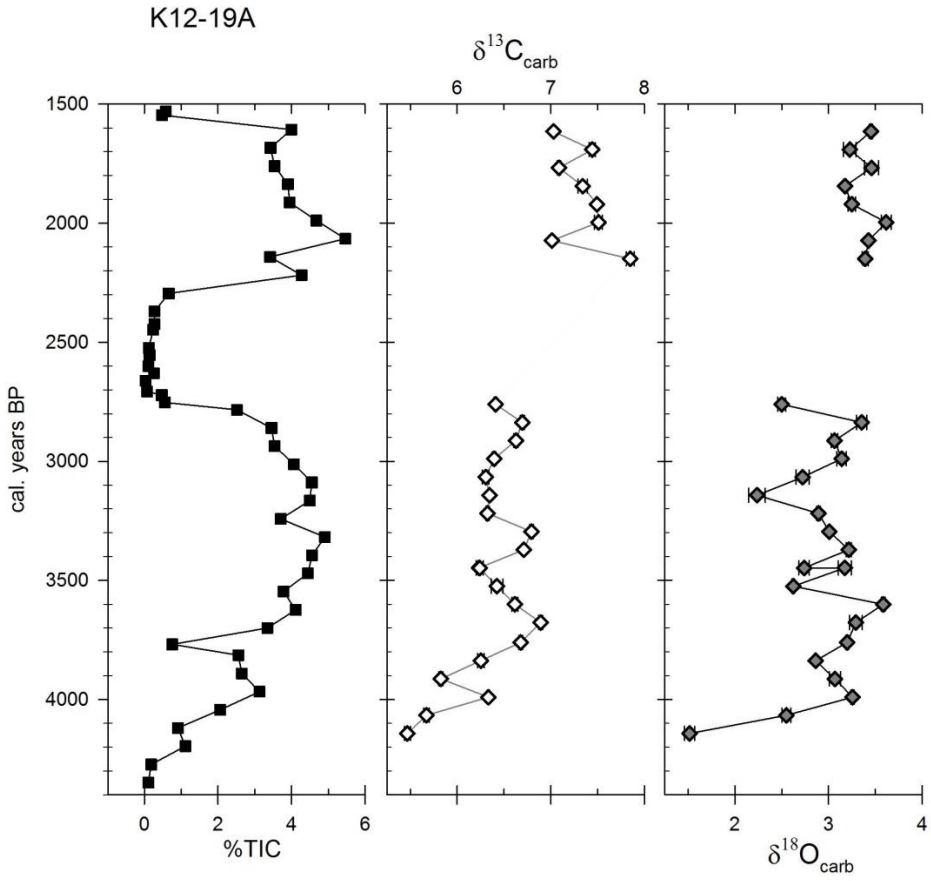

Figure 3.12 – Carbonate Isotopes core K12-19A
Percent TIC and δ-values for ^{13}C and ^{18}O of the carbonate fraction versus age, cal yr BP (estimated from ^{14}C). Isotope values reported in per mil deviation from VPDB with error bars of 1SD

3.5 BULK ORGANIC ISOTOPES

3.5.1 ORGANIC ISOTOPES OF K12-15A

$\delta^{13}C_{org}$ is remarkably consistent at about -26‰ from the base of the core (691 cm) up to ~300 cm. There is a dramatic enrichment from -25‰ to -16‰ in $\delta^{13}C_{org}$ above 300 cm depth, but this occurs after the onset of carbonate deposition at 4.2 kyr (horizon B), and well into that carbonate interval (Figure 3.13). This is followed by a highly variable period, but generally trending towards lighter values (less negative), until an enriched interval appears again in the upper-most 0.5 m of core, though this is the disturbed portion of K12-15A. The $\delta^{15}N_{org}$ profile displays more variability than $\delta^{13}C_{org}$ in the lower portion of this core, with values that range from 2 - 8‰, but that then stabilize around 4‰ between 420 cm and 340 cm depth. Overlying this interval, $\delta^{15}N_{org}$ values drop to around -2‰ at 300 cm depth, after which the values rise gradually back to near 4 or 5‰ by 200 cm depth.

All brown layer events in this core show dramatic isotopic changes with $\delta^{13}C_{org}$ depletion by about -5‰ and $\delta^{15}N_{org}$ enrichment by about 4‰, clearly standing out in the isotopic record of the last 2,700 years.

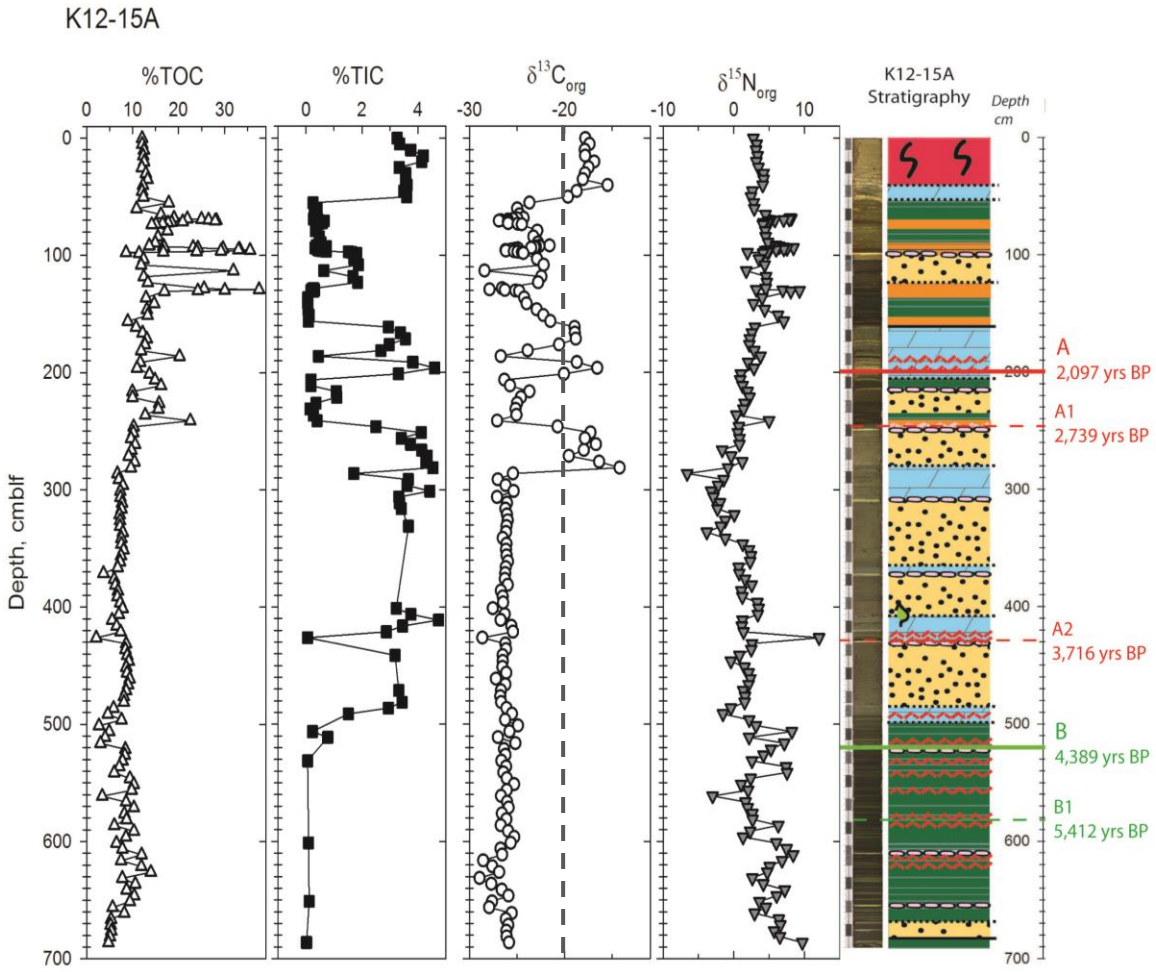

Figure 3.13 – Bulk Organic Isotopes core K12-15A

Percent TOC, TIC, and δ-values for ^{13}C and ^{15}N of bulk organic sediments versus depth in K12-15A.Carbon isotope values reported in per mil deviation from VPDB, nitrogen from atmospheric N_2.Stratigraphy of 15A with horizons correlated to 19A for reference. Dashed line in ^{13}C for reference to carbonate excursions in section 4.4.1.

3.5.2 Organic Isotopes of K12-19B

Both carbon and nitrogen show a very consistent signal in the undated core 19B with $\delta^{13}C_{org}$ ~ -25‰ and $\delta^{15}N_{org}$ ~ 3‰ down the whole core (Figure 3.14). There is a slight depletion trend of the $\delta^{15}N_{org}$ signal from ~4‰ at 64 cm depth to ~2‰ at the core top. The $\delta^{13}C_{org}$ of the brown layers show a slight depletion similar to that of the brown layers of core 15A but with a much subdued change of only -1 to -2‰ (compared to -5‰). Only the deeper brown-layer (55 cm depth) shows the $\delta^{15}N_{org}$ enrichment similar to the 15A brown layers, but, again, with only 2‰ change compared to the 4 or 5‰ shift in 15A.

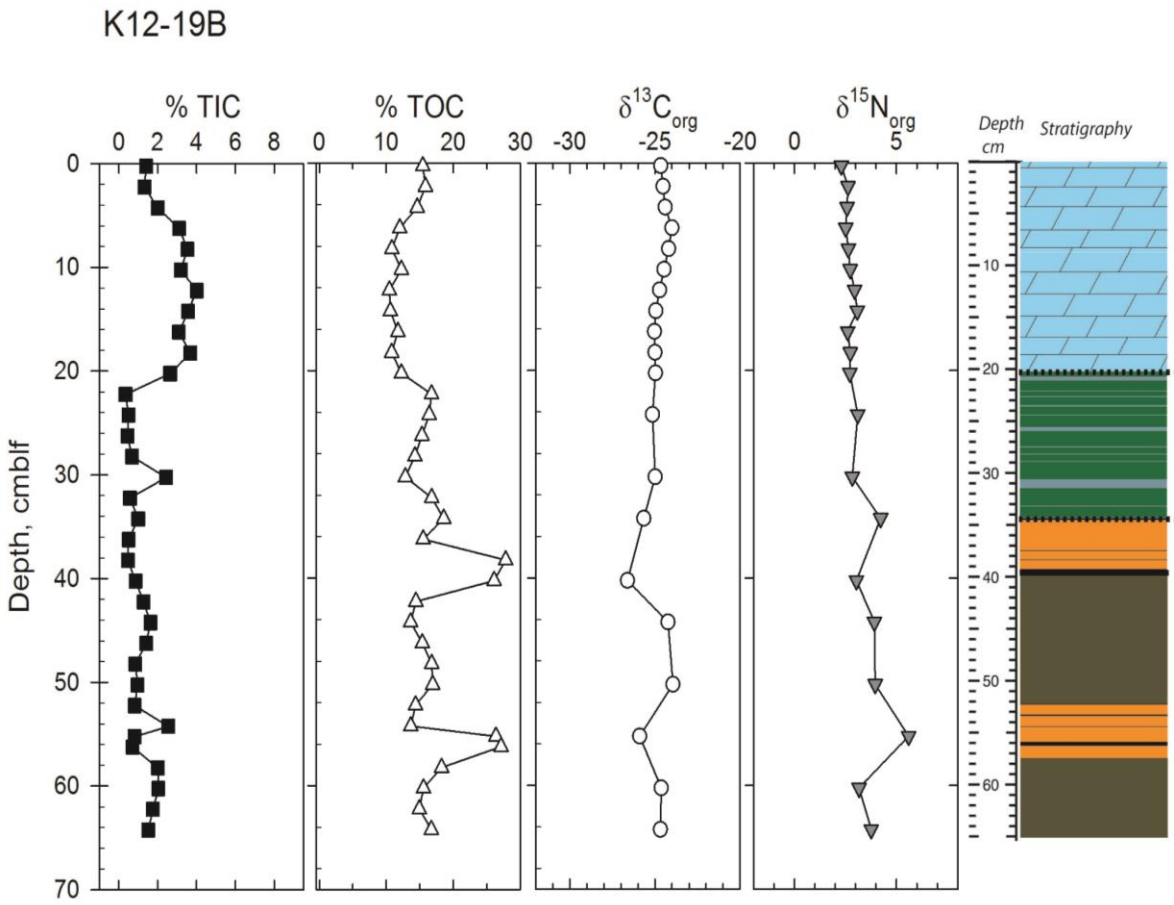

Figure 3.14 – Bulk organic isotopes core K12-19B
Percent TIC, TOC, and δ-values for ^{13}C and ^{15}N of bulk organic sediments versus depth in K12-19B.Carbon isotope values reported in per mil deviation from VPDB, nitrogen from atmospheric N_2. Stratigraphy of 19B at right for reference.

3.5.3 Organic Isotopes of K13-8A

Isotopic composition of carbon and nitrogen varies with age in core 8A, with $\delta^{13}C_{org}$ values between -31‰ and -23‰ and $\delta^{15}N_{org}$ values between -1‰ and 7‰ (Figure 3.15). The $\delta^{15}N_{org}$ signal averages around 3‰ with a few notable excursions: a depletion to -1‰ at 1590 AD (i.e. the brown layer at 47.5 cm depth) and an enrichment to 7‰ at 1890 AD (i.e. at 12.5 cm depth, above the upper brown layer). The $\delta^{13}C_{org}$ of the brown layers also show a similar depletion trend to that of other brown layers discussed above with a shift of -6‰ for the older brown-layer (47.5 cm depth) and -2‰ for the younger (13.5 cm depth). Although the younger brown layer (1880 AD) shows a $\delta^{15}N_{org}$ enrichment of 2‰, the older layer shows the opposite trend, with a -4‰ depletion.

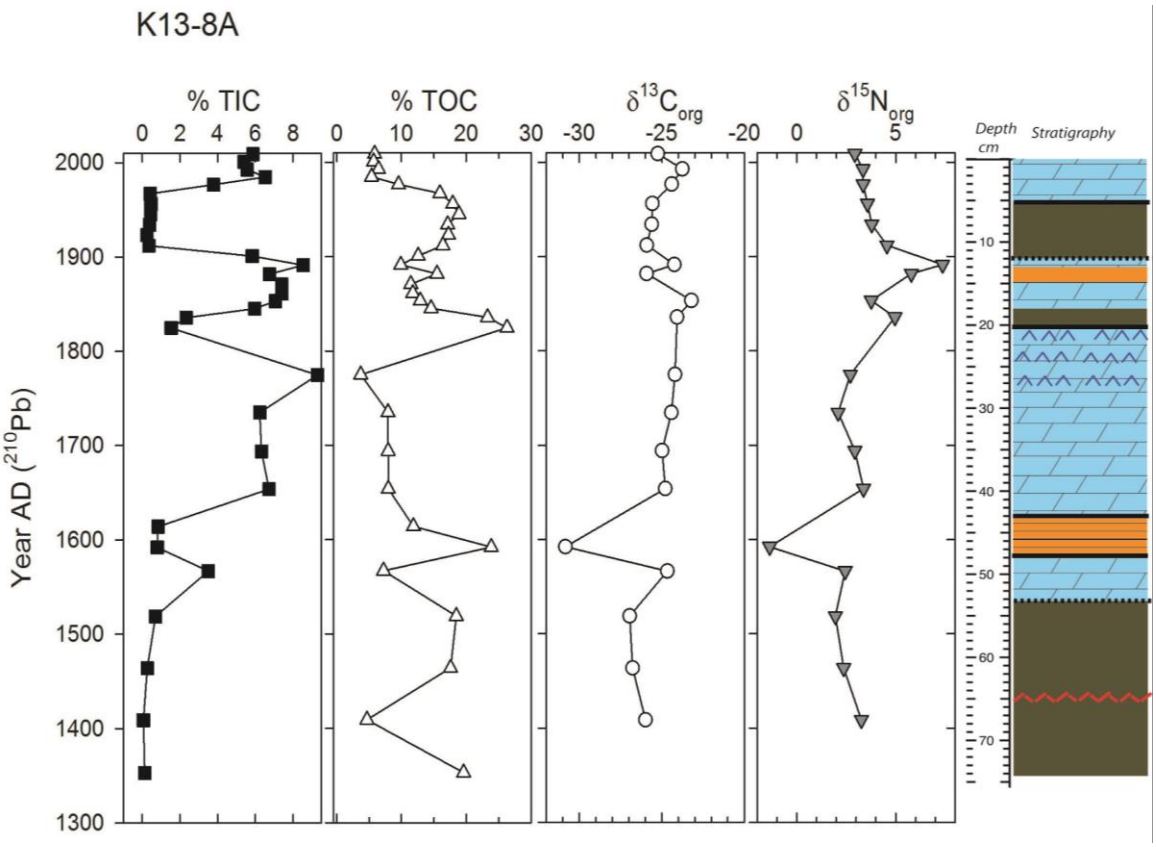

Figure 3.15 – Bulk organic isotopes core K13-8A
Percent TIC, TOC, and δ-values for ^{13}C and ^{15}N of bulk organic sediments versus calendar year (from ^{210}Pb age model) in K13-8A. Carbon isotope values reported in per mil deviation from VPDB, nitrogen from atmospheric N_2. Stratigraphy of 8A at right for reference.

4 DISCUSSION

4.1 THE HOLOCENE STRATIGRAPHIC RECORD OF LAKE KIVU

4.1.1 LAKE KIVU 11,700 YEARS BP TO ~1,000 YEARS BP

Nearly the entire Holocene history of Lake Kivu is encompassed in our two piston cores K12-19A and K12-15A, from ~11,790 cal yr BP in 19A, to <1,000 cal yr BP in 15A (Table 3.1 and Figure 3.6). The coarse sands and cobble at the base of 19A suggest that Lake Kivu was a much shallower lake with water levels at least 350 m lower than present day at this time, approximately at end of the Younger Dryas. Overlying this coarse deposit, the sediments are organic-rich (mean TOC ~10%) and laminated (i.e. not disturbed by biota), suggesting that lake level rose quickly and the shoreline became more distant from the coring site. The early Holocene in both cores 19A and 15A indicate a deep, productive lake with organic-rich, laminated sediments until around 4,230 cal yr BP (330 cm depth in 19A), at which time both cores reveal an onset of carbonate deposition (Figure 3.6). This second-half of the Holocene history, 4.2 ka to present, records significant limnological changes to Lake Kivu. The lithology alternates between carbonate-rich (TIC > 3%) and organic-rich intervals (TOC ≥ 15%). Carbonate precipitation and preservation in the lacustrine environment is not uncommon, but strongly suggests major limnological changes from previous conditions. Sapropelic (brown layer) intervals just a few centimeters thick, which reach or exceed 30% TOC, also occur after 4.2 ka, however, they are not present in the organic-rich sediments prior. Clearly, lake conditions dramatically changed at or slightly before 4,200 BP and the succeeding record alternates between carbonate and non-carbonate sediments, suggesting a dynamic lake environment. This post-4.2 ka period will be discussed in more detail in section 4.5.

The gross TIC/ TOC stratigraphy and lithologic observations from 19A (Figure 3.3) are similar to those described by Haberyan and Hecky (1987) for their core K-10, which contained two distinct carbonate-rich intervals. Each of these is overlain by sapropelic brown layers. Core K-10 displays a general trend of centric diatom to pennate diatom dominance up-core, including the presence of *Chaetoceros spp.* in their zone C (i.e. at the termination of the first carbonate interval; their Figures 5 and 7. See Appendix 4, Figure C).

From 11.8 ka until 8.2 ka (600 cm depth, 19A; Figure 3.3) the diatom taxon *Stephanodiscus* was dominant with variable occurrence of *Nitzschia* spp., which suggests fluctuations in water column stability and Si-limitation affecting the diatom community composition (Stoffers and Hecky, 1978; Kilham, Kilham, and Hecky, 1986). After 8.2 ka *Nitzschia* became increasingly

more abundant until 2.8 ka, when these became the dominant diatom taxon. Previous studies on Lake Kivu (e.g. Stoffers and Hecky, 1978; Haberyan and Hecky, 1987) have demonstrated that a high ratio of dissolved Si:P in the photic zone and strong stratification indeed favors the needle-like *Nitzschia* diatoms. Hence this biological record for Lake Kivu suggests the water column is presently more stable than in the early Holocene. Indeed, the *Nitzschia* dominance beginning at 2.8 ka indicates that the present extreme stratification of the lake has more or less persisted ever since.

The genus *Chaetoceros* is typically marine and is often found in relatively saline lakes (i.e. salinity > 3ppt; Hammer *et al.*, 1983). Its presence in the microfossil record was interpreted by Haberyan and Hecky (1986) to reflect the onset of the modern crenogenic meromictic condition of the lake. In K12-19A *Chaetoceros* occurs from 2,600 BP to 1,910 BP which is younger than the age of 5,000 BP reported by Haberyan and Hecky (1987). Previous workers did not encounter *Chaetoceros* in plankton collections from the modern lake, and Haberyan and Hecky (1987) concluded that lake surface salinity during the *Chaetoceros* interval, their zone B-C transition, must have been higher than at present (i.e. more hospitable to *Chaetoceros* and greater than 3ppt). More recent studies by Pasche *et al*. (2010), however, have found this genus in modern sediments (< 260 years old) (see Map, Figure 1.3) and will be discussed further in the following section.

4.1.2 LAKE KIVU ~700 YEARS BP TO PRESENT

The recent and modern history of Lake Kivu is captured in our two gravity cores K13-8A and K12-19B. Core 8A (96 m water depth) reveals a dynamic record of the lake over the past 700 years or so, from approximately 1315 AD to today, based on extrapolation of sedimentation rates determined from ^{210}Pb analyses (Table 3.3). The deeper core 19B (352 m water depth) most likely represents the modern interval after ~1400 AD (i.e. the ^{210}Pb-age of the ash layer in 8A at 65.5 cm depth which was not recovered in 19B). Both cores contain two brown layers which, if taken as distinct, lake-wide events, suggest that these cores overlap temporally (Figure 3.9). The older brown layer occurs at about 1590 AD followed by the most recent brown layer at ~1880 AD (Figure 3.15). These cores show effects of their relative locations within the water column. The most recent period of aragonite sedimentation is recorded in the top-most sections of both cores, but with apparently more preservation (i.e. higher % TIC) in the shallower 8A core than in the deeper core, 19B. This is expected given the decreasing pH trend with depth reported by Tassi *et al.* (2009) from 8.8 at the surface to 6.2 at 350 m depth in the main basin. Core 19B does not record the ~400 year aragonite interval that occurs between the two brown layers in 8A (1550 AD to 1900 AD; Figure 3.9), perhaps reflecting more acidic or corrosive deep water at that time,

which might have dissolved the carbonate supplied from the above surface waters. Variability of carbonate deposition in 8A suggests there have been fluctuations in the water chemistry following changing primary productivity levels (i.e. nutrients), changing chemocline and mixing depths (i.e. carbonate preservation potential), or some combination of both. This topic is further explored in section 4.5.

The pennate diatom dominance (*Nitzschia*) from both cores 8A and 19B agrees with the general trend found in the upper strata of piston core 19A and with diatom stratigraphy reported by Pasche *et al.* (2010) for their nearby Kibuye core (Figure 1.3). The general *Nitzschia* dominance in the microfossil record suggests that the current medium to high surface pH and alkalinity, as well as the strong stratification regime and high Si:P in the water column (Gasse *et al.*, 1983), has persisted for the past 600 years (i.e. the record encompassed by both gravity cores). While I did not find specimens of *Chaetoceros (muelleri)* in the few smear slides that I examined from the uppermost carbonate interval of core 8A, Pasche *et al.* (2010) report this species in their Kibuye core, in the upper carbonate-rich sediments (0-8 cm). This modern record of *Chaetoceros* means the current surface salinity (~ 1100 mg/L total dissolved solids; Tassi *et al.*, 2009) is tolerated by this unique species, and perhaps, their earlier occurrence from 2.6 ka to 1.9 ka marks a time when conditions were not much different from today.

4.1.3 REGIONAL HOLOCENE CLIMATE

Freshwater carbonate sedimentation is largely controlled by two factors: (1) biogenic uptake of CO_2 (photosynthesis) and (2) physical-chemical (e.g. temperature) effects on the solubility of CO_3^{2-} (Kelts and Hsü, 1978). The precipitation of inorganic carbonate minerals from the water column (typically from the epilimnion) requires supersaturation with respect to calcium carbonate to be reached. Supersaturation in the lacustrine environment is commonly induced during phytoplankton bloom events when CO_2 uptake raises the pH and enables the precipitation of $CaCO_3$. This is dependent on nutrient availability in the epilimnion. Indeed, Pasche *et al.* (2010) attribute carbonate deposition over the last 60 years in Lake Kivu to higher productivity as inferred from changes in the nutrient budget of the epilimnion (Muvundja *et al.*, 2009; Pasche *et al.*, 2009). Calcite (and aragonite) solubility is also temperature dependent, and increases with decreasing temperature (Wetzel, 1975; Kelts and Hsü, 1978). In addition to photosynthesis and temperature, enhanced evaporation and mixing of chemically-unique water bodies can also induce supersaturation within a lake system.

Carbonate abundance in lacustrine sediments is sometimes taken as a proxy for relative degree of evaporation (i.e. the aridity of a region). Thus, all else being equal, the bulk TIC record

can be compared to other paleoclimatic proxies to deduce regional climate trends through time. Our TIC record (K12-19A) was compared to three other proxy records of past aridity from nearby lakes for the last 12,000 cal yr BP: (1) the deuterium content of plant leaf wax in sediments from Lake Challa, Tanzania (Tierney *et al.*, 2011), (2) the same index from Lake Tanganyika (Tierney *et al.*, 2008), and (3) the Mg/Ca ratio in calcite from Lake Edward (Russel *et al.*, 2003). All three of these lakes record the end of the regional pluvial known as the African Humid Period (AHP), which lasted roughly from 14 ka to 5 ka (deMenocal *et al.*, 2000), with a brief return to drier conditions during the Younger Dryas around 12 ka (Talbot *et al.*, 2007)(Figure 4.1). The timing of this East African pluvial event agrees well with the evidence for rising lake levels in Kivu at the end of the Younger Dryas (i.e. the onset of deep-water sedimentation over the shallow-water coarse sand at 11.8 ka), and with the onset of carbonate deposition in Kivu shortly after the termination of the AHP in the region (i.e. increased aridity after 5 ka).

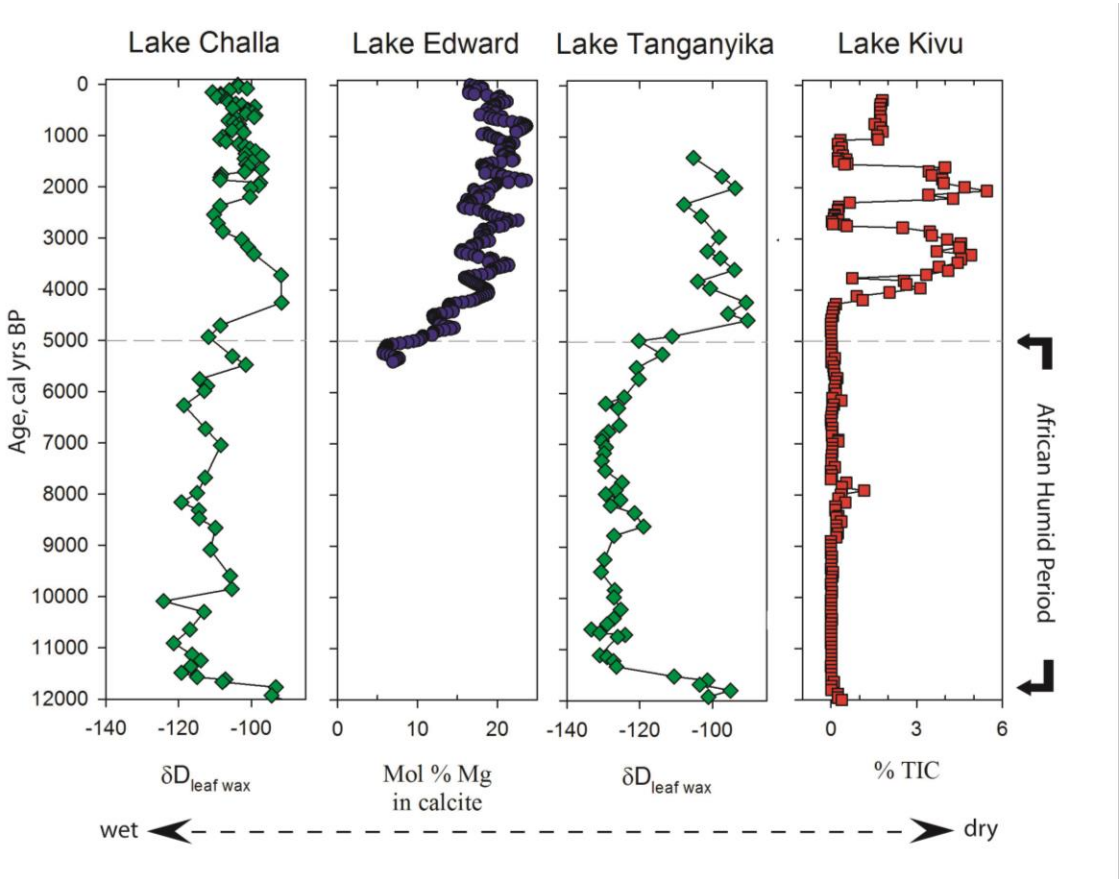

Figure 4.1 Regional Holocene climate records
Comparison and timing of regional climate proxies from three other African Lakes. Axes are positioned so that data to the right suggest more arid conditions than data to the left. δD of plant leaf waxes from Lake Tanganyika (Tierney *et al.*, 2008) and Lake Challa (Tierney *et al.*, 2011); mol% Mg in calcite from Lake Edward (Russell *et al.*, 2003); %TIC (this study, K12-19A) versus age in cal yr BP. See Fig. 1.1 for lake locations.

4.2 $CaCO_3$ SATURATION AND PRECIPITATION

4.2.1 ARAGONITE MINERALOGY

Aragonite ($CaCO_3$) was found to be the dominant carbonate mineral in all of the calcareous sediments analyzed by X-ray diffraction. Previously reported mineralogy from Lake Kivu (e.g. Stoffers and Fischbeck, 1974; Stoffers and Hecky, 1978; Botz *et al.*, 1988) record the presence of calcite, Mg-calcite, dolomite ($CaMg(CO_3)_2$), siderite ($FeCO_3$), and monohydrocalcite ($CaCO_3 \cdot H_2O$) species. The reasons for this discrepancy may be due to both the relatively low sampling resolution down-core that was employed in this study and, perhaps more importantly, the location of the cores that were analyzed for mineralogy. Sediment mineralogy reported from Northern basin cores (K-10 and K-12 in Stoffers and Hecky, 1978; Appendix 4, Figure B) was similar to our findings, with aragonite as the dominant phase and lesser amounts of siderite. Cores from the far southern end of the lake, in Bukavu basin (K-15) and south of Idjwi island (K-1 and K-13), areas from which we have no cores for comparison, reveal carbonate mineral variability (Appendix 4).

Given the high Mg^{2+} content relative to Ca^{2+} of present-day Kivu (main basin Mg:Ca = 12:1 by weight; Tassi *et al.*, 2009), aragonite mineralogy is expected for the precipitated authigenic carbonates (Müller *et al.*, 1972). This suggests that Mg/Ca of Lake Kivu has always been high ($\geq$ 12, which is required for aragonite mineralogy), at least in the Eastern basin, since carbonate deposition began 4,230 year ago. Mineral variability of the sediments from the southern Bukavu basin (Stoffers and Hecky, 1978; core K-15) can be explained by the lower Mg/Ca ratio currently present in that part of the lake (Mg:Ca = ~7:1 mg/L; Tassi *et al.*, 2009). At Mg/Ca ratios between 2 -12 by weight, Mg-calcite forms as the authigenic carbonate mineral with diagenetic dolomite also occurring in the sediments (Müller *et al.*, 1972).

The entire Bukavu basin is shallow (<100 m water depth) and, given the continuous carbonate record found in K-15, has always been favorable to carbonate preservation. Previous studies have concluded that the variable Bukavu basin sediment mineralogy reflects fluctuations in lake level including linkage to the main basin of the lake and the Ruzizi river outflow (Stoffers and Fischbeck, 1974; Stoffers and Hecky, 1978). Most of the ages from these earlier cores are not reliable however, because ages were estimated from sedimentation rates derived from radiometric ^{14}C analysis of bulk lacustrine sediments, which likely have a significant reservoir effect from the geogenic CO_2 released into the water column. A detailed correlation to our better-dated cores (i.e. from terrestrial macro fossils) is not possible at this time.

4.2.2 *MECHANISMS FOR ARAGONITE SATURATION*

As mentioned above, climate can be a major driver of authigenic carbonate precipitation in lacustrine systems in that higher temperature and evaporation induce supersaturation. In this regard, it appears that Kivu responded to the major climatic transition that occurred in the Holocene, i.e. the termination of the African Humid Period. However, not all tropical rift lakes precipitate and preserve $CaCO_3$ and the conditions necessary for aragonite supersaturation in Kivu are worth investigating. The degree of carbonate saturation in natural waters is determined by the ion activity product (IAP) and the equilibrium constant, K_i (Kelts and Hsü, 1978). The IAP for $CaCO_3$ is the product of the ion activities of (Ca^{2+}) and (CO_3^{2-}) and the equilibrium constant, K_c, is temperature dependent. Saturation is achieved when IAP > K_c.

$$Saturation\ Index, \Omega = log \frac{[Ca^{2+}][CO_3^{2-}]}{K_c}$$

The system is saturated when $\Omega > 0$; supersaturated when $\Omega > 1$; undersaturated when $\Omega < 0$

Schmid *et al.* (2009) and Pasche *et al.* (2009) reported the surface (0-50 m) waters of Kivu to be saturated or slightly supersaturated ($\Omega = 0.8$ to 1.3) with respect to calcite. Aragonite saturation was not reported in either study, but the difference between aragonite and calcite should not change the overall demonstration presented here. Both studies report the underlying water column (100 - 475 m water depth) as near equilibrium ($\Omega = 0$), however Schmid *et al.* (2009) report values of Ω around -0.16 (slightly undersaturated), while Pasche *et al.* (2009) report Ω around 0.125. Regardless, these values demonstrate that Lake Kivu's epilimnion is currently favorable for $CaCO_3$ precipitation.

In addition to saturation considerations, there must be a source of the calcium and magnesium ions that are delivered to the lacustrine system. Erosion and weathering of the surrounding catchment soils and rocks are typical sources of detrital carbonates and of Ca^{2+}, Mg^{2+}, and HCO_3^- ions and are delivered via surface inflows (Kelts and Hsü, 1978). The Kivu catchment is located within an active volcanic terrain to the north and south and Precambrian metamorphic bedrock to the east and west (Degens *et al.*, 1972) and as such, an erosional source alone does not seem to satisfy the solute requirements (i.e. there is no limestone or Ca-rich sedimentary rock unit present in the catchment).

A simple Ca^{2+} budget was constructed for Lake Kivu using reported, modern-day solute concentrations of the lake and surrounding water-bodies (Table 4.1). Inputs include the surface

tributaries and the sub-aquatic hydrothermal seeps, while carbonate burial and the Ruzizi River are the lake's only output of dissolved calcium. Precipitation was not considered here.

Table 4.1: Lake Kivu Annual Calcium Budget

Calcium budget based on modern-day measurements with calculations described in text.

		$[Ca^{2+}]^{*}$ mg/l	Flow rate** km^3/y	Annual amount kg Ca/ y	Potential Sed Flux*** g Ca/ m^2 y
IN	Surface Streams	4.7	2.4	1.13×10^7	
	Hydrothermal seeps	84	1.3	10.9×10^7	
OUT	Ruzizi R.	4.6	3.6	1.66×10^7	
EXCESS				10.4×10^7	**43.85**

*Concentrations from Degens et al. (1972) with hydrothermal seep $[Ca^{2+}]$ as mean from two surface hot springs: Kaukula and Kakondo.

**Surface stream discharge compiled from 21 rivers by Muvundja *et al.* (2009), hydrothermal seeps from Schmid *et al.* (2005), and outlet measured at Ruzizi I Hydropower Plant (1941 to 2005).

*** Potential sediment flux assumes uniform Ca burial rate across the entire lake floor area (2.37×10^9 m^2).

Concentrations reported by Degens *et al.* (1972) and flow rates compiled by Muvundja *et al.* (2009) were used to calculate the annual amount (in kg of Ca^{2+} per year) contributed (lost) by each source (sink) in Table 4.1. Degens *et al.* (1972) measured $[Ca^{2+}]$ in two creeks, Lwiro (6.7 mg/L) and Kabindi (2.7 mg/L), as well as in two surface hotsprings, Kaukula (85.5 mg/L) and Kakondo (82.2 mg/L), of which the averages were used for the surface stream and hydrothermal inputs, respectively.

Currently the Ruzizi river removes more calcium (1.66×10^7 kg Ca /y) than the lake basin receives from the surrounding terrain (1.13×10^7 kg Ca /y) in a given year. The hydrothermal seeps, though contributing only ~1/3 of the total water inflow (Schmid *et al.*, 2005), contain a substantial amount of $[Ca^{2+}]$ compared to surface inflows and indeed yield an estimated annual contribution of 10.9×10^7 kg Ca /y, an order of magnitude higher than the surface runoff. The estimated residence time of Ca^{2+} in Kivu is on the order of 270 years (based on modern lake concentrations and flow rates). The "excess" amount in Table 4.1 refers to the annual supply of calcium available for $CaCO_3$ precipitation.

The solute concentrations of hydrothermal seeps within Lake Kivu have not been measured directly and, my assumption that they are the same as concentrations from nearby surface hot springs is examined further here. The assumption is that the sub-lacustrine hydrothermal waters that enter the lake are fed by the same altered groundwater source that fills the nearby hot springs. In fact chemical composition data reported by Tassi *et al.* (2009) from various depths in all the basins of Kivu agree well with this assumption. Schmid *et al.* (2005) place the two main sub-lacustrine inflows at 180 m and 250 m depth and when the [Ca^{2+}] from Tassi *et al.* (2009) are compared at 200 m and 275 m depth (i.e. just below the depth of inflow), the values bracket the 84 mg/L hot spring concentration (78 mg/L and 119 mg/L, respectively). A range of annual excess Ca^{2+} delivered to the lake was calculated from these main basin concentrations and yield 9.61 x10^7 kg Ca /y to 14.9 x10^7 kg Ca /y.

Taking this budget one step further, a sedimentation flux was estimated in terms of g Ca /m^2 y, assuming that $CaCO_3$ was deposited uniformly across the entire lake floor, with lake floor area equal to the lake surface area (2.37 x10^9 m^2). This resultant value of 43.85 g Ca /m^2 y (Table 4.1) offers an approximation that can be compared to actual burial rates of Ca calculated from our sediment cores.

Mass Accumulation Rates (MAR) were calculated for various intervals from cores K13-8A and K12-19A using the Linear Sedimentation Rate (LSR), porosity, and dry bulk density.

$$MAR\left(\frac{g}{cm^2\ yr}\right) = LSR\left(\frac{cm}{yr}\right) * (1 - \emptyset) * \rho_{\text{dry bulk}}\left(\frac{g}{cm^3}\right)$$

Estimates of LSR came from the appropriate age model derived for each core: 19A (AMS ^{14}C), 0.065 cm/y; 8A (^{210}Pb – carbonate interval), 0.124 cm/y. Porosity and dry bulk density were estimated for both cores with the method described earlier (section 2.4.2 - ^{210}Pb dating of bulk sediments) and the appropriate mean used for the interval considered. Assuming all TIC measured in these cores is $CaCO_3$ (i.e. all TIC is aragonite) the following conversion was used to find %Ca (by weight) of the interval.

$$\%Ca = \frac{\%TIC}{0.12} * 0.4$$

Where 0.12 is the weight fraction of carbon and 0.4 is the weight fraction of calcium in $CaCO_3$.

After determining the weight % Ca, a Calcium Mass Accumulation Rate (MAR_{Ca}) was estimated.

$$MAR_{Ca}\left(\frac{gCa}{cm^2\ yr}\right) = MAR * \frac{\%Ca}{100}$$

The results of these calculations show reasonable agreement between the Ca deposition rate that is required to balance the Ca budget of the lake (Table 4.1), and the Ca burial rate that we measure in our cores (Table 4.2).

Table 4.2: Carbonate Mass Accumulation Rates and Ca^{2+} flux.
Estimates from the carbonate intervals of K13-8A and K12-19A.

Core - lithology	depth interval, cm	ρ, g/cc	LSR, cm/y	MAR, g/ m^2 y	% TIC	% Ca	MAR_{Ca}, g Ca / m^2 y	Annual, kg Ca/ y
8A - carbonate	0-5	2.37	0.124	235.1	5.43	18.1	**42.55**	10.1 x10^7
8A - carbonate	25-40.5	2.31	0.124	200.5	7.15	23.8	**47.79**	11.3 x10^7
19A - carbonate	158-198	2.09	0.065	68.4	4.07	13.6	**9.28**	2.2 x10^7
19A - carbonate	235-327.5	1.97	0.065	141.9	3.23	10.8	**15.28**	3.62 x10^7

Dry bulk density(ρ) and porosity (φ) estimated as described in section 2.4.2.

Porosity values used: 0.92 (8A, 0-5cm); 0.93 (8A, 25-40.5cm); 0.95 (19A, 158-198cm); 0.89 (19A, 235-327.5cm)

The shallower and more recent carbonate intervals from 8A yield very similar MAR_{Ca} values to the sediment flux of 43.85 g Ca/ m^2 y estimated from the Ca^{2+} balance and suggests that the Ca-budget is accurate. However the smaller MAR_{Ca} and annual Ca flux calculated for the two carbonate intervals of the deep, offshore core 19A is inadequate for a balanced budget using modern inputs. There is a lot of carbonate deposition in the very shallow, near shore modern waters of Lake Kivu, including the formation of calcareous crusts on submerged rocks and along the shoreline (Beadle, 1974; T. Johnson and R. Hecky, pers. communication, March 2014). It is possible that this shallow water sink for Ca, driven mainly by the high productivity of the littoral zone, is more important at times than the aragonite burial in the deep basins offshore. Or perhaps the influx of Ca^{2+} from which aragonite could precipitate was smaller at the time of deep-water carbonate burial in the lake's history, from 4.1 ka to 1.9 ka (i.e. lower rates of hydrothermal input). Uncertainties lie in the fact that the hydrothermal seeps have not been sampled directly and the calculation in Table 4.2 assumes these two cores are representative of the entire lake.

Regardless, the above demonstration suggests the dominant input of Ca^{2+} to the lake is hydrothermal waters and hence, the likely calcium source for Kivu's carbonate supersaturation. In fact, it would take on the order of 300 years for modern Lake Kivu to become undersaturated ($\Omega \leq 0$) with respect to calcite if the hydrothermal inputs were to stop, all else being equal. This suggests that the hydrothermal contribution toward calcite saturation operates on a timescale of decades to centuries.

Stoffers and Hecky (1978) compared the sedimentology of lakes Kivu and Tanganyika and reported late Holocene carbonate deposition in both records, but with a delayed onset of carbonate deposition in Tanganyika. The Ruzizi river is the hydrologic link between these two lakes and this delay could be explained by the solute connection, with Tanganyika receiving a high proportion of major ions from Kivu, but requiring some time to achieve supersaturation within the water column. Hence, there is a clear source for the Tanganyika carbonate supersaturation: solute spill-over from upstream Lake Kivu. This delayed carbonate onset in Tanganyika has been confirmed by more recent dating (i.e. from macro fossils) in Tanganyika cores, indicating that carbonates occur no earlier than about 2,400 BP (J. Russell and A. Cohen, pers. communication, May 2014).

4.3 THE ISOTOPIC COMPOSITION OF ARAGONITE

The covariance of $\delta^{13}C$ with $\delta^{18}O$ in the aragonite minerals is most striking when all samples are plotted against each other (Figure 4.2). Lake Kivu is considered hydrologically open, yet even the modern aragonites plot with "heavy" $\delta^{18}O$, more in a range typical of carbonates from closed basin lakes (Talbot, 1990). Similar to open lakes however, the ^{18}O range of carbonates in this study is less variable than the ^{13}C range (3.5‰ versus 6.8‰, respectively). Compared to other African lakes, aragonites of Kivu appear quite enriched in $\delta^{13}C$ suggesting an enriched source of dissolved inorganic carbon (DIC). These data do, however, encompass the range reported by Botz *et al.* (1988) for aragonites from the northern and eastern basins of Lake Kivu (their sites 5-7, Appendix 4, Fig. D), 4.3‰ to 5.8‰ $\delta^{13}C$ and 0.7‰ to 4.3‰ $\delta^{18}O$, and despite the ^{13}C-enrichment, the $\delta^{18}O$ values are similar to those reported from other African lakes (e.g. Turkana, Natron, and Bostumtwi), although these are closed-basin lakes.

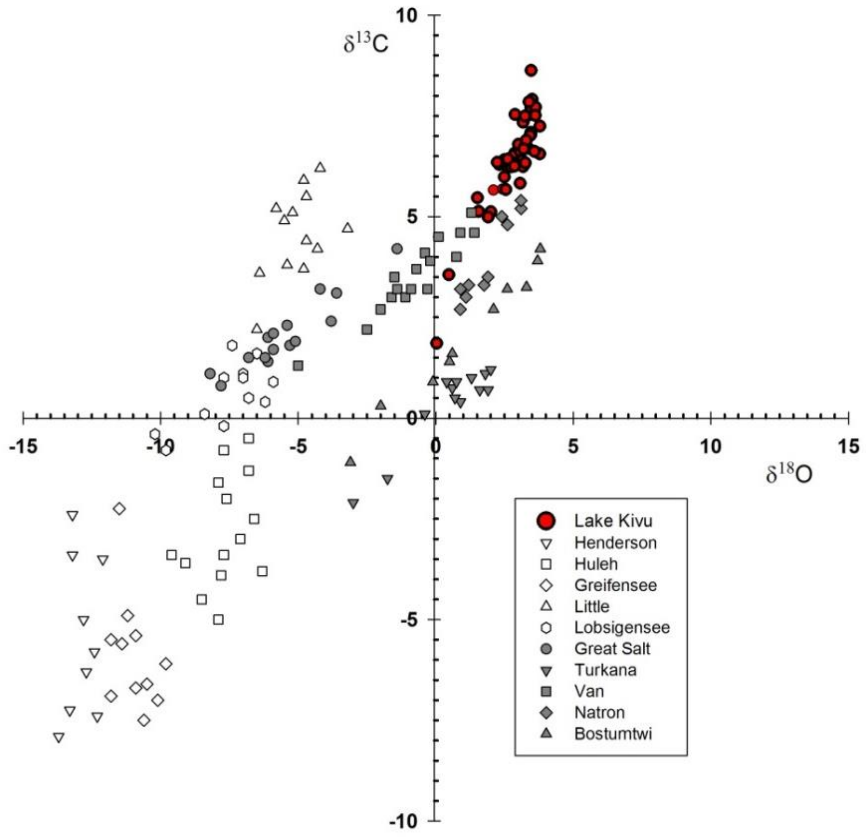

Figure 4.2 - Primary Carbonates Cross-plot of $\delta^{13}C$ and $\delta^{18}O$
Cross-plot of $\delta^{13}C$ (y-axis) and $\delta^{18}O$ (x-axis) with all Lake Kivu carbonate data (this study) plotted in red-filled circles. For reference, primary carbonate data from other lakes around the world are also plotted: closed lakes (filled symbols) and open lakes (open symbols). Modified from Talbot (1990).

4.3.1 $\delta^{13}C$ OF ARAGONITE

The carbonate stable isotopes describe an enriched system in terms of both carbon and oxygen when compared to other primary lacustrine carbonates (Figure 4.2). With only kinetic fractionation taking place as the $CaCO_3$ precipitates out of the surface waters, the resulting isotopic signature of $\delta^{13}C_{carb}$ would be expected (from Faure, 1977):

$$\delta^{13}C_{carb} = (\delta^{13}C_{DIC} + 1000)(1.00185) - 1000$$

where $\delta^{13}C_{DIC}$ is the isotopic composition of the dissolved inorganic carbon pool from which aragonite forms.

Based on the modern $\delta^{13}C_{DIC}$ value reported by Tassi *et al.* (2009) of 3.35‰ from the surface of the main basin, precipitating aragonites are expected to be 5.21‰ $\delta^{13}C$. This is ~ 1‰ lower than what is measured from the upper-most (0-1cm) in cores 8A and 19B, whose values are 6.23‰ and 6.29‰, respectively (Figures 3.10 and 3.11). However, when compared to the mean of all aragonites measured, this expected $\delta^{13}C_{arg}$ (5.21‰) is more similar to the 19B aragonites (0-61 cm average) of 5.47‰ than to the 8A aragonites (0-58 cm average) of 7.00‰. Again, this could be evidence of near shore versus offshore effects on the carbonate record from higher productivity and CO_2 drawdown in the shallow water, and hence, isotopic enrichment, occurring closer to shore, represented here by core 8A. The aragonitic crusts in core 8A (20-27 cm depth, Fig. 3.2; ca. 1740 – 1800 AD, Fig. 3.11) are particularly enriched in $\delta^{13}C_{arg}$, up to 8.62‰, which, if due to a much enriched DIC pool from high productivity in the near shore, suggests a much shallower environment than today (i.e. less than the current 96 m water depth) at the coring site.

The $\delta^{13}C$ per mil values of the aragonites from 19A (5.46‰ – 7.84‰, Figure 3.12) were used to estimate a possible range of isotopic composition of formation waters (i.e. solving for $\delta^{13}C_{DIC}$) at their time of deposition. Near the onset of carbonate deposition, 4,100 BP, $\delta^{13}C_{DIC}$ = 3.6‰, increasing to 4.54‰ by 2,800 BP. The DIC pool then becomes more enriched, up to 5.94‰, by the beginning of the next carbonate interval around 2,100 BP. This suggests that either these ancient formation waters were more enriched than today, and/or, as with 8A, this location was much shallower and closer to shore with higher productivity and recycling of nutrients during the 4.1 to 1.6 ka carbonate interval.

Another useful equation is the fractionation expected in equilibrium between solid $CaCO_3$ and gaseous CO_2 (also from Faure, 1977):

$$\delta^{13}C_{carb} = \left(\delta^{13}C_{CO_2} + 1000\right)(1.01017) - 1000$$

Where $\delta^{13}C_{CO2}$ is the isotopic composition of the aqueous CO_2 in solution and $\delta^{13}C_{carb}$ is the isotopic composition of the precipitated carbonate mineral at 25°C.

Fumarolic gas samples collected within Nyiragongo crater (e.g. Tedesco *et al.*, 2010), roughly 20 km north of Lake Kivu, yield a $\delta^{13}C_{CO2}$ of -3.65‰, which we use with the equations above to estimate that $\delta^{13}C_{arg}$ = 6.48‰. This result is similar to the modern aragonites of 8A and 19B, 6.23‰ and 6.29‰, respectively. The authors point out that $\delta^{13}C_{CO2}$ discharges vary spatially however, from -3.55‰ at Nyiragongo to -11.63‰ on the western side of Kabuno bay, and from -8.1‰ along the eastern shore to -5.6‰ in the surface waters of Lake Kivu. These more depleted values, closer to those of the Eastern basin, result in lower estimated $\delta^{13}C_{arg}$ values (4.4‰) for the aragonites expected from 8A and 19B, again suggesting there are more factors affecting the carbonate fractionation than just kinetics alone.

Lastly, the carbonate intervals of 19A were used to calculate a range of $\delta^{13}C_{CO2}$, -4.66‰ to -2.3‰, for the formation waters 4,100 BP to 1,600 BP, and these estimates are consistent with modern $\delta^{13}C_{CO2}$ discharged from Nyiragongo crater, -4.04‰ to -3.55‰ (Tedesco *et al.*, 2010). Although these values are temporally disconnected and the actual $\delta^{13}C_{CO2}$ of hydrothermal fluids 3,000 – 4,000 years ago are unknown, these estimates suggest that the source waters for aragonite precipitation were quite enriched in $^{13}C_{CO2}$.

The above calculations demonstrate that the isotopic signature of the Kivu aragonite is significantly impacted by the local volcanic source of CO_2 rather than from just atmospheric or biogenic sources of CO_2 alone, which are typically depleted to around -7‰ or less (Leng and Marshall, 2004).

4.3.2 $\delta^{18}O$ OF ARAGONITE

The oxygen isotopic composition of the aragonite depends on temperature and the isotopic composition of the surface water. The expected $\delta^{18}O_{arg}$ can be calculated, or vice versa to find the temperature of formation waters, assuming isotopic equilibrium has been reached between the aragonite and surface water. Kim *et al.* (2007) describe the following relationship for synthetic aragonite:

$$1000 \ln \alpha_{a-w} = 17.88 \pm 0.13 \left(\frac{103}{T}\right) - 31.14 \pm 0.46$$

$$\alpha_{a-w} = \frac{\left(1000 + \delta^{18}O_{aragonite}\right)}{\left(1000 + \delta^{18}O_{water}\right)}$$

where temperature (T) is in °K, α is the fractionation factor, and $\delta^{18}O$ is reported as ‰ deviation from V-SMOW standard.

The actual fractionation from formation waters to aragonite is ε:

$$\varepsilon_{a-w} = (\alpha - 1) * 1000$$

To compare with our $\delta^{18}O_{arg}$ in VPBD, values were converted using:

$$\delta^{18}O_{VSMOW} = 1.03086 * \delta^{18}O_{VPDB} + 30.86$$

Modern-day lake $\delta^{18}O_{water}$ VSMOW values for Lake Kivu range from 1.2‰ in the north to 3.4‰ in the south (Tassi *et al.*,2009), and along with an average surface temperature of 24.3°C (Schmid *et al.*,2005) should yield $\delta^{18}O_{arg}$ between 30.45‰ and 32.82‰ VSMOW, or -0.26‰ and 1.97‰ VPDB (Table 4.3). Modern aragonites from 8A and 19B have $\delta^{18}O_{arg} \cong 2.5$‰ VPDB, i.e. heavier than expected. The lake water, therefore, is likely enriched in $\delta^{18}O$ compared to meteoric water (by -1.5‰ VSMOW; Katsev, 2014) due to evaporation across the basin.

Table 4.3: Fractionation Factors Water to Aragonite for various temperatures using equation from Kim *et al.* (2007).

temp. °C (°K)	$\alpha_{A\text{-}W}$	$\varepsilon_{A\text{-}W\ VSMOW}$	$\varepsilon_{A\text{-}W\ VPDB}$
24.3 (297.45)	1.02939	29.39	-1.426
25 (298.15)	1.02925	29.25	-1.562
30 (303.15)	1.02823	28.23	-2.551

The $\delta^{18}O$ values of aragonite from 19A vary from 1.51‰ to 3.62‰ VPDB (Figure 3.11). If we assume that these carbonates formed in isotopic equilibrium with the lake water and we further assume a lake surface temperature of 25°C (298.15°K), then the $\delta^{18}O$ VSMOW of the water is estimated to range from 3.07‰ to 5.18‰. The $\delta^{18}O$ record shows enrichment from onset of carbonate deposition at 4.2ka into the ensuing carbonate interval to 2.2 ka (Figure 4.3) and which likely resulted from variable and strengthening aridity following the AHP, i.e. increased evaporative effects on the formation waters.

The paleorecords from Tanganyika (e.g. Tierney *et al.*, 2008) and Edward (Russell *et al.*, 2003) indicate a dramatic shift to more arid climate at the end of the AHP (~5 ka). Lake Edward, specifically, exhibits variability in the %Mg in calcite record on a ~700 -year timescale over the past 5,000 years that appears roughly similar in the lower carbonate interval of Kivu (Figure 4.3). Russell *et al.* (2003) concluded that a maximum low lake level occurred sometime between 4 ka to 2 ka, which was followed by a transgression phase beginning around 1800 BP (geochemical data not shown here), with lake level believed to have risen to its present level by ~1500 BP. All records indicate an increase in aridity between 5 ka and 4 ka and even, to a lesser extent, a peak of aridity at, or slightly after, 2,000 years BP.

This increased regional aridity and the $\delta^{18}O_{arg}$ enrichment in Lake Kivu beginning at 4.2 ka, as well as evidence for carbonate mineral variability in the Bukavu sediment cores (e.g. Stoffer and Hecky, 1978) suggest intense evaporation, and perhaps periodic closure of Lake Kivu in the post-AHP.

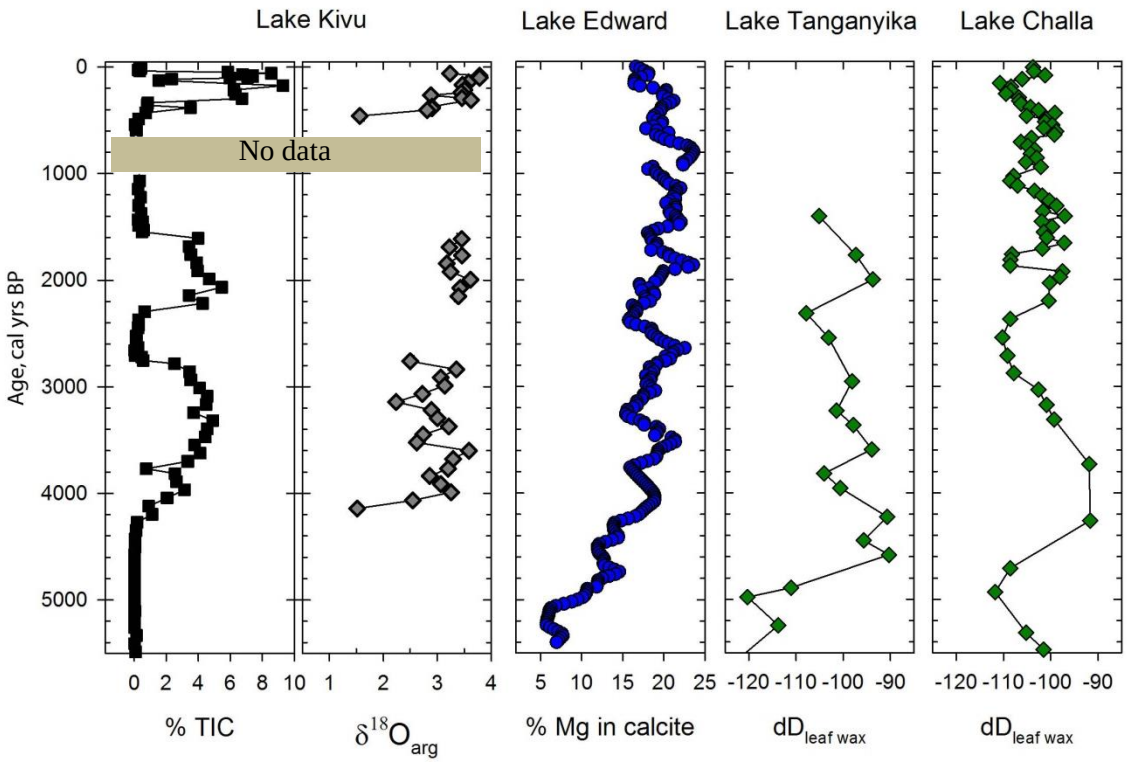

Figure 4.3 Regional paleoclimate records since 5.5 ka.
The same paleorecords shown in Fig. 4.1 but only for the post African Humid Period, from 5.5 ka to 0ka. References are the same for Fig 4.1 and axes are aligned so that data to the right suggest more arid conditions than data to the left. Percent TIC and $\delta^{18}O_{arg}$ (in ‰ deviation from VPDB) from Lake Kivu with the most recent, 0 to 500 yrs BP, from core 8A. Mole % Mg in calcite from Lake Edward and δD of plant leaf waxes from Lakes Tanganyika and Challa. Shaded bar represents the gap in data between the undisturbed, lower sections of core 19A and the base of core 8A.

4.4 THE ISOTOPIC COMPOSITION OF BULK ORGANIC MATTER

Evidence from the carbonate minerals point to an enriched source of $\delta^{13}C_{DIC}$, which we attribute to a significant volcanic source of CO_2 coming into the lake. We further explore this hypothesis by considering the $\delta^{13}C$ of the bulk organic matter (OM). With the dissolved inorganic carbon (DIC) in a lake being the carbon source for aquatic primary productivity, mainly epilimnic and littoral zone photosynthesis, any isotopically enriched DIC (i.e. from Kivu's deeper water) should show up in the $\delta^{13}C$ of the bulk organic matter preserved in the sediments.

4.4.1 $\delta^{13}C_{org}$ OF CORE K12-15A

The bulk OM $\delta^{13}C$ and $\delta^{15}N$ results from core K12-15A show several significant changes during the Holocene (Figure 3.13). The large (>10‰) shift in $\delta^{13}C_{org}$ at 290 cm depth (approx. 3,000 yr. BP) in 15A and subsequent shifts to heavier $\delta^{13}C_{org}$ during both carbonate intervals (TIC >2%) that follow, are consistent with the interpretation (from the carbonate sediment record) that the onset of hydrothermal activity in the lake occurred around 4.2 ka. When plotted as $\delta^{13}C_{org}$ versus C/N (weight %), these post-3ka excursions (i.e. when $\delta^{13}C_{org} \geq$ -21‰; samples to the right of the dashed line in Fig. 3.13) clump together with heavier $\delta^{13}C_{org}$ and higher C/N than all other non-calcareous post-3ka samples (open squares, Figure 4.4).

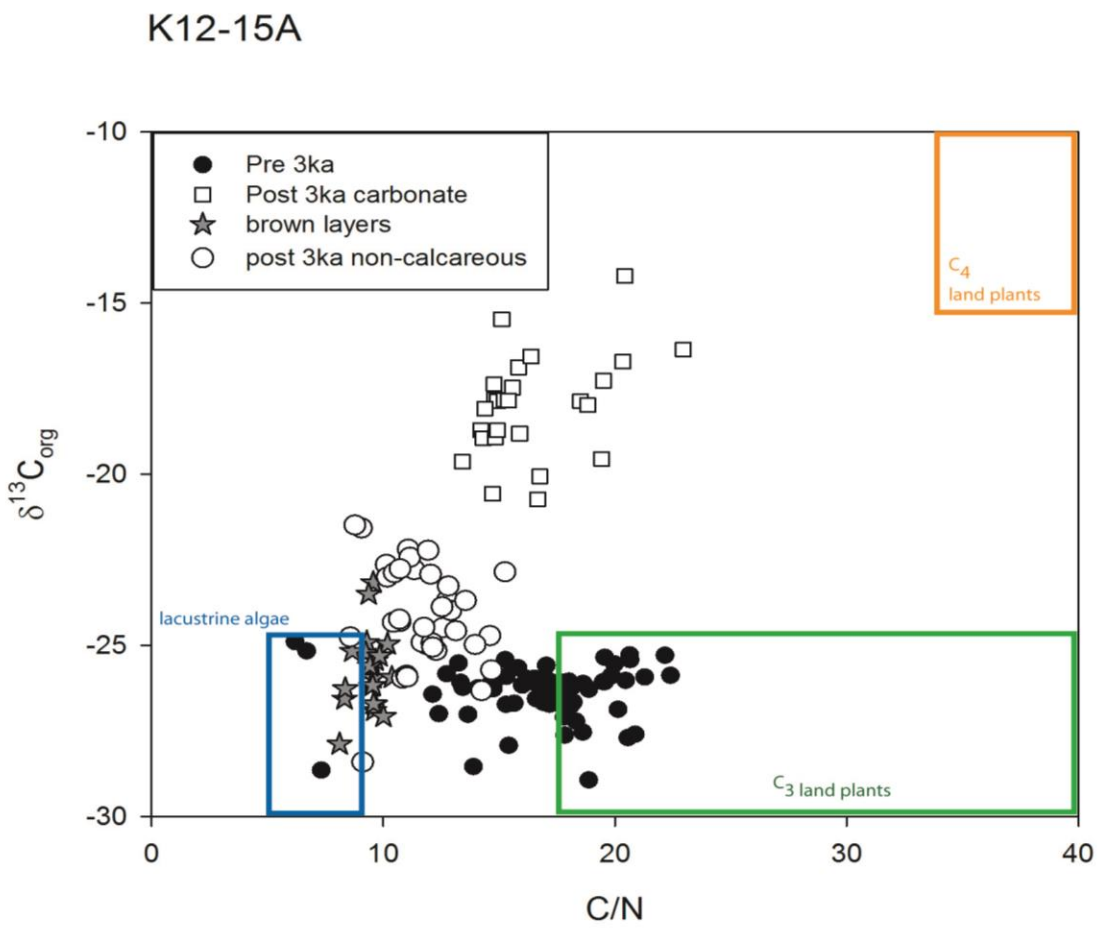

Figure 4.4 Bulk Organic Matter Cross-Plot from all samples of K12-15A
Comparison of the $\delta^{13}C_{org}$ signal with the C/N weight ratio of all samples from 15A to highlight sources of organic matter to lake sediments. Boxes indicate generalized ranges of lacustrine algae (blue), C_3 land plants (green), and C_4land plants (orange) as reviewed in Meyers (2003).

In 15A, OM samples from 7,160 BP (base of core) to 3,000 BP fall into a range between that expected from lacustrine algae and C_3 land plants (black circles, Figure 4.4). The increased $^{13}C_{org}$ after 3 ka could be due to increased aridity, which could result in increased input of organic matter from C_4 land plants, or a switch from $CO_{2(aq)}$ to HCO^-_3 as the dominant DIC source for photosynthesis (Meyers, 2003). The established link between modern-day sub-aquatic hydrothermal inputs and [HCO^-_3] (e.g. Tassi *et al.*, 2009) however, and the relatively low C/N ratio of < 25 (C_4 land plants C/N typically >35) suggest that this signal reflects the influence of hydrothermal input to Kivu's DIC pool. In addition, this large and sustained shift (~10‰) in $\delta^{13}C_{org}$ occurs over a core interval of just 5cm (286 cm to 281 cm depth in 15A) which argues against the possibility of terrestrial vegetation shifts (i.e. this would require some time to establish) and instead could have been caused by a sudden influx of volcanogenic CO_2 at depth. However, all the inorganic signals discussed thus far have indicated that hydrothermal influence started before 4.2 ka, making the timing of this $\delta^{13}C_{org}$ signal rather unusual. Why there are no significant deviations in the $\delta^{13}C_{org}$ record before ~3 ka, such as at the onset of carbonate deposition at 500 cm depth in 15A, or even during the three preceding turbidite intervals, which presumably bring enriched material from near shore to offshore, cannot be determined from these data (Fig. 3.13). Core 15A was not dated directly, however, and age assignments in this core are based on stratigraphic correlations to core 19A, which have some uncertainty. The isotopic composition of the bulk organic matter from the dated core 19A should be investigated in order to better constrain this timing.

4.4.2 $\delta^{13}C_{org}$ OF CORES K12-19B AND K13-8A

The C/N weight ratio and $\delta^{13}C$ of the bulk organic matter from cores K12-19B and K13-8A reveal the likely sources of organic matter for the last 700 years (Figure 4.5). Samples from within carbonate intervals in neither core show the dramatic shift as seen in the post- 3 ka carbonate intervals of 15A (Fig. 4.4). Instead, all samples plot consistently below -23‰ and in a range of C/N that typifies the early Holocene for Lake Kivu. Perhaps the enriched post-3ka carbonate samples from 15A result from processes restricted to the Northern basin and close proximity to hydrothermal seep locations. Bulk carbon and nitrogen data (not shown here) collected from the main basin of Lake Kivu in January of 2011 (S. Katsev, pers. communication, May 2014) reveal that particulate organic carbon and nitrogen (POC and PON, respectively) from the epilimnion have an average C/N ratio of around 15 (range 5 to 16). Samples from 8A (black

circles, Figure 4.5) plot with higher C/N than those of 19B (open circles, Fig. 4.5), again pointing to the near shore versus offshore effects discussed earlier.

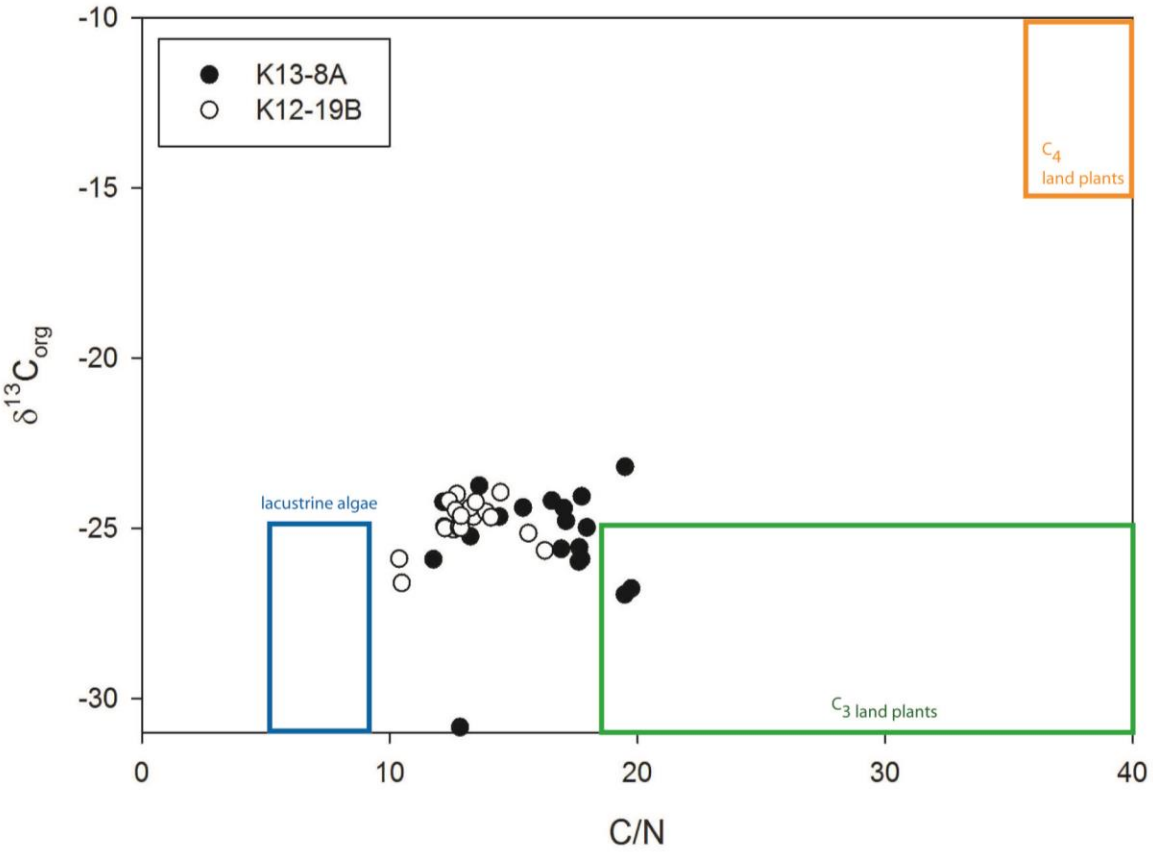

Figure 4.5 Bulk Organic Matter Cross-Plot from all samples of K12-19B and K13-8A
Comparison of the $\delta^{13}C_{org}$ signal with the C/N weight ratio of all samples from cores 19B and 8A to highlight sources of organic matter to lake sediments. Boxes indicate generalized ranges of lacustrine algae (blue), C_3 land plants (green), and C_4land plants (orange) as reviewed in Meyers (2003).

4.4.3 ISOTOPIC COMPOSITION OF KIVU'S BROWN LAYERS

Our sediment records, as well as those of previous studies (e.g. cores of the Woods Hole Lake Kivu expedition, 1971), clearly show that the unique brown layers only show up after the onset of calcareous deposition at 4.2 ka, or more specifically after the end of the first carbonate interval at ~2,740 BP (Figure 3.6; Table 3.2). They show up distinctly at the termination of carbonate intervals in core 19A, while in 15A they also occur as separate intervals within the laminated, organic-rich diatomaceous units (Fig. 3.6). In core 8A, the brown layers occur within aragonite intervals. The brown layers appear in both shallow and deep-water records, implying that they occurred as lake-wide events, with the most recent layer deposited as recently as 1880 AD (Fig. 3.15).

Depletion of the $\delta^{13}C_{org}$ of all brown layers sampled from all three cores suggests a biogenic source, most likely of algal and microbial origins (Hollander and Smith, 2001). The brown layers of 15A, and to a lesser extent those of 19B, exhibit $\delta^{15}N$ enrichment (Fig. 3.13 and 3.14). In general, enrichment in $\delta^{15}N$ can result from changing importance of ammonia, nitrate or nitrogen fixation as substrates for algal growth, denitrification of anoxic bottom waters, as well as increased input of fertilizers and sewage from the surrounding landscape (Meyers, 2003). Decreases in $\delta^{15}N$ can result from increased nitrogen fixation by cyano- or anaerobic bacteria. Many studies suggest the currently high levels of CH_4 in the anoxic bottom waters of Kivu are the result of microbial reduction and bacterial activity (e.g. Tassi *et al.*, 2009; see also Degens *et al.*, 1972; Schmid *et al.*, 2005; Pasche *et al.*, 2011). The oxycline in Lake Kivu is at ~50 m water depth, and hence most of the water column is permanently anoxic. Thus, the denitrification of anoxic bottom waters likely occurs quite regularly, if not continually, in Kivu. If the $\delta^{15}N$ enrichment in the brown layers is a reflection of this process, then it is unclear why they would show up as distinct strata in Lake Kivu sediments, i.e. as discrete events, rather than as continuous deposition. The contradictory $\delta^{15}N$ signals of brown layers from 8A (i.e. older layer showing $\delta^{15}N$ depletion to -1.4‰; Figure 3.15) suggest that bulk carbon and nitrogen stable isotopic compositions alone may not be enough to elucidate the meaning of the brown layers. The extent to which a strong methanogenic system, such as the one currently operating in Kivu's unique environment, affects the isotopic composition of the DIC pool is outside the limits of this study but should be investigated further in future Lake Kivu sediment record analyses, especially in the context of both hydrothermal seep and meromixis onset.

5 CONCLUSIONS ON THE HOLOCENE CARBONATE RECORD OF LAKE KIVU: RELATIVE IMPACTS OF CLIMATE AND HYDROTHERMAL SEEPS

The sediment cores recovered in 2012-2013 from the main basins (northern and eastern) in Lake Kivu capture a limnologic history of Kivu during the Holocene. AMS radiocarbon dating of recovered terrestrial macrofossils as well as ^{210}Pb-dating analysis reveal an almost continuous record of sedimentation since 11,700 years BP. At the end of the Younger Dryas (~11.7 ka) Kivu was a much shallower (-350 m) and smaller basin than today as evidenced by coarse sands and cobbles in the base of core K12-19A. Lake levels rose rapidly with the onset of the regional pluvial known as the African Humid Period at 11.7 ka, with stratigraphic evidence for a deep, productive lake from then until about 5 ka. The late-Holocene sediment record of Lake Kivu displays alternating periods of calcareous and non-calcareous sedimentation. Aragonite was identified as the dominant carbonate mineral phase for all calcareous intervals investigated in cores K12-19A/B and K13-8A, suggesting that the weight ratio of dissolved Mg:Ca in the water column has been high (i.e. > 12) since carbonate deposition began.

This study has demonstrated that the deposition of carbonates in Lake Kivu is overwhelmingly influenced by substantial sub-lacustrine inputs of Ca^{2+}. This hydrothermal input appears to have started about 4,230 years BP, as evidenced by the onset of carbonate deposition as well as by the abrupt enrichment of the $\delta^{13}C_{org}$ in the deep-water sediments of Kivu's northern basin (15A). Based on the solute budget and mass accumulation rates of Ca^{2+} of modern-day Lake Kivu, initiation of $CaCO_3$ (aragonite) deposition at 4.2 ka could not have proceeded without the prior onset of hydrothermally Ca-enriched waters to the Kivu Basin. Conditions became favorable for $CaCO_3$ deposition starting at 4.2 ka, after the onset of hydrothermal activity and increased regional aridity in the post-African Humid Period. The influence of these hydrothermal waters has persisted since then and indeed occurs in the lake today.

Climate influences the chemistry of surface waters as well as controlling meteoric water as the source for the hydrothermal groundwater. There might also be a substantial climate signal over-printed on the carbonate record in addition to hydrothermal effects. The more severe regional aridity after 5,000 BP (Fig. 4.3) might also have impacted Kivu's water chemistry and water column stability. A comparison of the Kivu carbonate record (% TIC and $\delta^{18}O_{arg}$) with regional paleorecords of aridity since 5 ka, especially with that of Lake Edward, indicate fairly

close correspondence, with aridity peaking around 4,000 years BP and perhaps again, but to a lesser extent, around 2,000 years BP.

A comparison of the carbonate record in core 8A with late-Holocene Lake Edward data (e.g. Russell and Johnson, 2007) reveals agreement for a Little Ice Age drought from 1400 AD to 1750 AD, over which time there was increasing % TIC and enrichment of $\delta^{18}O_{arg}$ (Fig. 3.11). This agreement with Lake Edward breaks down during the drought of the Dark Ages (~1.4 ka to 1 ka) however, as core 19A contains no carbonates in this interval, perhaps due to its deep-water setting (Figure 4.3). In modern Lake Kivu, precipitation (1,470 mm/yr; Muvundja *et al.,* 2014) is nearly equal to evaporation (1,530 mm/yr; Muvundja *et al.,* 2014) over the lake basin and yet the $\delta^{18}O_{arg}$ of modern aragonites appear to be enriched over the expected fractionation (i.e. $\delta^{18}O_{arg} \cong 2.5‰$ vs. the expected -0.26‰ to 1.97‰). Therefore the imprint of climate on the carbonate record is still an open question. Apparently, no breaks exist in the carbonate-rich intervals of either Lake Edward (Russell et al., 2003) or Tanganyika (Stoffers and Hecky, 1978) after the termination of the African Humid Period. Differences among the records point to additional, internal influences on Kivu's carbonate record. One possibility is that Kivu's fluctuating carbonate record in the late-Holocene is due to variable hydrothermal inputs.

In the late-Holocene there were at least 4 intervals in which carbonates did not accumulate in the last 4 millennia. The shortest break in aragonite deposition occurred over just a 2 cm interval in core 8A (~1820 – 1835 AD, Fig. 3.11) and other intervals of non-calcareous sediments suggest that these cessations lasted on the order of decades to centuries. A number of mechanisms could cause carbonate deposition to cease. The simplest mechanism is that $CaCO_3$ production stops in the surface waters due to nutrient limitation and low primary productivity. Indeed, this is the interpretation offered by Pasche *et al.* (2010) for the most recent onset of carbonate deposition (~50 years ago) reported for their Kibuye core (i.e. that nutrient input and primary productivity increased starting ~1960 AD). However, the large reservoir of Ca^{2+} in the lake (estimated at 3,250 $x10^7$ kg Ca) compared to the amount that leaves via the Ruzizi river (1.66 $x10^7$ kg Ca/yr; Table 4.1) suggests that lower primary productivity alone cannot account for complete carbonate cessation. Another possible mechanism for variable carbonate deposition would be a change of water column preservation potential. As mentioned in previous sections, carbonate preservation is linked to a number of water column factors such as pH, temperature, and pressure. Preservation is complicated in Lake Kivu by the number of contributing sources of water and solutes, all influencing the water chemistry. Episodic disruption of carbonate sedimentation might therefore reflect a history of variable sub-lacustrine input of hydrothermal water to the lake. This would certainly be impacted by changes in regional volcanic activity and, perhaps, even by tectonic re-

configuration ("re-plumbing") of the hydrothermal groundwater system in the Kivu basin. At this time however, a clear mechanism for $CaCO_3$ cessation in the sediment record has not been established.

Results of this study reveal relative concordance with bulk stratigraphy previously reported by Haberyan and Hecky (1987) but with a shift in timing of hydrothermal onset. Here I report hydrothermal onset to begin just prior to 4,230 years BP with the occurrence of $CaCO_3$ sedimentation as opposed to the long-standing interpretation of hydrothermal onset marked by the first appearance of organic-rich, brown layers (Fig. C, Appendix 4), dated by Haberyan and Hecky (1987) to occur around 5,000 years BP. Stratigraphically, this first brown layer overlies a significant carbonate-rich interval and our new chronology for Lake Kivu sediments estimates an age for this brown layer that is much later in the Holocene (e.g. 2,740 years BP). Again, however, this study demonstrates the relatively high degree of influence that the Ca-rich, sub-lacustrine hydrothermal waters have on the $CaCO_3$ sedimentation/ deposition potential of Lake Kivu, thus making the carbonate sediment record a valid indicator of hydrothermal activity.

6 SUGGESTIONS FOR FUTURE WORK

Future research in the Kivu basin should include the collection of more groundwater hydrology data to better constrain the "plumbing" of the basin and exactly which solutes (and how much) are supplied via this route. Groundwater from the region should be analyzed for stable isotopes of ^{13}C, ^{18}O, and deuterium in addition to major ion concentrations. The study should concentrate on the Virunga volcanic field along Kivu's north shore, but include data from around the basin and at varying proximities to the lake. Perhaps, in addition to these hydrologic tracers, the volcanic history of the region could also be compiled and compared to certain volcanic geochemical tracers in the sediment record. Certainly constraining the timing of major volcanic/ tectonic events would help elucidate their relative influence on the late-Holocene record and especially in the context of carbonate deposition turning on and off.

More work needs to be done to understand the origin and significance of the unique brown sediment layers that are found in the late-Holocene Kivu sediments. Analyses for specific biomarkers and their isotopic composition will surely help resolve some first order stratigraphic observations and will have implications for the late-Holocene history of Lake Kivu.

I have presented in this study a relatively robust age model for the Holocene sediments of Lake Kivu. Additional sedimentological and geochemical analyses on these cores will continue to add to the refinement of interpreting Kivu's unique paleolimnology, within the context of the regional history.

BIBLIOGRAPHY

Appleby, P. G., Birks, H. H., Flower, R. J., Rose, N., Peglar, S. M., Ramdani, M., . . . Fathi, A. A. (2001). Radiometrically determined dates and sedimentation rates for recent sediments in nine North African wetland lakes (the CASSARINA project). *Aquatic Ecology, 35*(3-4), 347-367. doi: 10.1023/a:1011938522939

Beadle, L. (1974). *The inland waters of tropical Africa* (1 ed.). London: Longman Group Limited.

Botz, R., Stoffers, P., Faber, E., & Tietze, K. (1988). Isotope geochemistry of carbonate sediments from Lake Kivu (East-Central Africa) (Vol. 69, pp. 299-308): Chemical Geology.

Degens, E. (1973). Salts in the Sea (Vol. 243, pp. 504-507): Nature.

Degens, E., von Herzen, R., Wong, H.-K., Deuser, W., & Jannasch, H. (1972). Lake Kivu: Structure, Chemistry and Biology of an East African Rift Lake (Vol. 62, pp. 245-277): Geol Rundsch.

deMenocal, P., Ortiz, J., Guilderson, T., & Sarnthein, M. (2000). Coherent high- and low-latitude climate variability during the holocene warm period. *Science, 288*(5474), 2198-2202. doi: 10.1126/science.288.5474.2198

Faure, G. (1977). *Principles of isotope geology*.

Gale, S. J. (2009). Event chronostratigraphy: A high-resolution tool for dating the recent past. *Quaternary Geochronology, 4*(5), 391-399. doi: 10.1016/j.quageo.2008.12.003

Gasse, F. (1986). *East African diatoms : taxonomy, ecological distribution*. Berlin: J. Cramer.

Gasse, F., Talling, J. F., & Kilham, P. (1983). DIATOM ASSEMBLAGES IN EAST AFRICA CLASSIFICATION DISTRIBUTION AND ECOLOGY. *Revue d'Hydrobiologie Tropicale, 16*(1), 3-34.

Haberyan, K. A., & Hecky, R. E. (1987). THE LATE PLEISTOCENE AND HOLOCENE STRATIGRAPHY AND PALEOLIMNOLOGY OF LAKES KIVU AND TANGANYIKA ZAIRE. *Palaeogeography Palaeoclimatology Palaeoecology, 61*(3-4), 169-198. doi: 10.1016/0031-0182(87)90048-4

Hammer, U., Shamess, J., & Haynes, C. (1983). The distribution and abundance of algae in saline lakes of Saskatchewan, Canada (Vol. 105, pp. 1-26): Hydrobiologia.

Heiri, O., Lotter, A. F., & Lemcke, G. (2001). Loss on ignition as a method for estimating organic and carbonate content in sediments: reproducibility and comparability of results. *Journal of Paleolimnology, 25*(1), 101-110. doi: 10.1023/a:1008119611481

Hoefs, J. (1997). *Stable Isotope Geochemistry* (4 ed.). Berlin: Springer-Verlag.

Hollander, D. J., & Smith, M. A. (2001). Microbially mediated carbon cycling as a control on the delta C-13 of sedimentary carbon in eutrophic Lake Mendota (USA): New models for interpreting isotopic excursions in the sedimentary record. *Geochimica Et Cosmochimica Acta, 65*(23), 4321-4337. doi: 10.1016/s0016-7037(00)00506-8

Johnson, T., & Odada, E. (1996). *The limnology, climatology and paleoclimatology of the East African Lakes* (T. Johnson & E. Odada Eds.). Amsterdam: Gordon & Breach Publishers.

Johnson, T. C., Brown, E. T., & Shi, J. (2011). Biogenic silica deposition in Lake Malawi, East Africa over the past 150,000 years. *Palaeogeography Palaeoclimatology Palaeoecology, 303*(1-4), 103-109. doi: 10.1016/j.palaeo.2010.01.024

Kelts, K., & Hsu, K. (1978). Freshwater Carbonate Sedimentation. In A. Lerman (Ed.), *Lakes: chemistry, geology and physics*. New York: Springer-Verlag.

Kilham, P., Kilham, S., & Hecky, R. (1986). Hypothesized resource relationships among African planktonic diatoms. (Vol. 31, pp. 1169-1181): Limnology and Oceanography.

Kim, S.-T., O'Neil, J. R., Hillaire-Marcel, C., & Mucci, A. (2007). Oxygen isotope fractionation between synthetic aragonite and water: Influence of temperature and Mg2+ concentration. *Geochimica Et Cosmochimica Acta, 71*(19), 4704-4715. doi: 10.1016/j.gca.2007.04.019

Leng, M. J., & Marshall, J. D. (2004). Palaeoclimate interpretation of stable isotope data from lake sediment archives. *Quaternary Science Reviews, 23*(7-8), 811-831. doi: 10.1016/j.quascirev.2003.06.012

MacKenzie, A. B., Hardie, S. M. L., Farmer, J. G., Eades, L. J., & Pulford, I. D. (2011). Analytical and sampling constraints in Pb-210 dating. *Science of the Total Environment, 409*(7), 1298-1304. doi: 10.1016/j.scitotenv.2010.11.040

Meyers, P. A. (2003). Applications of organic geochemistry to paleolimnological reconstructions: a summary of examples from the Laurentian Great Lakes. *Organic Geochemistry, 34*(2), 261-289. doi: 10.1016/s0146-6380(02)00168-7

Mueller, G., Irion, G., & Foerstner, U. (1972). Formation and diagenesis of inorganic Ca-Mg carbonates in the lacustrine environment. (pp. 158-164): Naturwissenschaften.

Muvundja, F., Weust, A., Isumbisho, M., Kaningini, M., Pasche, N., Rinta, P., & Schmid, M. (2014). Modelling Lake Kivu water level variations over the last seven decades (Vol. 47, pp. 21-33): Limnologica.

Muvundja, F. A., Pasche, N., Bugenyi, F. W. B., Isumbisho, M., Mueller, B., Namugize, J.-N., . . . Wueest, A. (2009). Balancing nutrient inputs to Lake Kivu. *Journal of Great Lakes Research, 35*(3), 406-418. doi: 10.1016/j.jglr.2009.06.002

Pasche, N., Alunga, G., Mills, K., Muvundja, F., Ryves, D. B., Schurter, M., . . . Schmid, M. (2010). Abrupt onset of carbonate deposition in Lake Kivu during the 1960s: response to recent environmental changes. *Journal of Paleolimnology, 44*(4), 931-946. doi: 10.1007/s10933-010-9465-x

Pasche, N., Dinkel, C., Mueller, B., Schmid, M., Wueest, A., & Wehrli, B. (2009). Physical and biogeochemical limits to internal nutrient loading of meromictic Lake Kivu. *Limnology and Oceanography, 54*(6), 1863-1873. doi: 10.4319/lo.2009.54.6.1863

Pasche, N., Schmid, M., Vazquez, F., Schubert, C. J., Wueest, A., Kessler, J. D., . . . Buergmann, H. (2011). Methane sources and sinks in Lake Kivu. *Journal of Geophysical Research-Biogeosciences, 116*. doi: 10.1029/2011jg001690

Robbins, J. (1978). Geochemical and geographical applications of radioactive lead. In J. Nriagu (Ed.), *Biogeochemistry of Lead* (pp. 285-337). Amsterdam: Elsevier.

Robbins, J. & Edington, D. (1975). Determination of recent sedimentation rates in Lake Michigan using lead-210 and cesium-137. *Geochem. Cosmochim. Acta, 39, 245*.

Rozanski, K., Araguas-Araguas, L., & Gonfiantini, R. (1993). Isotopic patterns in modern global precipitation. (Vol. 78, pp. 1-36): Geophycial Monographs.

Russell, J. M., & Johnson, T. C. (2007). Little Ice Age drought in equatorial Africa: Intertropical Convergence Zone migrations and El Nino-Southern Oscillation variability. *Geology, 35*(1), 21-24. doi: 10.1130/g23125a.1

Russell, J. M., Johnson, T. C., Kelts, K. R., Laerdal, T., & Talbot, M. R. (2003). An 11 000-year lithostratigraphic and paleohydrologic record from Equatorial Africa: Lake Edward, Uganda-Congo. *Palaeogeography Palaeoclimatology Palaeoecology, 193*(1), 25-49. doi: 10.1016/s0031-0182(02)00709-5

Santisteban, J. I., Mediavilla, R., Lopez-Pamo, E., Dabrio, C. J., Zapata, M. B. R., Garcia, M. J. G., . . . Martinez-Alfaro, P. E. (2004). Loss on ignition: a qualitative or quantitative method for organic matter and carbonate mineral content in sediments? *Journal of Paleolimnology, 32*(3), 287-299. doi: 10.1023/B:JOPL.0000042999.30131.5b

Schmid, M., Busbridge, M., & Wueest, A. (2010). Double-diffusive convection in Lake Kivu. *Limnology and Oceanography, 55*(1), 225-238. doi: 10.4319/lo.2010.55.1.0225

Schmid, M., Halbwachs, M., Wehrli, B., & Wuest, A. (2005). Weak mixing in Lake Kivu: New insights indicate increasing risk of uncontrolled gas eruption. *Geochemistry Geophysics Geosystems, 6*. doi: 10.1029/2004gc000892

Schnurrenberger, D., Russell, J., & Kelts, K. (2003). Classification of lacustrine sediments based on sedimentary components. *Journal of Paleolimnology, 29*(2), 141-154. doi: 10.1023/a:1023270324800

Sharp, Z. (2007). *Principles of stable isotope geochemistry* (C. Rapp Ed. 1 ed.). New Jersey: Pearson Prentice Hall.

Steinman, B. A., & Abbott, M. B. (2013). Isotopic and hydrologic responses of small, closed lakes to climate variability: Hydroclimate reconstructions from lake sediment oxygen isotope records and mass balance models. *Geochimica Et Cosmochimica Acta, 105*, 342-359. doi: 10.1016/j.gca.2012.11.027

Stoffers, P., & Fischbeck, R. (1974). Monohydrocalcite in the sediments of Lake Kivu (East Africa) (Vol. 21, pp. 163-170): Sedimentology.

Stoffers, P., & Hecky, R. (1978). Late Pleistocene-Holocence evolution of the Kivu-Tanganyika Basin (Vol. 2, pp. 43-55): Int. Asssociation of Sedimentologists.

Talbot, M. (1990). A review of the paleohydrological interpretation of carbon and oxygen isotopic ratios in primary lacustrine carbonates. (Vol. 80, pp. 261-279): Chemical Geology.

Talbot, M. R., Filippi, M. L., Jensen, N. B., & Tiercelin, J.-J. (2007). An abrupt change in the African monsoon at the end of the Younger Dryas. *Geochemistry Geophysics Geosystems, 8*. doi: 10.1029/2006gc001465

Tassi, F., Vaselli, O., Tedesco, D., Montegrossi, G., Darrah, T., Cuoco, E., . . . Huertas, A. D. (2009). Water and gas chemistry at Lake Kivu (DRC): Geochemical evidence of vertical and horizontal heterogeneities in a multibasin structure. *Geochemistry Geophysics Geosystems, 10*. doi: 10.1029/2008gc002191

Tedesco, D., Tassi, F., Vaselli, O., Poreda, R. J., Darrah, T., Cuoco, E., & Yalire, M. M. (2010). Gas isotopic signatures (He, C, and Ar) in the Lake Kivu region (western branch of the East African rift system): Geodynamic and volcanological implications. *Journal of Geophysical Research-Solid Earth, 115*. doi: 10.1029/2008jb006227

Tierney, J. E., Lewis, S. C., Cook, B. I., LeGrande, A. N., & Schmidt, G. A. (2011). Model, proxy and isotopic perspectives on the East African Humid Period. *Earth and Planetary Science Letters, 307*(1-2), 103-112. doi: 10.1016/j.epsl.2011.04.038

Tierney, J. E., Russell, J. M., Huang, Y., Damste, J. S. S., Hopmans, E. C., & Cohen, A. S. (2008). Northern hemisphere controls on tropical southeast African climate during the past 60,000 years. *Science, 322*(5899), 252-255. doi: 10.1126/science.1160485

Wetzel, R. (1975). The inorganic carbon complex *Limnology: lake and river ecosystems* (3 ed.): Academic Press.

APPENDIX 1

SEDIMENT CORE DATA TABLES

K12-19A BULK

Section	Depth in section (cm)	cmblf (sed top)	Cal Years BP	NOTE	% TIC	% OC loi	% water content	Si:Ti (XRF)	(proxy) %Bsi	g/cm3 bulk dry sed	porosity, ϕ
19A_1	90-90.5	**72.25**	807	disturbed	1.80	14.79	0.928	NA			
19A_1	95-95.5	**77.25**	872	disturbed	1.75	15.47	0.930	NA			
19A_1	100-100.5	**82.25**	938	disturbed	1.72	14.73	0.927	NA			
19A_1	105-105.5	**87.25**	1003	disturbed	1.74	14.87	0.928	NA			
19A_1	110-110.5	**92.25**	1068	disturbed	1.72	14.88	0.930	NA			
19A_1	115-115.5	**97.25**	1133	disturbed	1.76	15.04	0.926	NA			
19A_1	120-120.5	**102.25**	1198	disturbed	1.54	14.79	0.930	NA			
19A_1	125-125.5	**107.25**	1263	disturbed	1.72	15.18	0.929	NA			
19A_1	130-130.5	**112.25**	1328	disturbed	1.81	14.54	0.929	NA			
19A_1	135-135.5	**117.25**	1393	disturbed	1.61	14.89	0.929	NA			
19A_1	140-140.5	**122.25**	1458	disturbed	1.66	15.86	0.931	NA			
19A_2	0-0.5	**122.75**	1465		0.33		0.918	0.427	53.84	2.30	0.963
19A_2	5-5.5	**127.75**	1530		0.25	14.34	0.928	0.578	75.49	1.69	0.956
19A_2	10-10.5	**132.75**	1595		0.38	15.63	0.943	0.058	1.11	2.13	0.972
19A_2	15-15.5	**137.75**	1660		0.28	15.54	0.939	0.500	64.29	1.72	0.964
19A_2	20-20.5	**142.75**	1725		0.42	16.81	0.930	0.194	20.62	1.96	0.963
19A_2	23.5-24	**146.5**	1774		0.24	12.36	0.931	0.258	29.76	2.05	0.965
19A_2	25-25.5	**148**	1794		0.54	16.99	0.934	0.318	38.32	1.84	0.963
19A_2	27-27.5	**150**	1820		0.26	12.58	0.925	0.317	38.19	1.99	0.961
19A_2	30-30.5	**153**	1859	BL	0.58	30.34	0.914	0.130	11.44	1.57	0.943
19A_2	31-31.5	**154**	1872	BL	0.48	31.40	0.914	0.133	11.88	1.54	0.942
19A_2	35-35.5	**158**	1924		3.99	10.74	0.915	0.293	34.68	2.07	0.957
19A_2	40-40.5	**163**	1989		3.43	12.70	0.921	0.202	21.77	2.09	0.960
19A_2	45-45.5	**168**	2054		3.53	12.02	0.911	0.154	14.87	2.16	0.957
19A_2	50-50.5	**173**	2119		3.90	12.80	0.912	0.296	35.08	2.00	0.954
19A_2	55-55.5	**178**	2184		3.95	12.41	0.909	0.291	34.45	2.02	0.953
19A_2	60-60.5	**183**	2249		4.68	11.86	0.913	0.317	38.09	2.01	0.955
19A_2	65-65.5	**188**	2314		5.46	10.02	0.891	0.061	1.57	2.31	0.950
19A_2	70-70.5	**193**	2380	ash?	3.42	7.50	0.870	0.218	23.97	2.25	0.938
19A_2	75-75.5	**198**	2445		4.27	12.05	0.913	0.441	55.87	1.89	0.952
19A_2	80-80.5	**203**	2510		0.66	15.64	0.941	0.569	74.20	1.65	0.963
19A_2	85-85.5	**208**	2575		0.27	16.16	0.943	0.442	56.04	1.75	0.967
19A_2	88.5-89	**211.5**	2620		0.27	14.66	0.932	0.214	23.45	2.01	0.965
19A_2	90-90.5	**213**	2640		0.24	15.54	0.933	0.221	24.49	1.98	0.965

Section	Depth in section (cm)	cmblf (sed top)	Cal Years BP	NOTE	% TIC	% OC loi	% water content	Si:Ti (XRF)	(proxy) %Bsi	g/cm3 bulk dry sed	porosity, ϕ
19A_2	95-95.5	**218**	2705		0.12	16.53	0.908	0.124	10.54	2.04	0.953
19A_2	97-97.5	**220**	2731		0.14	17.46	0.917	0.255	29.26	1.88	0.954
19A_2	100-100.5	**223**	2770		0.10	13.27	0.914	0.233	26.17	2.04	0.956
19A_3	0-0.5	**225**	2796		0.25	14.59	0.884	NA			
19A_3	2-2.5	**227**	2822	BL	0.03	17.86	0.892	0.145	13.55	1.97	0.942
19A_3	5-5.5	**230**	2861		0.07	10.80	0.906	0.459	58.39	1.91	0.949
19A_3	6-6.5	**231**	2874	BL	0.47	19.27	0.902	0.276	32.24	1.80	0.943
19A_3	8-8.5	**233**	2900	BL	0.55	14.69	0.859	0.088	5.47	2.13	0.929
19A_3	10-10.5	**235**	2926		2.51	11.01	0.873	0.391	48.69	1.97	0.931
19A_3	15-15.5	**240**	2991		3.46	8.73	0.794	0.177	18.17	2.24	0.896
19A_3	20-20.5	**245**	3057		3.54	8.39	0.804	0.132	11.77	2.30	0.904
19A_3	25-25.5	**250**	3122		4.07	8.51	0.822	0.367	45.35	2.07	0.906
19A_3	30-30.5	**255**	3187		4.55	8.09	0.816	0.573	74.72	1.90	0.894
19A_3	35-35.5	**260**	3252		4.50	8.43	0.822	0.473	60.43	1.98	0.901
19A_3	40-40.5	**265**	3317		3.71	9.15	0.822	0.774	103.41	1.68	0.886
19A_3	45-45.5	**270**	3382		4.90	8.32	0.798	0.881	118.72	1.60	0.864
19A_3	50-50.5	**275**	3447		4.56	8.38	0.803	0.529	68.44	1.93	0.887
19A_3	55-55.5	**280**	3512		4.44	7.96	0.792	0.633	83.27	1.85	0.875
19A_3	60-60.5	**285**	3577		3.78	8.40	0.829	0.631	82.95	1.83	0.899
19A_3	65-65.5	**290**	3642		4.11	7.88	0.793	0.572	74.59	1.91	0.879
19A_3	70-70.5	**295**	3708		3.34	8.67	0.816	0.467	59.61	1.98	0.898
19A_4	2-2.5	**299.5**	3766		0.75	4.74	0.763	0.379	47.05	2.19	0.876
19A_4	5-5.5	**302.5**	3805		2.55	6.64	0.820	0.252	28.91	2.24	0.911
19A_4	10-10.5	**307.5**	3870		2.64	8.27	0.823	0.449	56.98	2.01	0.903
19A_4	15-15.5	**312.5**	3935		3.13	7.98	0.818	0.618	81.18	1.86	0.893
19A_4	20-20.5	**317.5**	4001		2.06	8.54	0.796	0.403	50.46	2.04	0.888
19A_4	25-25.5	**322.5**	4066		0.91	10.56	0.861	0.606	79.44	1.79	0.917
19A_4	30-30.5	**327.5**	4131		1.11	9.14	0.832	0.360	44.32	2.06	0.911
19A_4	35-35.5	**332.5**	4196		0.18	9.17	0.880	0.661	87.31	1.78	0.929
19A_4	40-40.5	**337.5**	4261		0.10	7.43	0.874	0.196	20.92	2.27	0.940
19A_4	45-45.5	**342.5**	4326		0.06	8.11	0.788	0.336	40.81	2.12	0.887
19A_4	50-50.5	**347.5**	4391		0.06	10.96	0.796	0.650	85.78	1.73	0.871
19A_4	55-55.5	**352.5**	4456		0.02	12.71	0.833	0.600	78.58	1.72	0.896
19A_4	60-60.5	**357.5**	4521		0.01	13.18	0.825	0.542	70.28	1.76	0.892
19A_4	65-65.5	**362.5**	4586		0.01	12.05	0.831	0.506	65.16	1.83	0.900
19A_4	70-70.5	**367.5**	4652		0.01	12.73	0.833	0.718	95.48	1.61	0.889

Section	Depth in section (cm)	cmblf (sed top)	Cal Years BP	NOTE	% TIC	% OC loi	% water content	Si:Ti (XRF)	(proxy) %Bsi	g/cm3 bulk dry sed	porosity, ϕ
19A_4	75-75.5	**372.5**	4717		0.02	13.08	0.841	0.550	71.40	1.75	0.903
19A_4	80-80.5	**377.5**	4782		0.01	12.62	0.855	0.997	135.33	1.35	0.889
19A_5	1-1.5	**383**	4853		0.02	12.70	0.832	0.289	34.20	2.01	0.909
19A_5	5-5.5	**387**	4905		0.04	13.14	0.849	0.307	36.78	1.98	0.918
19A_5	10-10.5	**392**	4971		0.01	12.26	0.871	0.765	102.22	1.58	0.915
19A_5	15-15.5	**397**	5036		0.02	12.16	0.861	0.316	38.01	2.00	0.925
19A_5	20-20.5	**402**	5101		0.14	11.01	0.840	0.366	45.18	1.99	0.913
19A_5	25-25.5	**407**	5166	ash?	0.02	8.84	0.811	0.144	13.46	2.27	0.907
19A_5	30-30.5	**412**	5231		0.08	10.40	0.864	0.359	44.13	2.02	0.928
19A_5	35-35.5	**417**	5296		0.10	10.08	0.866	0.480	61.46	1.92	0.926
19A_5	40-40.5	**422**	5361		0.13	10.33	0.879	0.468	59.76	1.92	0.933
19A_5	45-45.5	**427**	5426		0.22	10.55	0.878	0.779	104.12	1.62	0.922
19A_5	50-50.5	**432**	5491		0.17	10.27	0.856	0.558	72.64	1.84	0.916
19A_5	55-55.5	**437**	5556		0.15	10.38	0.867	0.636	83.70	1.76	0.920
19A_5	60-60.5	**442**	5622		0.13	12.36	0.883	0.442	56.01	1.88	0.934
19A_5	65-65.5	**447**	5687		0.18	11.05	0.883	0.803	107.57	1.59	0.923
19A_6	1.5-2	**452.5**	5758		0.04	11.41	0.869	0.284	33.37	2.06	0.932
19A_6	5-5.5	**456**	5804		0.37	17.65	0.895	0.118	9.73	2.00	0.945
19A_6	10-10.5	**461**	5869		0.11	7.79	0.896	1.425	196.50	1.12	0.906
19A_6	15-15.5	**466**	5934		0.04	8.71	0.899	0.284	33.44	2.15	0.950
19A_6	20-20.5	**471**	5999		0.04	12.87	0.905	0.296	35.09	2.00	0.950
19A_6	25-25.5	**476**	6064		0.02	11.62	0.886	0.589	76.95	1.77	0.932
19A_6	30-30.5	**481**	6129		0.01	4.83	0.901	0.119	9.89	2.43	0.957
19A_6	35-35.5	**486**	6194		0.01	8.45	0.884	0.473	60.47	1.98	0.938
19A_6	40-40.5	**491**	6259		0.05	7.66	0.861	0.446	56.57	2.03	0.926
19A_6	45-45.5	**496**	6325		0.03	8.78	0.871	0.259	29.85	2.17	0.936
19A_6	50-50.5	**501**	6390		0.04	6.68	0.870	0.683	90.44	1.84	0.925
19A_6	55-55.5	**506**	6455		0.26	11.93	0.891	0.349	42.77	1.98	0.942
19A_6	57-57.5	**508**	6481	Diatomite	0.26	3.13	0.895	0.858	115.40	1.80	0.939
19A_6	60-60.5	**511**	6520		0.05	8.10	0.859	0.362	44.51	2.09	0.927
19A_6	65-65.5	**516**	6585		0.05	8.04	0.889	0.377	46.79	2.08	0.943
19A_6	70-70.5	**521**	6650		0.05	8.60	0.871	0.492	63.15	1.96	0.929
19A_6	75-75.5	**526**	6715		0.03	8.29	0.853	0.279	32.79	2.16	0.926
19A_6	80-80.5	**531**	6780		0.02	6.56	0.864	0.329	39.87	2.17	0.932
19A_6	85-85.5	**536**	6845		0.01	4.98	0.854	0.254	29.15	2.30	0.931
19A_6	90-90.5	**541**	6910	silt, mica	0.13	4.74	0.608	0.067	2.38	2.48	0.793

Section	Depth in section (cm)	cmblf (sed top)	Cal Years BP	NOTE	% TIC	% OC loi	% water content	Si:Ti (XRF)	(proxy) %Bsi	g/cm3 bulk dry sed	porosity, ϕ
19A_6	95-95.5	**546**	6976	f. sand/silt	0.00	8.01	0.755	0.075	3.61	2.36	0.879
19A_6	100-100.5	**551**	7041	silt	0.03	8.13	0.761	0.064	2.06	2.37	0.883
19A_6	105-105.5	**556**	7106		0.00	6.10	0.810	0.189	19.80	2.32	0.908
19A_6	110-110.5	**561**	7171		0.54	4.21	0.876	0.364	44.83	2.22	0.940
19A_6	115.5-116	**566.5**	7243	silt	0.38	5.45	0.582	0.087	5.24	2.44	0.772
19A_6	120-120.5	**571**	7301	silt	1.16	6.19	0.629	0.085	5.05	2.41	0.803
19A_6	125-125.5	**576**	7366	f. sand/silt	0.36	7.65	0.699	0.078	3.95	2.37	0.847
19A_6	130-130.5	**581**	7431	f.sand, mica	0.27	2.23	0.454	0.145	13.58	2.49	0.674
19A_6	135-135.5	**586**	7496		0.50	6.83	0.843	0.200	21.49	2.29	0.925
19A_6	140-140.5	**591**	7561		0.17	6.55	0.882	0.650	85.67	1.88	0.933
19A_6	145-145.5	**596**	7627		0.16	8.18	0.856	0.444	56.22	2.01	0.923
19A_7	3-3.5	**603.5**	7724		0.26	11.62	0.865	0.228	25.45	2.10	0.931
19A_7	5-5.5	**605.5**	7750		0.18	11.19	0.864	0.321	38.75	2.03	0.928
19A_7	10-10.5	**610.5**	7815		0.36	12.10	0.871	0.594	77.75	1.75	0.922
19A_7	15-15.5	**615.5**	7880		0.19	10.12	0.802	0.164	16.24	2.21	0.899
19A_7	20-20.5	**620.5**	7946		0.19	10.77	0.846	0.216	23.74	2.14	0.921
19A_7	25-25.5	**625.5**	8011		0.24	12.14	0.856	0.196	20.81	2.11	0.926
19A_7	30-30.5	**630.5**	8076		0.18	16.54	0.874	0.217	23.83	1.95	0.931
19A_7	35-35.5	**635.5**	8141		0.00	13.74	0.854	0.186	19.43	2.07	0.924
19A_7	40-40.5	**640.5**	8206		0.00	10.54	0.843	0.322	38.82	2.05	0.916
19A_7	45-45.5	**645.5**	8271		0.00	10.38	0.859	0.474	60.64	1.91	0.921
19A_7	50-50.5	**650.5**	8336		0.00	9.45	0.848	0.500	64.36	1.92	0.915
19A_7	55-55.5	**655.5**	8401		0.04	9.38	0.820	0.535	69.26	1.89	0.896
19A_7	60-60.5	**660.5**	8466		0.02	11.28	0.849	0.222	24.52	2.12	0.923
19A_7	65-65.5	**665.5**	8531		0.01	14.43	0.862	0.190	20.01	2.04	0.928
19A_7	70-70.5	**670.5**	8597		0.01	11.66	0.812	0.173	17.58	2.15	0.903
19A_7	75-75.5	**675.5**	8662		0.06	10.11	0.748	0.096	6.52	2.27	0.871
19A_7	80-80.5	**680.5**	8727		0.05	9.90	0.747	0.105	7.82	2.27	0.870
19A_7	85-85.5	**685.5**	8792		0.01	14.98	0.846	0.247	28.11	1.97	0.916
19A_7	90-90.5	**690.5**	8857		0.01	12.26	0.831	0.205	22.11	2.10	0.912
19A_7	95-95.5	**695.5**	8922		0.01	12.27	0.846	0.176	18.01	2.13	0.921
19A_7	100-100.5	**700.5**	8987		0.04	12.76	0.834	0.155	15.02	2.13	0.915
19A_7	105-105.5	**705.5**	9052		0.01	14.75	0.846	0.121	10.13	2.10	0.920
19A_7	110-110.5	**710.5**	9117		0.01	11.40	0.822	0.112	8.88	2.22	0.911
19A_7	115-115.5	**715.5**	9182		0.01	19.33	0.863	0.123	10.42	1.94	0.925

Section	Depth in section (cm)	cmblf (sed top)	Cal Years BP	NOTE	% TIC	% OC loi	% water content	Si:Ti (XRF)	(proxy) %Bsi	g/cm3 bulk dry sed	porosity, ϕ
19A_7	120-120.5	**720.5**	9248		0.01	15.66	0.881	0.330	40.06	1.87	0.933
19A_7	125-125.5	**725.5**	9313		0.01	12.14	0.840	0.334	40.61	1.99	0.913
19A_7	130-130.5	**730.5**	9378		0.01	13.59	0.862	0.346	42.31	1.93	0.924
19A_7	135-135.5	**735.5**	9443		0.03	11.98	0.848	0.201	21.55	2.11	0.922
19A_7	140-140.5	**740.5**	9508		0.01	11.25	0.850	0.115	9.32	2.22	0.926
19A_7	145-145.5	**745.5**	9573		0.01	10.58	0.834	0.301	35.90	2.07	0.912
19A_8	0-0.5	**750.5**	9638		0.01	7.65	0.858	0.263	30.38	2.20	0.930
19A_8	5-5.5	**755.5**	9703		0.01	8.68	0.825	0.252	28.81	2.18	0.911
19A_8	10-10.5	**760.5**	9768		0.01	8.99	0.785	0.297	35.25	2.12	0.886
19A_8	15-15.5	**765.5**	9833		0.01	10.85	0.832	0.243	27.55	2.11	0.913
19A_8	20-20.5	**770.5**	9899		0.02	9.20	0.733	0.233	26.19	2.18	0.857
19A_8	25-25.5	**775.5**	9964		0.02	8.03	0.823	0.306	36.61	2.15	0.909
19A_8	30-30.5	**780.5**	10029		0.02	12.18	0.851	0.318	38.35	2.00	0.919
19A_8	35-35.5	**785.5**	10094		0.01	8.92	0.788	0.403	50.48	2.03	0.883
19A_8	40-40.5	**790.5**	10159		0.02	8.43	0.822	0.446	56.61	2.00	0.902
19A_8	45-45.5	**795.5**	10224		0.01	8.97	0.737	0.153	14.74	2.26	0.863
19A_8	50-50.5	**800.5**	10289		0.01	11.25	0.684	0.180	18.59	2.16	0.824
19A_8	55-55.5	**805.5**	10354		0.01	10.00	0.715	0.207	22.48	2.17	0.845
19A_8	60-60.5	**810.5**	10419		0.01	10.31	0.739	0.108	8.25	2.26	0.865
19A_8	65-65.5	**815.5**	10484		0.10	7.17	0.807	0.148	14.00	2.32	0.907
19A_8	70-70.5	**820.5**	10550		0.01	7.20	0.737	0.158	15.37	2.31	0.866
19A_8	75-75.5	**825.5**	10615		0.03	10.12	0.788	0.086	5.16	2.28	0.895
19A_8	80-80.5	**830.5**	10680		0.24	8.29	0.660	0.077	3.88	2.35	0.820
19A_8	85-85.5	**835.5**	10745	mixed sand	0.24	0.87	0.165	0.080	4.27	2.59	0.339
19A_8	88-88.5	**838.5**	10784	sand	0.38	2.15	0.253	NA			

K12-15A BULK

Section	section depth (cm)	cmblf	NOTE	%TIC	%OC EA	%water content
15A-1K-1	0-0.5	**0.25**	disturbed	3.261	12.09	0.882
15A-1K-1	5-5.5	**5.25**	disturbed	3.344	12.10	0.878
15A-1K-1	10-10.5	**10.25**	disturbed	3.7421	12.48	0.874
15A-1K-1	15-15.5	**15.25**	disturbed	4.2016	12.31	0.875
15A-1K-1	20-20.5	**20.25**	disturbed	4.1367	12.50	0.872
15A-1K-1	25-25.5	**25.25**	disturbed	3.3274	12.03	0.870
15A-1K-1	30-30.5	**30.25**	disturbed	3.5631	12.90	0.874
15A-1K-1	35-35.5	**35.25**	disturbed	3.5584	13.26	0.865
15A-1K-1	40-40.5	**40.25**		3.6126	12.26	0.806
15A-1K-1	45-45.5	**45.25**		3.4997	12.07	0.906
15A-1K-1	50-50.5	**50.25**		3.6012	12.34	0.886
15A-1K-1	55-55.5	**55.25**		0.2563	17.88	0.905
15A-1K-1	60-60.5	**60.25**		0.397	10.84	0.906
15A-1K-1	65-65.5	**65.25**		0.291	16.16	0.915
15A-1K-1	68-68.5	**68.25**	BL	0.3071	19.01	0.914
15A-1K-1	68.5-69	**68.75**	BL	0.3735	21.92	0.916
15A-1K-1	69-69.5	**69.25**	BL	0.2647	24.99	0.918
15A-1K-1	69.5-70	**69.75**	BL	0.4157	26.53	0.919
15A-1K-1	70-70.5	**70.25**	BL	0.432	28.23	0.924
15A-1K-1	70.5-71	**70.75**	BL	0.6475	27.97	0.924
15A-1K-1	71-71.5	**71.25**	BL	0.5748	20.87	0.922
15A-1K-1	71.5-72	**71.75**		0.574	18.51	0.923
15A-1K-1	72-72.5	**72.25**		0.5822	17.73	0.925
15A-1K-1	72.5-73	**72.75**		0.4532	16.51	0.929
15A-1K-1	73-73.5	**73.25**		0.4022	15.05	0.931
15A-1K-1	73.5-74	**73.75**		0.3693	14.15	0.934
15A-1K-1	79-79.5	**79.25**		0.3333	17.59	0.935
15A-1K-1	84-84.5	**84.25**		0.4715	15.51	0.935
15A-1K-1	89-89.5	**89.25**		0.5355	14.93	0.931
15A-1K-1	91.5-92	**91.75**		0.3748	13.63	0.921
15A-1K-1	92-92.5	**92.25**		0.5512	16.71	0.921
15A-1K-1	92.5-93	**92.75**		0.7272	16.83	0.919
15A-1K-1	93-93.5	**93.25**	BL	0.4328	23.15	0.917
15A-1K-1	93.5-94	**93.75**	BL	0.3245	24.20	0.911
15A-1K-1	94-94.5	**94.25**	BL	0.5639	29.67	0.919
15A-1K-1	94.5-95	**94.75**	BL	0.4262	33.25	0.921

Section	section depth (cm)	cmblf	NOTE	%TIC	%OC EA	%water content
15A-1K-1	95-95.5	**95.25**	BL	0.4167	33.01	0.921
15A-1K-1	95.5-96	**95.75**	BL	0.4603	35.54	0.921
15A-1K-1	96-96.5	**96.25**	BL	0.56835	29.21	0.917
15A-1K-1	96.5-97	**96.75**	BL	0.7179	23.91	0.908
15A-1K-1	97-97.5	**97.25**		1.5155	16.67	0.911
15A-1K-1	97.5-98	**97.75**		1.6321	8.58	0.925
15A-1K-1	98-98.5	**98.25**		1.8064	11.42	0.912
15A-1K-2	0-0.5	**103.25**		1.7144	12.38	0.857
15A-1K-2	5-5.5	**108.25**		1.8681	11.85	0.859
15A-1K-2	10-10.5	**113.25**	BL	0.6362	31.91	0.900
15A-1K-2	15-15.5	**118.25**		1.67385	12.41	0.873
15A-1K-2	20-20.5	**123.25**		1.8468	13.32	0.867
15A-1K-2	25-25.5	**128.25**	BL	0.2671	25.54	0.901
15A-1K-2	26-26.5	**129.25**	BL	0.2037	37.51	0.908
15A-1K-2	26.5-27	**129.75**	BL	0.3146	30.05	0.898
15A-1K-2	27-27.5	**130.25**	BL	0.1769	24.18	0.889
15A-1K-2	27.5-28	**130.75**		0.2714	16.94	0.889
15A-1K-2	33-33.5	**136.25**		0.05887	12.91	0.910
15A-1K-2	38-38.5	**141.25**		0.06174	14.70	0.918
15A-1K-2	43-43.5	**146.25**		0.06845	13.10	0.914
15A-1K-2	48-48.5	**151.25**		0.1118	13.28	0.904
15A-1K-2	53-53.5	**156.25**		0.08765	8.95	0.906
15A-1K-2	58-58.5	**161.25**		2.9483	10.74	0.872
15A-1K-2	63-63.5	**166.25**		3.3766	12.19	0.884
15A-1K-2	68-68.5	**171.25**		3.5484	13.11	0.899
15A-1K-2	73-73.5	**176.25**		2.976	12.69	0.879
15A-1K-2	78-78.5	**181.25**		2.6733	11.84	0.900
15A-1K-2	83-83.5	**186.25**		0.4482	20.21	0.883
15A-1K-2	88-88.5	**191.25**		3.8185	11.66	0.883
15A-1K-2	93-93.5	**196.25**		4.5942	10.97	0.865
15A-1K-2	98-98.5	**201.25**		3.3034	13.67	0.896
15A-1K-2	103-103.5	**206.25**		0.1756	14.87	0.919
15A-1K-2	108-108.5	**211.25**		0.1739	16.20	0.917
15A-1K-2	113-113.5	**216.25**		1.0774	9.97	0.870
15A-1K-2	118-118.5	**221.25**		1.0911	9.99	0.868
15A-1K-3	3-3.5	**226.25**		0.356	15.78	0.923
15A-1K-3	8-8.5	**231.25**		0.1441	15.59	0.908

Section	section depth (cm)	cmblf	NOTE	%TIC	%OC EA	%water content
15A-1K-3	13-13.5	**236.25**		0.2572	12.76	0.900
15A-1K-3	18-18.5	**241.25**	BL	0.3942	22.57	0.887
15A-1K-3	23-23.5	**246.25**		2.5031	10.22	0.831
15A-1K-3	28-28.5	**251.25**		4.1156	10.14	0.802
15A-1K-3	33-33.5	**256.25**		3.4002	9.66	0.800
15A-1K-3	38-38.5	**261.25**		3.7381	10.55	0.797
15A-1K-3	43-43.5	**266.25**		4.1333	9.74	0.791
15A-1K-3	48-48.5	**271.25**		4.3259	9.14	0.781
15A-1K-3	53-53.5	**276.25**		4.2846	10.41	0.774
15A-1K-3	58-58.5	**281.25**		4.5327	9.64	0.782
15A-1K-3	63-63.5	**286.25**		1.7056	6.69	0.749
15A-1K-3	68-68.5	**291.25**		3.6541	7.02	0.802
15A-1K-3	73-73.5	**296.25**		3.6158	7.89	0.783
15A-1K-3	78-78.5	**301.25**		4.4246	7.32	0.739
15A-1K-3	83-83.5	**306.25**		3.3225	7.36	0.751
15A-1K-3	88-88.5	**311.25**		3.3375	7.71	0.781
15A-1K-3	93-93.5	**316.25**		3.4111	7.60	0.779
15A-1K-3	98-98.5	**321.25**			7.21	0.782
15A-1K-3	103-103.5	**326.25**			7.28	0.779
15A-1K-3	108-108.5	**331.25**		3.6631	7.27	0.777
15A-1K-3	113-113.5	**336.25**			7.87	0.778
15A-1K-3	118-118.5	**341.25**			7.58	0.778
15A-1K-3	123-123.5	**346.25**			7.57	0.782
15A-1K-3	128-128.5	**351.25**			8.05	0.778
15A-1K-4	4-4.5	**356.25**			7.50	0.772
15A-1K-4	9-9.5	**361.25**			7.27	0.777
15A-1K-4	14-14.5	**366.25**			6.77	0.723
15A-1K-4	19-19.5	**371.25**			3.67	0.808
15A-1K-4	24-24.5	**376.25**			6.01	0.740
15A-1K-4	29-29.5	**381.25**			6.25	0.743
15A-1K-4	34-34.5	**386.25**			6.82	0.727
15A-1K-4	39-39.5	**391.25**			6.71	0.723
15A-1K-4	44-44.5	**396.25**			7.32	0.748
15A-1K-4	49-49.5	**401.25**		3.2265	7.84	0.743
15A-1K-4	54-54.5	**406.25**		3.7469	7.05	0.736
15A-1K-4	59-59.5	**411.25**		4.7347	5.54	0.723
15A-1K-4	64-64.5	**416.25**		3.4534	6.51	0.766

Section	section depth (cm)	cmblf	NOTE	%TIC	%OC EA	%water content
15A-1K-4	69-69.5	**421.25**		2.8704	7.41	0.769
15A-1K-4	74-74.5	**426.25**		0.0574	2.10	0.634
15A-1K-4	79-79.5	**431.25**			8.61	0.759
15A-1K-4	84-84.5	**436.25**			8.44	0.764
15A-1K-4	89-89.5	**441.25**		3.1849	8.82	0.771
15A-1K-4	94-94.5	**446.25**			9.16	0.772
15A-1K-4	99-99.5	**451.25**			8.64	0.772
15A-1K-4	104-104.5	**456.25**			8.79	0.767
15A-1K-4	109-109.5	**461.25**			9.38	0.771
15A-1K-4	114-114.5	**466.25**			9.00	0.772
15A-1K-4	119-119.5	**471.25**		3.3159	8.61	0.766
15A-1K-4	124-124.5	**476.25**			8.11	0.761
15A-1K-4	129-129.5	**481.25**		3.4353	8.11	0.747
15A-1K-5	4-4.5	**486.25**		2.9427	5.87	0.712
15A-1K-5	9-9.5	**491.25**		1.5123	4.63	0.789
15A-1K-5	14-14.5	**496.25**			7.61	0.790
15A-1K-5	19-19.5	**501.25**			2.71	0.537
15A-1K-5	24-24.5	**506.25**		0.2267	4.92	0.807
15A-1K-5	29-29.5	**511.25**		0.7747	4.01	0.681
15A-1K-5	34-34.5	**516.25**			3.02	0.588
15A-1K-5	39-39.5	**521.25**			8.41	0.780
15A-1K-5	44-44.5	**526.25**			8.31	0.785
15A-1K-5	49-49.5	**531.25**		0.05688	7.82	0.653
15A-1K-5	54-54.5	**536.25**			7.13	0.773
15A-1K-5	59-59.5	**541.25**			5.99	0.756
15A-1K-5	64-64.5	**546.25**			9.42	0.780
15A-1K-5	69-69.5	**551.25**			10.25	0.772
15A-1K-5	74-74.5	**556.25**			9.79	0.795
15A-1K-5	79-79.5	**561.25**			3.40	0.665
15A-1K-5	84-84.5	**566.25**			8.57	0.789
15A-1K-5	89-89.5	**571.25**			10.28	0.810
15A-1K-5	94-94.5	**576.25**			8.22	0.803
15A-1K-5	99-99.5	**581.25**			8.69	0.821
15A-1K-5	104-104.5	**586.25**			6.03	0.816
15A-1K-5	109-109.5	**591.25**			10.29	0.852
15A-1K-5	114-114.5	**596.25**			8.56	0.804
15A-1K-5	119-119.5	**601.25**		0.09167	6.50	0.793

Section	section depth (cm)	cmblf	NOTE	%TIC	%OC EA	%water content
15A-1K-5	124-124.5	**606.25**			7.78	0.834
15A-1K-6	2-2.5	**611.25**			11.96	0.842
15A-1K-6	7-7.5	**616.25**			7.49	0.870
15A-1K-6	12-12.5	**621.25**			11.91	0.839
15A-1K-6	17-17.5	**626.25**			13.97	0.845
15A-1K-6	22-22.5	**631.25**			7.78	0.887
15A-1K-6	27-27.5	**636.25**			10.60	0.840
15A-1K-6	32-32.5	**641.25**			8.67	0.827
15A-1K-6	37-37.5	**646.25**			10.38	0.841
15A-1K-6	42-42.5	**651.25**		0.11351	9.41	0.859
15A-1K-6	47-47.5	**656.25**			5.65	0.843
15A-1K-6	52-52.5	**661.25**			8.21	0.823
15A-1K-6	57-57.5	**666.25**			5.32	0.795
15A-1K-6	62-62.5	**671.25**			5.23	0.711
15A-1K-6	67-67.5	**676.25**			5.39	0.753
15A-1K-6	72-72.5	**681.25**			5.09	0.734
15A-1K-6	77-77.5	**686.25**		0.01638	4.75	0.793

K12-19B BULK

cmblf (sed top)	NOTE	%TIC	%OC loi	%water content	Si:Ti (XRF)	(proxy) %Bsi	g/cm3 bulk dry sed	porosity, ϕ
0.25		1.408	15.45	0.918	NA			
2.25		1.322	15.85	0.909	NA			
4.25		1.999	14.61	0.909	0.172	17.36	2.05	0.953
6.25		3.115	12.00	0.893	0.184	19.09	2.13	0.947
8.25		3.534	10.84	0.893	0.247	28.17	2.11	0.946
10.25		3.185	12.25	0.911	0.152	14.63	2.15	0.956
12.25		4.005	10.45	0.900	0.080	4.23	2.28	0.954
14.25		3.570	10.60	0.903	0.203	21.82	2.16	0.953
16.25		3.093	11.72	0.906	0.138	12.54	2.18	0.954
18.25		3.686	10.81	0.906	0.131	11.53	2.22	0.955
20.25		2.644	12.26	0.907	0.098	6.85	2.20	0.955
22.25		0.347	16.76	0.926	0.167	16.78	1.99	0.961
24.25		0.503	16.40	0.925	0.255	29.26	1.92	0.960
26.25		0.453	15.33	0.923	0.231	25.80	1.98	0.959
28.25		0.693	14.28	0.923	0.245	27.89	2.00	0.960
30.25		2.445	12.85	0.916	0.222	24.57	2.07	0.957
32.25		0.583	16.78	0.929	0.275	32.21	1.89	0.961
34.25		1.004	18.59	0.925	0.190	20.03	1.91	0.959
36.25		0.501	15.49	0.924	0.186	19.42	2.01	0.961
38.25	BL	0.469	27.81	0.930	0.300	35.66	1.50	0.953
40.25	BL	0.867	26.11	0.933	0.380	47.17	1.48	0.953
42.25		1.283	14.43	0.939	0.198	21.16	2.04	0.969
44.25		1.630	13.62	0.938	0.107	8.10	2.15	0.970
46.25		1.413	15.38	0.939	0.054	0.51	2.14	0.971
48.25		0.855	16.77	0.948	0.093	6.18	2.06	0.974
50.25		0.969	16.93	0.944	0.243	27.58	1.91	0.970
52.25		0.825	14.37	0.937	0.394	49.12	1.86	0.965
54.25		2.554	13.65	0.921	0.290	34.25	1.98	0.958
55.25	BL	0.814	26.38	0.916	0.254	29.17	1.59	0.945
56.25	BL	0.715	27.13	0.927	0.140	12.81	1.67	0.955
58.25	BL	2.009	18.25	0.928	0.115	9.35	1.99	0.962
60.25		2.048	15.56	0.932	0.262	30.29	1.94	0.964
62.25		1.765	14.94	0.933	0.176	17.94	2.04	0.966
64.25		1.523	16.74	0.938	0.110	8.56	2.04	0.969

K13-8A BULK

cmblf (sed top)	Year, AD	NOTE	%TIC	%OC loi	%water content	Si:Ti (XRF)	(proxy) %Bsi	g/cm3 bulk dry sed	porosity, ϕ
0.5	2009		5.88	5.85	0.841	0.148	13.93	2.37	0.926
1.5	2001		5.41	5.70	0.844	0.077	3.85	2.44	0.929
2.5	1993		5.58	6.48	0.836	0.081	4.42	2.41	0.924
3.5	1985		6.52	5.39	0.773	0.185	19.30	2.35	0.889
4.5	1977		3.78	9.56	0.854	0.115	9.22	2.27	0.930
5.5	1967		0.43	15.91	0.905	0.124	10.57	2.06	0.951
6.5	1956		0.46	17.91	0.920	0.207	22.47	1.91	0.957
7.5	1945		0.44	18.88	0.923	0.106	7.96	1.98	0.960
8.5	1934		0.38	17.13	0.915	0.102	7.47	2.04	0.957
9.5	1923		0.26	17.24	0.907	0.063	1.86	2.07	0.953
10.5	1912		0.35	16.38	0.916	0.143	13.32	2.02	0.957
11.5	1901		5.84	12.56	0.843	0.107	8.08	2.18	0.921
12.5	1891		8.55	9.90	0.690	0.212	23.17	2.17	0.829
13.5	1882	BL	6.75	15.47	0.801	0.097	6.69	2.10	0.894
14.5	1871		7.40	11.44	0.783	0.091	5.87	2.23	0.890
15.5	1861		7.40	11.75	0.803	0.213	23.28	2.11	0.896
16.5	1853		7.07	12.90	0.827	0.091	5.83	2.19	0.913
17.5	1845		5.97	14.57	0.861	0.096	6.62	2.13	0.929
18.5	1836		2.33	23.27	0.931	0.144	13.36	1.80	0.961
19.5	1825		1.54	26.27	0.940	0.152	14.60	1.69	0.964
25.5	1775		9.30	3.72	0.778	0.291	34.45	2.30	0.890
30.5	1735		6.23	7.93	0.879	0.130	11.37	2.31	0.944
35.5	1694		6.33	7.96	0.877	0.152	14.64	2.29	0.942
40.5	1654		6.73	7.98	0.867	0.118	9.66	2.32	0.938
45.5	1614		0.84	11.84	0.930	0.107	8.12	2.21	0.967
47.5	1592	BL	0.80	23.83	0.901	0.069	2.70	1.85	0.944
50.5	1567		3.51	7.23	0.860	0.238	26.93	2.24	0.932
55.5	1519		0.71	18.45	0.922	0.105	7.87	1.99	0.959
60.5	1464		0.27	17.56	0.910	0.055	0.77	2.07	0.954
65.5	1409		0.01	4.67	0.770	0.022	-3.99	2.52	0.894
70.5	1353		0.13	19.59	0.925	0.120	10.00	1.94	0.960

K12-19A Stable Isotopes, carbonates

cmblf	Age, cal BP	d13C VPDB	C std dev	d18O VPDB	O std dev	
123.5	1081	14.67	0.670	-28.76	1.206	low voltage
133.5	1233	12.70	0.844	-32.28	0.879	low voltage
143.5	1386	11.78	0.594	-34.93	0.490	low voltage
153.5	1539	1.86	0.030	0.04	0.020	
158.5	1615	7.03	0.004	3.45	0.018	
163.5	1691	7.44	0.034	3.23	0.068	
168.5	1768	7.09	0.019	3.46	0.075	
173.5	1844	7.34	0.048	3.18	0.013	
178.5	1920	7.49	0.008	3.25	0.040	
183.5	1997	7.51	0.042	3.62	0.054	
188.5	2073	7.01	0.006	3.43	0.014	
193.5	2150	7.85	0.042	3.39	0.033	
203.5	2302	14.30	1.724	-27.45	1.289	low voltage
213.5	2455	12.10	0.842	-33.27	2.178	low voltage
223.5	2608	14.33	1.711	-32.43	0.952	low voltage
233.5	2760	6.41	0.015	2.50	0.043	
238.5	2837	6.70	0.024	3.35	0.053	
243.5	2913	6.63	0.022	3.06	0.036	
248.5	2990	6.39	0.019	3.14	0.051	
253.5	3066	6.30	0.034	2.72	0.070	
258.5	3142	6.35	0.007	2.24	0.088	
263.5	3219	6.32	0.019	2.89	0.019	
268.5	3295	6.79	0.020	3.01	0.007	
273.5	3371	6.71	0.004	3.22	0.028	
278.5	3448	6.23	0.006	2.74	0.055	
278.5	3448	6.24	0.039	3.17	0.070	
283.5	3524	6.42	0.064	2.62	0.015	
288.5	3600	6.62	0.032	3.59	0.020	
293.5	3677	6.89	0.022	3.29	0.068	
299	3761	6.68	0.020	3.20	0.015	
304	3837	6.25	0.035	2.86	0.010	
309	3913	5.83	0.023	3.07	0.060	
314	3990	6.33	0.013	3.26	0.020	
319	4066	5.67	0.030	2.55	0.046	
324	4143	5.47	0.032	1.51	0.054	
334	4295	1.70	0.513	-21.42	0.540	low voltage

cmblf	Age, cal BP	d13C VPDB	C std dev	d18O VPDB	O std dev	
344	4448	-3.45	1.152	-28.71	2.453	low voltage
354	4601	-2.77	1.850	-26.88	2.589	low voltage
364	4753	3.64	0.277	-28.32	1.379	low voltage
374	4906	-1.44	0.233	-28.51	1.738	low voltage
384	5059	-1.87	2.007	-32.06	0.565	low voltage
394	5212	2.03	0.549	-27.73	1.922	low voltage
404	5364	-2.41	1.718	-28.92	0.341	low voltage
414	5517	-1.64	0.665	-33.62	1.473	low voltage
424	5670	0.31	0.984	-21.46	2.444	low voltage
434	5822	6.38	1.162	-19.85	1.673	low voltage
442	5945	3.21	0.389	-24.42	0.489	low voltage
742.5	10534	-2.93	0.373	-28.15	0.425	low voltage
762.5	10839	-4.97	0.063	-28.60	0.623	low voltage

K12-19B Stable Isotopes, Carbonates

cmblf	d13C VPDB	C std dev	d18O VPDB	O std dev	
0.5	6.29	0.028	2.31	0.047	
10.5	5.66	0.023	2.09	0.026	
20.5	0.57	0.180	-12.26	0.143	low voltage
30.5	3.56	0.043	0.48	0.085	
35.5	-2.54	0.223	-17.01	0.181	low voltage
40.5	5.98	0.015	2.49	0.050	
45.5	5.12	0.036	2.00	0.049	
50.5	4.99	0.017	1.91	0.050	
55.5	5.68	0.012	2.43	0.058	
60.5	6.52	0.023	2.86	0.020	

K13-8A Stable isotopes, carbonates

cmblf	Year, AD	d13C VPDB	C std dev	d18O VPDB	O std dev	
1	2005	6.23	0.028	2.31	0.047	
4.2	1979	6.57	0.023	2.09	0.026	
12.9	1888	6.30	0.180	-12.26	0.143	low voltage
14.8	1868	6.56	0.043	0.48	0.085	
17	1849	7.24	0.223	-17.01	0.181	low voltage
21.5	1807	7.60	0.015	2.49	0.050	
24.5	1783	8.62	0.036	2.00	0.049	
30.5	1735	7.91	0.017	1.91	0.050	
33.5	1710	7.53	0.012	2.43	0.058	
36.5	1686	7.53	0.023	2.86	0.020	
40	1658	7.71	0.020	3.46	0.043	
43	1642	7.71	0.032	3.63	0.029	
49	1579	6.43	0.007	2.90	0.051	
51	1563	6.54	0.073	2.90	0.075	
53	1546	6.35	0.033	2.81	0.015	
58	1491	5.13	0.029	1.56	0.043	

K12-15A Stable isotopes, bulk OM

cmblf	NOTE	d13C VPDB	d15N N2	% C	% N	C/N
0.25	disturbed	-17.82	2.77	12.09	0.82	14.81
5.25	disturbed	-17.38	3.25	12.10	0.82	14.79
10.25	disturbed	-17.87	3.14	12.48	0.84	14.92
15.25	disturbed	-17.83	3.38	12.31	0.81	15.21
20.25	disturbed	-16.88	3.19	12.50	0.79	15.83
25.25	disturbed	-17.47	3.50	12.03	0.77	15.57
30.25	disturbed	-17.86	4.23	12.90	0.84	15.41
35.25	disturbed	-18.09	4.22	13.26	0.92	14.39
40.25		-15.47	4.09	12.26	0.81	15.12
45.25		-18.72	2.64	12.07	0.85	14.21
50.25		-19.64	2.44	12.34	0.92	13.42
55.25		-23.69	2.82	17.88	1.40	12.78
60.25		-24.98	2.89	10.84	0.91	11.86
65.25		-24.72	4.50	16.16	1.11	14.60

cmblf	NOTE	d13C VPDB	d15N N2	% C	% N	C/N
68.25	BL	-24.31	7.99	19.01	1.77	10.73
68.75	BL	-24.97	8.15	21.92	2.15	10.19
69.25	BL	-25.45	7.85	24.99	2.58	9.67
69.75	BL	-25.96	7.06	26.53	2.77	9.58
70.25	BL	-26.72	5.82	28.23	2.93	9.65
70.75	BL	-26.90	5.17	27.97	2.91	9.61
71.25	BL	-25.94	4.96	20.87	2.01	10.38
71.75		-25.96	4.81	18.51	1.71	10.84
72.25		-25.88	4.21	17.73	1.61	11.01
72.75		-25.93	4.21	16.51	1.50	11.04
73.25		-24.92	4.28	15.05	1.29	11.67
73.75		-24.49	4.13	14.15	1.13	12.57
79.25		-22.86	4.46	17.59	1.15	15.26
84.25		-23.27	4.53	15.51	1.21	12.81
89.25		-22.80	4.86	14.93	1.32	11.33
91.75		-21.58	5.99	13.63	1.50	9.07
92.25		-22.65	6.41	16.71	1.65	10.14
92.75		-23.01	6.46	16.83	1.65	10.18
93.25	BL	-23.17	7.03	23.15	2.42	9.57
93.75	BL	-23.51	8.46	24.20	2.58	9.38
94.25	BL	-24.91	7.54	29.67	3.19	9.29
94.75	BL	-25.23	7.09	33.25	3.59	9.25
95.25	BL	-25.61	6.00	33.01	3.50	9.43
95.75	BL	-26.20	4.74	35.54	3.75	9.47
96.25	BL	-26.17	4.45	29.21	3.06	9.55
96.75	BL	-25.32	4.97	23.91	2.43	9.84
97.25		-24.94	4.77	16.67	1.38	12.11
97.75		-24.48	1.94	8.58	0.73	11.76
98.25		-24.33	4.15	11.42	1.09	10.43
103.25		-22.89	3.56	12.38	1.18	10.48
108.25		-22.19	4.38	11.85	1.07	11.08
113.25	BL	-28.41	1.77	31.91	3.50	9.12
118.25		-22.43	4.57	12.41	1.11	11.16
123.25		-22.77	4.67	13.32	1.24	10.73
128.25	BL	-26.57	4.52	25.54	3.07	8.33
129.25	BL	-27.89	3.18	37.51	4.62	8.12
129.75	BL	-26.28	6.93	30.05	3.59	8.36
130.25	BL	-25.17	9.29	24.18	2.79	8.66

cmblf	NOTE	d13C VPDB	d15N N2	% C	% N	C/N
130.75		-24.76	8.07	16.94	1.97	8.58
136.25		-24.24	4.02	12.91	1.21	10.71
141.25		-23.99	2.80	14.70	1.14	12.92
146.25		-22.93	4.37	13.10	1.09	12.05
151.25		-22.23	6.26	13.28	1.11	11.94
156.25		-21.49	7.07	8.95	1.02	8.78
161.25		-18.95	2.99	10.74	0.75	14.31
166.25		-18.92	2.55	12.19	0.82	14.83
171.25		-18.82	2.27	13.11	0.83	15.88
176.25		-20.57	2.21	12.69	0.86	14.72
181.25		-23.88	2.92	11.84	0.94	12.54
186.25		-26.71	3.78	20.21	2.11	9.58
191.25		-18.72	2.02	11.66	0.78	14.93
196.25		-16.56	2.86	10.97	0.67	16.38
201.25		-20.06	1.01	13.67	0.82	16.76
206.25		-26.33	0.91	14.87	1.04	14.25
211.25		-25.73	1.24	16.20	1.10	14.67
216.25		-23.70	1.96	9.97	0.74	13.55
221.25		-24.58	2.22	9.99	0.76	13.14
226.25		-24.98	1.54	15.78	1.13	13.97
231.25		-25.15	1.37	15.59	1.27	12.28
236.25		-25.06	0.38	12.76	1.05	12.13
241.25	BL	-27.08	5.00	22.57	2.25	10.01
246.25		-20.73	0.72	10.22	0.61	16.66
251.25		-17.27	0.59	10.14	0.52	19.50
256.25		-17.86	0.81	9.66	0.52	18.51
261.25		-16.71	0.80	10.55	0.52	20.34
266.25		-17.98	-1.63	9.74	0.52	18.82
271.25		-19.55	-0.37	9.14	0.47	19.42
276.25		-16.36	1.20	10.41	0.45	22.94
281.25		-14.21	-0.80	9.64	0.47	20.42
286.25		-25.42	-6.59	6.69	0.44	15.27
291.25		-27.02	-1.42	7.02	0.51	13.66
296.25		-26.20	-2.22	7.89	0.47	16.77
301.25		-25.36	-3.20	7.32	0.37	19.56
306.25		-27.10	-2.87	7.36	0.41	17.80
311.25		-26.05	-1.95	7.71	0.43	18.01
316.25		-26.23	-2.30	7.60	0.44	17.09

cmblf	NOTE	d13C VPDB	d15N N2	% C	% N	C/N
321.25		-26.05	0.08	7.21	0.42	17.17
326.25		-25.98	-1.21	7.28	0.45	16.20
331.25		-26.10	-1.82	7.27	0.44	16.54
336.25		-26.16	-3.81	7.87	0.47	16.92
341.25		-26.50	-1.21	7.58	0.45	16.91
346.25		-26.10	1.28	7.57	0.44	17.29
351.25		-26.15	2.16	8.05	0.45	17.73
356.25		-26.08	2.43	7.50	0.42	17.76
361.25		-25.95	2.32	7.27	0.43	16.98
366.25		-26.18	0.69	6.77	0.40	16.89
371.25		-26.24	0.78	3.67	0.27	13.44
376.25		-26.27	1.62	6.01	0.41	14.75
381.25		-25.97	2.55	6.25	0.38	16.51
386.25		-26.69	1.06	6.82	0.39	17.49
391.25		-26.49	1.22	6.71	0.40	16.90
396.25		-26.46	3.34	7.32	0.42	17.53
401.25		-27.54	3.51	7.84	0.42	18.61
406.25		-26.29	3.41	7.05	0.37	18.86
411.25		-26.72	1.23	5.54	0.32	17.18
416.25		-25.59	1.13	6.51	0.38	17.04
421.25		-25.43	1.38	7.41	0.36	20.65
426.25		-28.65	12.07	2.10	0.29	7.33
431.25		-26.22	2.58	8.61	0.47	18.15
436.25		-26.15	2.47	8.44	0.48	17.75
441.25		-26.51	0.79	8.82	0.50	17.60
446.25		-26.49	-0.40	9.16	0.51	17.85
451.25		-26.54	1.51	8.64	0.50	17.31
456.25		-26.13	2.10	8.79	0.52	16.78
461.25		-27.22	2.35	9.38	0.51	18.32
466.25		-26.22	2.10	9.00	0.51	17.76
471.25		-26.67	1.32	8.61	0.51	16.91
476.25		-26.76	1.59	8.11	0.45	18.10
481.25		-26.66	1.55	8.11	0.45	18.20
486.25		-26.10	-0.40	5.87	0.34	17.49
491.25		-25.52	-1.53	4.63	0.35	13.25
496.25		-26.24	2.19	7.61	0.54	14.10
501.25		-24.90	3.14	2.71	0.44	6.20

cmblf	NOTE	d13C VPDB	d15N N2	% C	% N	C/N
506.25		-25.78	8.21	4.92	0.52	9.46
511.25		-27.00	2.17	4.01	0.32	12.40
516.25		-25.17	7.14	3.02	0.45	6.70
521.25		-26.37	5.26	8.41	0.47	17.74
526.25		-26.21	4.21	8.31	0.47	17.68
531.25		-26.63	2.57	7.82	0.45	17.28
536.25		-26.14	7.38	7.13	0.48	14.74
541.25		-26.43	7.54	5.99	0.49	12.14
546.25		-26.07	2.39	9.42	0.48	19.57
551.25		-25.30	1.04	10.25	0.46	22.16
556.25		-26.07	2.03	9.79	0.50	19.50
561.25		-26.68	-2.98	3.40	0.20	17.19
566.25		-26.03	1.66	8.57	0.42	20.46
571.25		-25.88	1.99	10.28	0.46	22.40
576.25		-26.58	2.64	8.22	0.46	17.96
581.25		-26.12	2.66	8.69	0.47	18.63
586.25		-26.70	6.29	6.03	0.39	15.66
591.25		-25.93	2.31	10.29	0.48	21.29
596.25		-25.29	1.31	8.56	0.41	20.64
601.25		-25.66	6.01	6.50	0.41	15.81
606.25		-26.73	7.48	7.78	0.51	15.30
611.25		-26.56	8.40	11.96	0.72	16.60
616.25		-28.55	6.83	7.49	0.54	13.90
621.25		-27.60	5.08	11.91	0.57	20.88
626.25		-26.87	4.74	13.97	0.69	20.14
631.25		-28.94	2.64	7.78	0.41	18.87
636.25		-27.70	4.19	10.60	0.52	20.55
641.25		-26.60	7.22	8.67	0.48	17.92
646.25		-25.89	6.07	10.38	0.52	19.85
651.25		-27.63	3.64	9.41	0.53	17.83
656.25		-27.93	4.54	5.65	0.37	15.42
661.25		-25.55	2.95	8.21	0.41	19.98
666.25		-26.17	6.38	5.32	0.33	16.00
671.25		-25.92	6.58	5.23	0.34	15.31
676.25		-26.11	5.72	5.39	0.37	14.65
681.25		-26.09	6.53	5.09	0.38	13.34
686.25		-25.83	9.70	4.75	0.37	12.74

K12-19B Stable isotopes, bulk OM

cmblf	NOTE	d13C VPDB	d15N N2	% C	% N	C/N
0.25		-24.66	2.30	15.73	1.17	13.39
2.25		-24.52	2.63	15.67	1.13	13.89
4.25		-24.40	2.59	13.77	1.04	13.26
6.25		-24.00	2.52	10.77	0.85	12.71
8.25		-24.19	2.65	9.95	0.80	12.40
10.25		-24.47	2.74	11.84	0.93	12.67
12.25		-24.73	2.95	9.49	0.74	12.87
14.25		-24.95	3.08	9.73	0.80	12.20
16.25		-25.03	2.62	10.53	0.84	12.58
18.25		-25.00	2.75	10.03	0.82	12.24
20.25		-24.97	2.73	11.57	0.90	12.79
24.25		-25.15	3.11	18.26	1.17	15.61
30.25		-24.99	2.85	12.41	0.96	12.89
34.25		-25.66	4.23	17.95	1.10	16.27
40.25	BL	-26.61	3.04	24.29	2.31	10.50
44.25		-24.23	3.92	12.27	0.91	13.48
50.25		-23.94	3.96	15.44	1.07	14.48
55.25	BL	-25.89	5.60	30.67	2.95	10.39
60.25		-24.63	3.17	23.63	1.83	12.88
64.25		-24.68	3.77	34.60	2.46	14.09

K13-8A Stable isotopes, bulk OM

cmblf	Year, AD	NOTE	d13C VPDB	d15N N2	% C	% N	C/N
0.5	2009		-25.24	2.94	6.26	0.47	13.26
2.5	1993		-23.75	3.35	5.97	0.44	13.62
4.5	1977		-24.40	3.36	10.17	0.66	15.39
6.5	1956		-25.57	3.58	20.55	1.16	17.66
8.5	1934		-25.61	3.79	19.24	1.14	16.93
10.5	1912		-25.91	4.56	17.44	0.98	17.74
12.5	1891		-24.23	7.37	3.67	0.30	12.16
13.5	1882	BL	-25.91	5.80	11.92	1.01	11.77
16.5	1853		-23.20	3.77	9.24	0.47	19.51
18.5	1836		-24.07	4.97	28.61	1.61	17.75
25.5	1775		-24.19	2.71	3.75	0.23	16.54
30.5	1735		-24.41	2.09	5.88	0.35	17.03
35.5	1694		-24.98	2.94	7.22	0.40	17.96
40.5	1654		-24.79	3.37	6.97	0.41	17.12
47.5	1592	BL	-30.85	-1.37	25.05	1.95	12.85
50.5	1567		-24.66	2.44	5.47	0.38	14.43
55.5	1519		-26.94	1.96	22.37	1.15	19.49
60.5	1464		-26.77	2.37	20.28	1.03	19.76
65.5	1409		-25.98	3.27	5.78	0.33	17.63

APPENDIX 2

AGE MODEL DATA TABLES

Kivu Samples for C14 dating

BETA	Sub sample label	Core/ section	depth in section, cm	depth, cmblf	description
347837	Kivu12-00	NA	NA		method blank, modern plant
347838	Kivu12-11A-2-15	11A-1K-2	15	137	unknown fibers
348195	Kivu12-11A-2-107	11A-1K-2	107	229	macrofossil unknown
347839	Kivu12-11A-4-40	11A-1K-4	40	378	macrofossil twig
347840	Kivu12-11A-6-5	11A-1K-6	5	499	wood
347841	Kivu12-11A-7-49	11A-1K-7	49	664.5	macrofossil leaf
347842	Kivu12-18A-6-131	18A-1K-6	131	794.5	macrofossil
347843	Kivu12-18B-1-61.5	18B-1G-1	61.5	61.5	brown layer base, twig
347844	Kivu12-19A-4-55	19A-1k-4	55	348	macrofossil twig
347845	Kivu12-19A-5-12.5	19A-1K-5	12.5	389	macrofossil twig
347846	Kivu12-19A-6-45.5	19A-1K-6	45.5	489	macrofossil twig
347847	Kivu12-19A-6-94	19A-1K-6	94	537.5	macrofossil twig
347848	Kivu12-19A-7-18	19A-1K-7	18	606	macrofossil wood
347849	Kivu12-19A-7-35	19A-1K-7	35	629	macrofossil wood
347850	Kivu12-19A-7-89.5	19A-1k-7	89.5	681	macrofossil wood
347851	Kivu12-19A-7-104.5	19A-1K-7	104.5	696	macrofossil unknown

Depth, cm	Years Cal BP
0	-805.58
100	721.62
200	2248.82
300	3776.02
400	5303.22
500	6830.42
600	8357.62
700	9884.82
800	11412.02
900	12939.22

Pb-210 Analysis (K13-8A) CRS Model V. 2 revised

avg. depth, cmblf	Median Yr	Sed Rate g/m2/yr	Pb-210 activity Bq/g	1 SD error	Pb-210 Excess Bq/g
0.5	2009.1	207.1	1.48E+00	7.91E-02	1.45E+00
1.5	2001.7	277.0	8.94E-01	4.84E-02	8.64E-01
2.5	1994.5	220.2	8.98E-01	4.97E-02	8.68E-01
3.5	1984.6	227.3	6.50E-01	3.58E-02	6.20E-01
4.5	1971.2	103.7	9.29E-01	5.18E-02	8.99E-01
5.5	1956.1	66.8	9.01E-01	5.11E-02	8.71E-01
6.5	1942.6	69.6	5.78E-01	3.35E-02	5.48E-01
7.5	1932.0	86.0	3.48E-01	2.22E-02	3.18E-01
8.5	1922.9	97.8	2.40E-01	1.68E-02	2.10E-01
9.5	1914.3	120.2	1.61E-01	1.25E-02	1.31E-01
10.5	1906.6	124.3	1.30E-01	9.50E-03	9.96E-02
11.5	1901.3	471.4	5.22E-02	4.46E-03	2.22E-02
12.5			2.75E-02	3.31E-03	
13.5			3.38E-02	3.60E-03	
14.5			2.96E-02	2.81E-03	
16.5			3.44E-02	3.99E-03	
18.5			7.95E-02	7.11E-03	
19.5			7.07E-02	6.62E-03	
25.5			8.94E-02	6.33E-03	
30.5			1.12E-01	8.19E-03	

^{210}Pb Age Model

Rates	years per cm
carbonate, 0-4cm	8.0627
organic, 5.5-8.5cm	11.023

Depth, cm	interval depth	Lith Unit	Year	value
0.5	0.5	carb	2008.97	2009
1.5	1.5	carb	2000.91	2001
2.5	2.5	carb	1992.84	1993
3.5	3.5	carb	1984.78	1985
4.2	4.2	carb	1979.14	1979
4.5	4.5	carb	1976.72	1977
5.5	0.5	org	1967.18	1967
6.5	1.5	org	1956.15	1956
7.5	2.5	org	1945.13	1945
8.5	3.5	org	1934.11	1934
9.5	4.5	org	1923.08	1923
10.5	5.5	org	1912.06	1912
11.5	6.5	org	1901.04	1901
12.5	0.5	carb	1891.49	1891
12.9	0.9	carb	1888.27	1888
13.5	0.5	org	1881.95	1882
14.5	1.5	org	1870.93	1871
14.8	1.8	org	1867.62	1868
15.5	0.5	carb	1861.39	1861
16.5	1.5	carb	1853.32	1853
17.5	2.5	carb	1845.26	1845
18.5	0.5	org	1835.72	1836
19.5	1.5	org	1824.69	1825
20.5	0.5	carb	1815.15	1815
21.5	1.5	carb	1807.09	1807
22.5	2.5	carb	1799.03	1799
23.5	3.5	carb	1790.96	1791
24.5	4.5	carb	1782.90	1783
25.5	5.5	carb	1774.84	1775
26.5	6.5	carb	1766.78	1767

Depth, cm	interval depth	Lith Unit	Year	value
27.5	7.5	carb	1758.71	1759
28.5	8.5	carb	1750.65	1751
29.5	9.5	carb	1742.59	1743
30.5	10.5	carb	1734.52	1735
31.5	11.5	carb	1726.46	1726
32.5	12.5	carb	1718.40	1718
33.5	13.5	carb	1710.34	1710
34.5	14.5	carb	1702.27	1702
35.5	15.5	carb	1694.21	1694
36.5	16.5	carb	1686.15	1686
37.5	17.5	carb	1678.09	1678
38.5	18.5	carb	1670.02	1670
39.5	19.5	carb	1661.96	1662
40.5	20.5	carb	1653.90	1654
41.5	21.5	carb	1645.83	1646
42.5	22.5	carb	1637.77	1638
43.5	0.5	org	1636.29	1636
44.5	1.5	org	1625.27	1625
45.5	2.5	org	1614.25	1614
46.5	3.5	org	1603.22	1603
47.5	4.5	org	1592.20	1592
48.5	0.5	carb	1582.66	1583
49.5	1.5	carb	1574.59	1575
50.5	2.5	carb	1566.53	1567
51.5	3.5	carb	1558.47	1558
52.5	4.5	carb	1550.41	1550
53.5	0.5	org	1540.86	1541
54.5	1.5	org	1529.84	1530
55.5	2.5	org	1518.82	1519
56.5	3.5	org	1507.79	1508
57.5	4.5	org	1496.77	1497
58.5	5.5	org	1485.75	1486
59.5	6.5	org	1474.73	1475
60.5	7.5	org	1463.70	1464
61.5	8.5	org	1452.68	1453
62.5	9.5	org	1441.66	1442
63.5	10.5	org	1430.63	1431

Depth, cm	interval depth	Lith Unit	Year	value
64.5	11.5	org	1419.61	1420
65.5	12.5	org	1408.59	1409
66.5	13.5	org	1397.56	1398
67.5	14.5	org	1386.54	1387
68.5	15.5	org	1375.52	1376
69.5	16.5	org	1364.50	1364
70.5	17.5	org	1353.47	1353
71.5	18.5	org	1342.45	1342
72.5	19.5	org	1331.43	1331
73.5	20.5	org	1320.40	1320
74	21	org	1314.89	1315

APPENDIX 3

X-RAY DIFFRACTION MINERAL ANALYSES

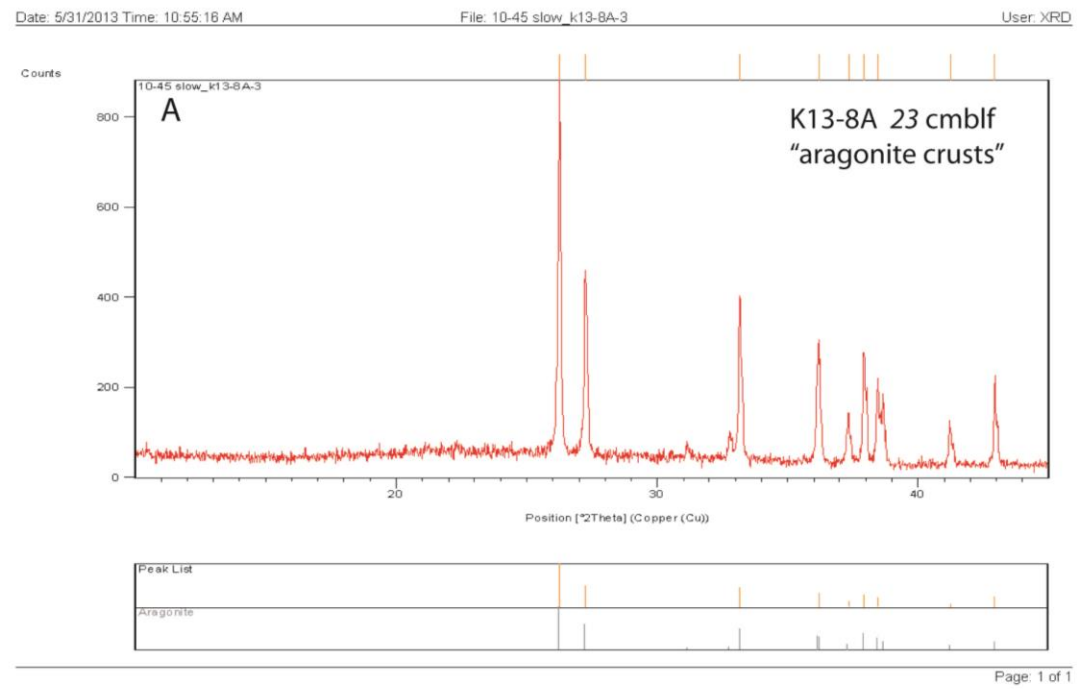

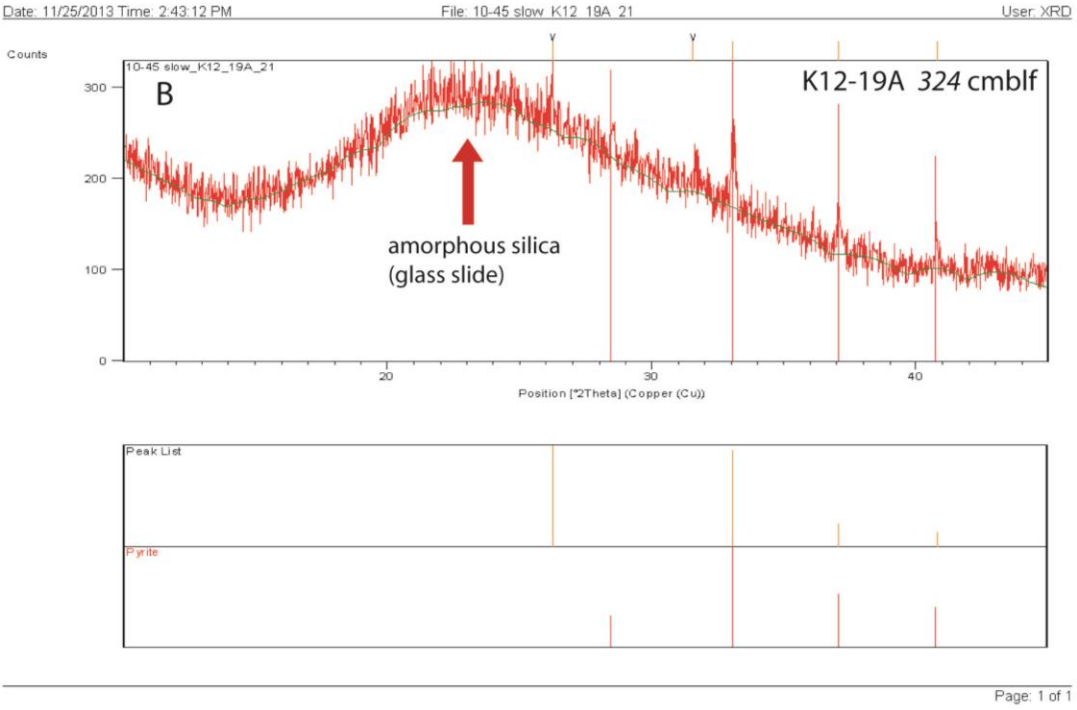

Figure A – Representative X-Ray Diffractograms

A and B represent the range in XRD signal strength and minerals present from all carbonate samples investigated. A - strong signal of aragonite from the hard crusts encountered in core 8A. B - sample that has low signal: noise ratio. Pyrite has a weak signal above the background amorphous silica "hump" generated from diatoms and glass slide.

APPENDIX 4

SELECT PREVIOUS STUDY CORES AND LOCATIONS

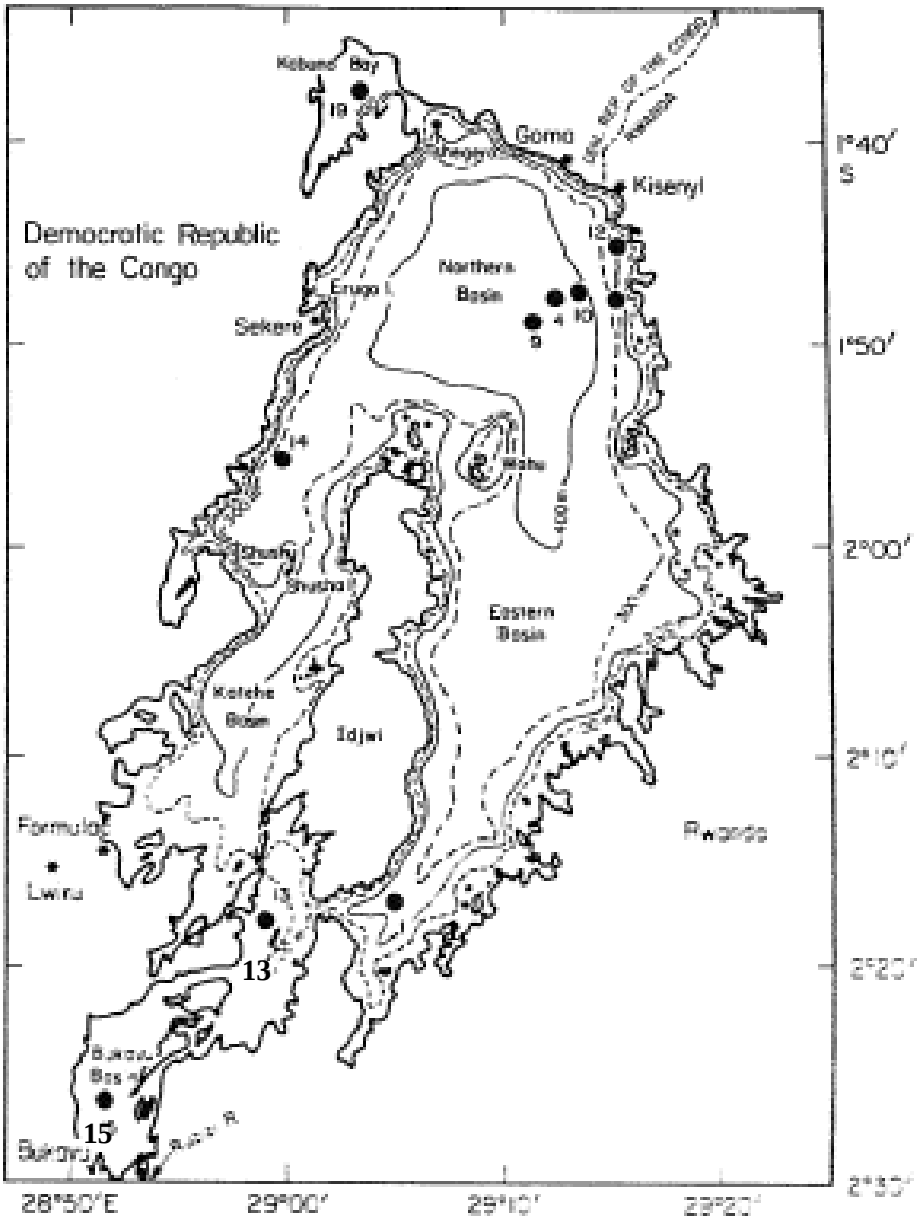

Figure A

Coring stations of the Woods Hole Oceanographic Institution 1971 expedition to Lake Kivu. From Fig. 1b of Stoffers and Hecky (1978).

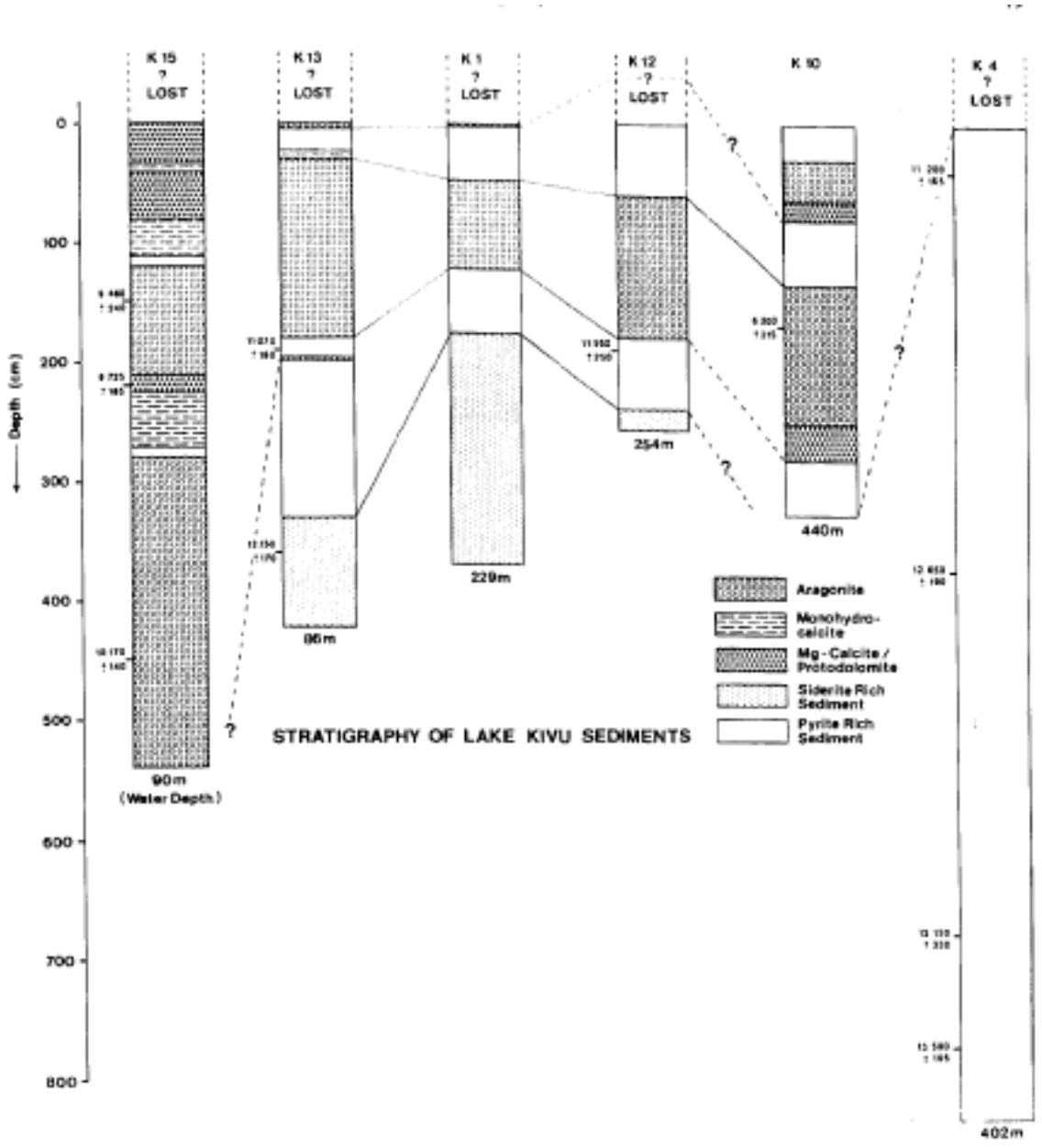

Figure B

Gross stratigraphy of Kivu cores from Stoffers and Hecky (1978); their figure 4. Stippled patterns are carbonate-rich sediments. See Fig. A for coring locations.

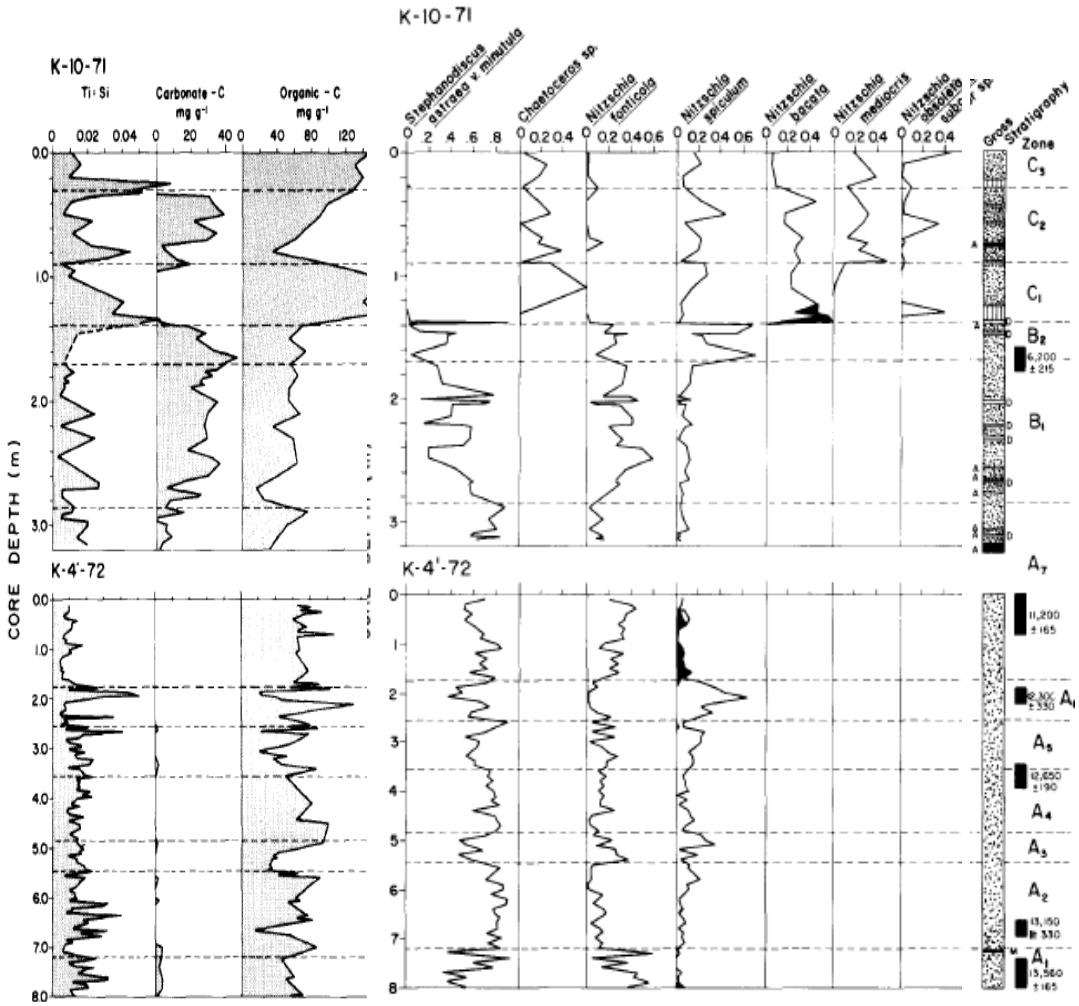

Figure C

Chemical and Diatom stratigraphy modified from Haberyan and Hecky (1987) figures 7 and 5, respectively. Note stratigraphy zone transitions (A-C) at right.

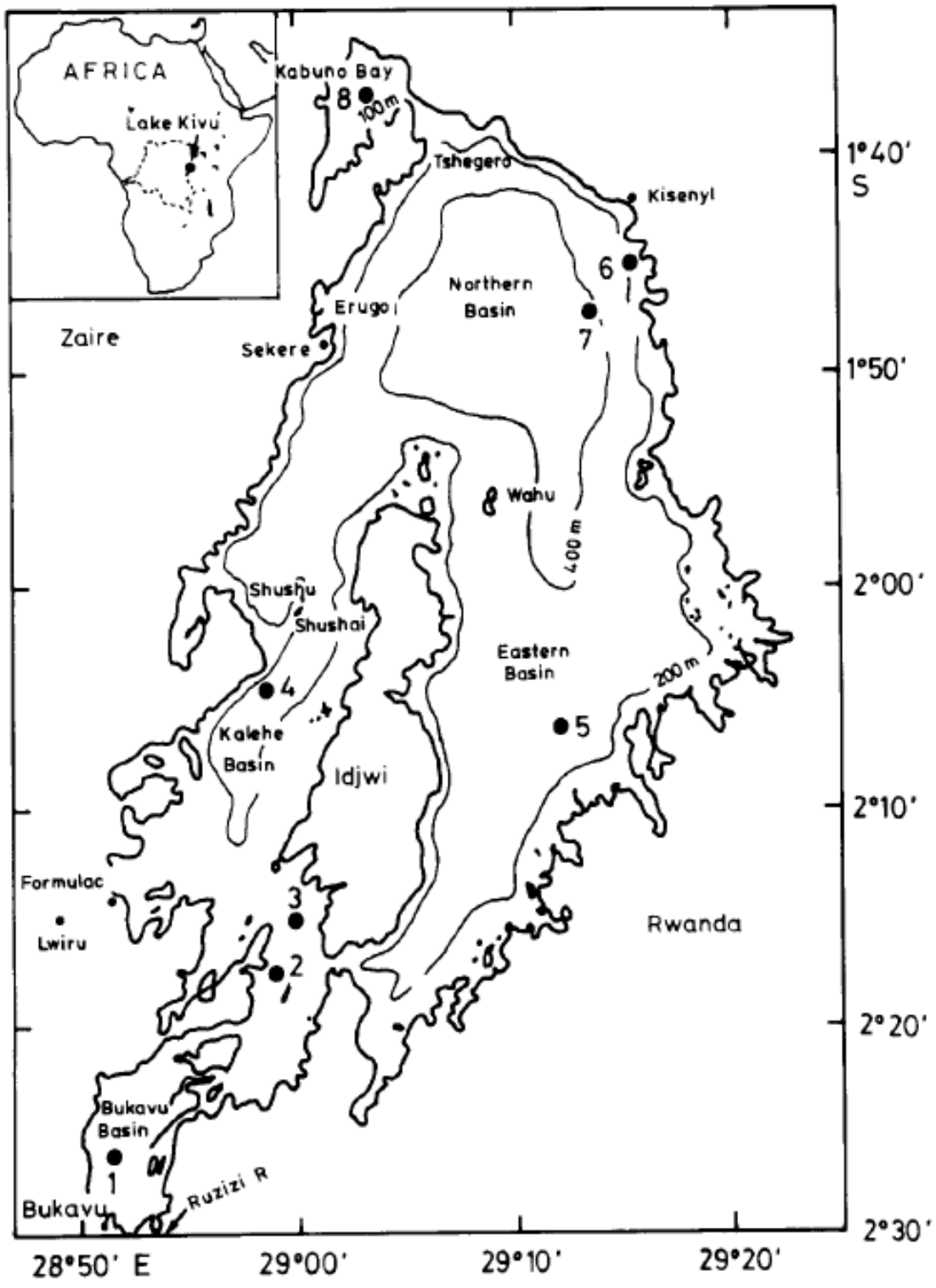

Figure D

Core locations of material analyzed by Botz *et al.* (1988) for inorganic carbonate isotope geochemistry. From their Fig. 1.